

| REPORT DOCUMENTATION PAGE  |             |                         |                            | Form Approved<br>OMB No. 0704-0188                    |  |
|--|-------------|-------------------------|----------------------------|---|--|
| Public reporting burden for this collection of information is estimated to average 1 hour per response, including the time for reviewing instructions, searching existing data sources, gathering and maintaining the data needed, and completing and reviewing this collection of information. Send comments regarding this burden estimate or any other aspect of this collection of information, including suggestions for reducing this burden to Department of Defense, Washington Headquarters Services, Directorate for Information Operations and Reports (0704-0188), 1215 Jefferson Davis Highway, Suite 1204, Arlington, VA 22202-4302. Respondents should be aware that notwithstanding any other provision of law, no person shall be subject to any penalty for failing to comply with a collection of information if it does not display a currently valid OMB control number. PLEASE DO NOT RETURN YOUR FORM TO THE ABOVE ADDRESS.   |             |                         |                            |   |  |
| 1. REPORT DATE (DD-MM-YYYY)<br>07/15/2002  |             | 2. REPORT TYPE<br>Final |                            | 3. DATES COVERED (From - To)<br>09/29/1999-12/30/2001 |  |
| 4. TITLE AND SUBTITLE<br>A Frontal Attack on Limiting Defects in GaN   |             |                         |                            | 5a. CONTRACT NUMBER                                   |  |
|  |             |                         |                            | 5b. GRANT NUMBER<br>N00014-99-1-1067                  |  |
|  |             |                         |                            | 5c. PROGRAM ELEMENT NUMBER<br>01PR04847-00            |  |
| 6. AUTHOR(S)<br>Hadis Morkoç   |             |                         |                            | 5d. PROJECT NUMBER                                    |  |
|  |             |                         |                            | 5e. TASK NUMBER                                       |  |
|  |             |                         |                            | 5f. WORK UNIT NUMBER                                  |  |
| 7. PERFORMING ORGANIZATION NAME(S) AND ADDRESS(ES)<br>Virginia Commonwealth University<br>PO Box 980568<br>Richmond, VA 23298-0568   |             |                         |                            | 8. PERFORMING ORGANIZATION REPORT NUMBER              |  |
| 9. SPONSORING / MONITORING AGENCY NAME(S) AND ADDRESS(ES)<br>ONR, Ballston Centre Tower<br>One, 800 N. Quincy Street<br>Arlington, VA 22217-5660   |             |                         |                            | 10. SPONSOR/MONITOR'S ACRONYM(S)                      |  |
|  |             |                         |                            | 11. SPONSOR/MONITOR'S REPORT NUMBER(S)                |  |
| 12. DISTRIBUTION / AVAILABILITY STATEMENT<br>Approved for Public Release; Distribution is Unlimited  |             |                         |                            |   |  |
| 13. SUPPLEMENTARY NOTES  |             |                         |                            |   |  |
| 14. ABSTRACT<br><br>GaN community, particularly under the leadership of Drs. Wood, Witt, and Litton, recognized that it is imperative that the extended, and point defects in GaN and related materials, and the mechanisms for their formation are understood. This is a first and an important step, which must be followed by defect reduction before full implementation of this material and its allied binaries/ternaries in devices. To establish benchmarks and identify the basic issues involved, a group of experts have joined forces to first fully characterize the HVPE grown material followed by attempts to find ways to reduce the defects an impurities in GaN in the outlying years. The group consisted of R. Molnar of Lincoln Labs, Dave Look of Wright State University, Jaime Freitas of NRL, Chris Van de Walle of Xerox PARC, L. Chernyak of UCF, Fred Pollak of Brooklyn College, Zuzanna Lilliental_Weber of LBNL, K. Saarinen of Helsinki University of Technology, L. Brillson of OSU, and Hadis Morkoç of VCU. There were others who performed related research, but their work is not included here. |             |                         |                            |   |  |
| 15. SUBJECT TERMS<br>GaN, semiconductors   |             |                         |                            |   |  |
| 16. SECURITY CLASSIFICATION OF:  |             |                         | 17. LIMITATION OF ABSTRACT | 18. NUMBER OF PAGES<br>55                             | 19a. NAME OF RESPONSIBLE PERSON<br>Hadis Morkoç        |
| a. REPORT  | b. ABSTRACT | c. THIS PAGE            |                            |   | 19b. TELEPHONE NUMBER (include area code) 804-827-3765 |

20020718 073

**Annual Report**  
**"A Frontal Attack on Limiting Point Defects in GaN"**  
Submitted to ONR and AFOSR

Attn: Dr. Colin E.C. Wood, Office of Naval Research,  
Code 312, Rm 607, 800 N. Quincy St., Arlington VA 22217  
VOICE: (703) 696 4218, FAX: (703) 696-2611, E-MAIL: Woodc@onr.navy.mil

Attn: Dr. Gerald L. Witt, AFOSR/NE  
801 North Randolph Street, Room 732, Arlington VA 22203-1977  
VOICE: 703-696-8571, FAX: 703-696-8481, E-MAIL: gerald.witt@afosr.af.mil

Submitted by: Hadis Morkoç  
School of Engineering, Virginia Commonwealth University  
Richmond, VA 23284

### Summary

GaN community, particularly under the leadership of Drs. Wood, Witt, and Litton, recognized that it is imperative that the extended, and point defects in GaN and related materials, and the mechanisms for their formation are understood. This is a first and an important step, which must be followed by defect reduction before full implementation of this material and its allied binaries/ternaries in devices. To establish benchmarks and identify the basic issues involved, a group of experts have joined forces to first fully characterize the HVPE grown material followed by attempts to find ways to reduce the defects and impurities in GaN in the outlying years. The group consisted of R. Molnar of Lincoln Labs, Dave Look of Wright State University, Jaime Freitas of NRL, Chris Van de Walle of Xerox PARC, L. Chernyak of UCF, Fred Pollak of Brooklyn College, Zuzanna Lilliental-Weber of LBNL, K. Saarinen of Helsinki University of Technology, L. Brillson of OSU, and Hadis Morkoç of VCU. There were others who performed related research, but their work is not included here.

The HVPE layers were grown by R. Molnar with free-standing GaN wafer provided by Y. J. Park of Samsung Advanced Institute of Technology. Dave Look and colleagues carried out the Hall, DLTS and PL measurements as well as keeping track of the wafer traffic with assistance in fabrication from the VCU group. Jaime Freitas and colleagues performed PL, Raman, ODMR and EPR measurements. Zuzanna Lilliental-Weber performed TEM and convergent beam electron diffraction experiments to determine the density and nature of extended defects, and the polarity of the films. Kimmo Sarinen performed positron annihilation experiments in an effort to determine Ga-vacancy concentration. L. Chernyak and colleagues employed electron beam probing and micro PL to determine the minority carrier diffusion length and lifetime in GaN. Chris van de Walle calculated formation energies of defects and basics pertaining to commonly observed background impurities in GaN such as C and O. Len Brillson performed the scanning micro cathodoluminescence experiments for probing the

evolution of deep defect related transitions from the interface to the surface in thick layers. Fred Pollak carried out the thermal conductivity measurements by scanning thermal microscopy. The impurity analysis was done by means of SIMS, which was carried out at Charles Evans Associates for a nominal fee. Hadis Morkoç developed chemical etches for defect density determination, undertook X-Ray, Hall, PL, and Raman measurements through collaborations, as well as providing fabrication support for DLTS samples for the group.

The first task of the group dealt with full characterization of HVPE GaN layers grown on sapphire at Lincoln Laboratories. This has been successfully completed. Serendipitously, free-standing GaN templates, separated from sapphire substrates by a laser process, became available to the investigators. All samples were analyzed for extended defects by TEM and chemical etches, polarity by Electric Force Microscopy and convergent beam electron diffraction (CBED), point defects by DLTS, optical quality and deep defects by PL, vacancies by positron annihilation, donor and acceptor like states within the gap by ODMR and EPR, and carrier transport targeted for defects and impurities by variable temperature and magnetic field dependent Hall measurements, including the differential variety.

Hydride VPE samples grown at Lincoln Laboratories with 1.5  $\mu\text{m}$ , 5.5  $\mu\text{m}$  and 55  $\mu\text{m}$  thicknesses were investigated for defects by TEM, and their polarity was found to be Ga-polarity, as expected, by CBED combined with simulations. The density of misfit dislocations at the substrate-epi interface was determined to be on the order of  $10^{13} \text{ cm}^{-2}$  based on high-resolution electron microscopy images. The threading dislocations are dominant from the interface to the top surface. Similar densities of all three types of these dislocations (edge, screw and mixed) were found. The highest density of threading dislocations (of the order of  $10^{10} \text{ cm}^{-2}$ ) was found closer the interface. The threading dislocation density decreased gradually with distance from the interface. For the 55  $\mu\text{m}$  sample, this density is about  $10^8 \text{ cm}^{-2}$  at the surface.

A 200  $\mu\text{m}$  thick laser separated and free-standing HVPE grown GaN template grown at Samsung was also characterized for its structural properties by transmission electron microscopy (TEM). Convergent Beam Electron Diffraction (CBED) was employed to determine the polarity of the free surface and the side juxtaposed to substrate before separation, which confirmed the epitaxial surface to be of Ga-polarity. The substrate side was confirmed to be N-face. The density of dislocations near the N-face was determined to be, in order,  $3 \pm 1 \times 10^7$  and  $4 \pm 1 \times 10^7$  by cross-sectional TEM and plan-view TEM, respectively. Identical observations on the Ga-face revealed the defect concentration to be less than  $1 \times 10^7 \text{ cm}^{-2}$  by plan-view TEM and  $5 \times 10^5 \text{ cm}^{-2}$  by cross-sectional TEM.

Defects in a 10  $\mu\text{m}$  thick GaN layer grown by HVPE at Lincoln Laboratory have been investigated by photo electrochemical (PEC) etching, and by wet etching in hot  $\text{H}_3\text{PO}_4$  acid and molten KOH. Threading vertical wires (i.e. whiskers) and hexagonal-shaped etch pits are formed on the etched sample surfaces by PEC and wet etching, respectively. Using atomic force microscopy, we find the density of "whisker-like" features to be  $2 \times 10^9 \text{ cm}^{-2}$ , the same value found for the etch-pit density on samples etched with both  $\text{H}_3\text{PO}_4$  and molten KOH. Values agree well with TEM results.

A free standing 300  $\mu\text{m}$  thick GaN template grown by hydride vapor phase epitaxy (HVPE), which has been reduced to 200  $\mu\text{m}$  by lapping and polishing, has been characterized for its structural and optical properties using X-ray diffraction, defect delineation etch followed by imaging with atomic force microscopy (AFM). The Ga-face and the N-face of the c-plane GaN exhibited a wide variation in terms of the defect density. The defect concentrations on Ga and N-faces were about  $5 \times 10^5 \text{ cm}^{-2}$  for the former and about  $1 \times 10^7 \text{ cm}^{-2}$  for the latter, again in good agreement with TEM results mentioned above.

High resolution X-ray rocking curves (omega scan) were measured by a Philips X'Pert MRD system equipped with four-crystal Ge monochromator in Lincoln layers and Samsung templates. The [002] symmetric and [104] asymmetric peaks in 10  $\mu\text{m}$  thick HVPE films by Lincoln Labs had FWHM values between 5.8 and 7.9, and 3.9 and 5.2, respectively. The Samsung template investigated had wide diffraction peaks (20.6 and 24 arcmin for [002] and [104] diffractions, respectively) on the Ga-face, similar on N-face, when a 2 mm slit size was used. When the slit size was reduced to 0.02 mm, the Ga and N-face [002] peaks reduced to 69 and 160 arcseconds. Using the particular geometry of the X-ray diffraction system in terms of the area covered by the incident beam, a bowing radius of 1.2 m was calculated to account for increased broadening with wider slits.

Specific impurities probed by SIMS as part of this investigation were nominally O, C, and Si. In the HVPE layer studied, both O and Si concentrations drop rapidly away from the surface into the sample- mainly due in part to the artifact of the technique and in part due to

condensates on the surface of the sample, down to about  $10^{17} \text{ cm}^{-3}$  for Si and high  $10^{16} \text{ cm}^{-3}$  for O. The Ga-face profile in the Samsung template indicated levels below mid  $10^{16} \text{ cm}^{-3}$  for all three of the impurities. The picture is different for the N-side, however, as it was juxtaposed to the substrate during growth and was mechanically polished after laser separation. The impurity concentration is, depending on the species, some 1-3 orders of magnitude higher than the case for the Ga-face. Particularly the concentration of O and C is high, albeit some drop occurs as one goes deeper into the film. This should be re-examined in a sample where the N-surface is etched to remove the damaged and highly conductive region.

Detailed transport measurements were undertaken in both Lincoln (AFRL) and Samsung HVPE (AFRL and VCU) materials in an effort to gain insight to impurities and defect including their depth profiles, and scattering events. In GaN grown on foreign substrates such as sapphire, regardless of the growth method, there exist an about 0.2  $\mu\text{m}$  region at the interface that is highly doped and exhibits nearly temperature independent carrier transport. Such layer complicates efforts, which utilize temperature activated processes occurring in the film to extract useful information such as accurate electrically active impurity concentrations and donor activation energies in n-type samples. Extraction of the effect of this layer has been dealt with in a variety of ways including detailed Hall measurements at high magnetic fields, differential Hall measurements involving sequential etching and measurements, and modeling. By investigating the films properties as a function of the layer thickness ranging from about 1 to 68  $\mu\text{m}$ , all the other parameters were kept the same, we determined the critical parameters as they evolve from the sapphire-GaN interface and up. A strong dependence on distance from the interface was observed with the averaged mobility figures increasing from  $190 \text{ cm}^2 \text{ V}^{-1} \text{ s}^{-1}$  in the 5  $\mu\text{m}$  film to  $740 \text{ cm}^2 \text{ V}^{-1} \text{ s}^{-1}$  in the 68  $\mu\text{m}$  film. The preliminary differential Hall measurements indicate that the mobility at the surface of the thick layer is about  $1200 \text{ cm}^2 \text{ V}^{-1} \text{ s}^{-1}$ .

The free-standing of the Samsung GaN template allowed the removal of about 30  $\mu\text{m}$  of what would have been the interfacial layer, before laser separation, to make sure that the measurements were not affected by it. In addition, Raman measurements were made in the sample used for Hall measurement to accurately determine the vibration mode frequencies for an accurate determination of the high frequency dielectric constant from the low frequency dielectric constant. Electron mobilities in this material were  $1425 \text{ cm}^2/\text{Vs}$  at  $T=273 \text{ K}$  and  $7385 \text{ cm}^2/\text{Vs}$  at  $48.2 \text{ K}$ . By using the most recent unscreened acoustic deformation potential and allowing only the acceptor concentration to vary ( $2.4 \times 10^{15} \text{ cm}^{-3}$  for the best fit), we obtained an excellent fit to the measured mobility in the temperature range of 30 – 273 K by using an iterative BTE method. In addition, an excellent fit for the temperature dependent electron concentration was also obtained utilizing the acceptor concentration determined from the

fit to the Hall data, and the charge balance equation. This led to a donor concentration of  $1.6 \times 10^{16} \text{ cm}^{-3}$ , and activation energy of 26 meV, the latter being the highest reported in the literature for GaN.

In the Samsung material, the  $\Gamma_5$  and  $\Gamma_6$  free excitons have been identified from emission measurements by utilizing polarization geometries where the E field is perpendicular to the c axis, favoring the  $\Gamma_5$  exciton, and E field parallel to the c-axis (incident beam from the edge of the wafer) favoring the  $\Gamma_6$  exciton. Focusing on the defect region of the PL spectrum, the N-face of the sample exhibited the usual yellow line. However, the Ga-face exhibited a broad band encompassing both yellow and green bands. Upon increased below gap radiation, the yellow band saturated while the green continued to grow. It is suggested that the green line is due to Ga vacancy, where as the yellow band may be due to the same vacancy complexed with dislocations which are more abundant on the N-face than on the Ga-face.

For deeper transitions associated with defects, experiments with variable excitation intensity and excitation energy showed two bands with maxima at about 2.15 eV (yellow luminescence) and 2.43 eV (green luminescence). Unlike in RMBE, RF-MBE and MOCVD and other HVPE grown GaN samples, the yellow luminescence in the free-standing template is weak and can be easily saturated. In contrast, the green luminescence is dominant and is attributed to the isolated defect involving gallium vacancy, whereas the yellow luminescence is related to the same defect bound to dislocation or surface bound structural defect.

Deep centers in n-GaN have been characterized by DLTS in HVPE-grown GaN of different thickness and dislocation densities, and Samsung templates. A collation of all the deep centers and their known characteristics are shown in Table V in the text. Centers  $A_1$  and  $E_1$  found in as-grown and thin HVPE-GaN are very similar to the centers  $A_2$  and E induced by electron-irradiation, indicating their point-defect nature. The main deep centers in n-GaN, such as  $A_1$ , B, and D, show higher concentrations in thinner samples, which suggests relevance to the high dislocation densities. Based on the anti-correlation between  $A_1$  and B, which can be observed in thin HVPE-GaN layers the defect B was tentatively assigned to  $N_{Ga}$ . Centers A, C, and D are not affected by 1-MeV electron-irradiation, thus ruling out the possibility of these centers being identical to any EI-induced centers; however, their nature remains unknown. 1-MeV electron irradiation creates  $V_N$ -related centers with thermal activation energies of 0.06 eV, and a center with  $E_T=0.85$  eV, which might be related to  $N_i$ . To shed light on the spatial distribution of defects away from the interface, HVPE-grown n-GaN layers with different thicknesses have been characterized by DLTS and TEM. The TEM results were discussed under the "TEM" section already. As the layer thickness decreases, an increase of deep centers, both in species and concentrations, was clearly

observed, which is believed to be closely associated with the significant increase of threading dislocations in the regions near the GaN/sapphire interface. Based on a comparison with EI-induced centers and an observation of anti-correlation,  $A_1$  is tentatively assigned to  $N_i$ , and B to  $N_{Ga}$ . The Samsung template exhibited a new trap B, with parameters  $E_T=0.53$  eV and  $\sigma_T=1.5 \times 10^{-15} \text{ cm}^2$  on the Ga-face, in addition to the four traps commonly observed in various epitaxial GaN layers. For the N-face sample, a N-vacancy related trap  $E_1$ , with  $E_T=0.18$  eV and  $\sigma_T=4 \times 10^{-17} \text{ cm}^2$ , was observed. On the other hand, the Ga-face sample contained trap C, with  $E_T=0.35$  eV and  $\sigma_T=1.6 \times 10^{-15} \text{ cm}^2$ . This trap may be related to surface damage caused by the RIE process employed. A new sample for which the damaged region is removed is under investigation. A Side benefit of the DLTS investigations is that the barrier heights of Ni/Au Schottky contacts were determined to be 1.27 eV and 0.75 eV for the Ga face and N face, respectively.

Electron beam and optical depth-profiling of thick (5.5 - 68  $\mu\text{m}$ ) n-type HVPE GaN samples were carried out using electron beam induced current (EBIC) and micro-photoluminescence (PL) to determine the minority carrier diffusion length,  $L$ , and minority carrier lifetime. The minority carrier diffusion length increased linearly from 0.25  $\mu\text{m}$ , at a distance of about 5  $\mu\text{m}$  from the GaN/sapphire interface, to 0.63  $\mu\text{m}$  at the GaN surface for a 36- $\mu\text{m}$ -thick sample. The increase in  $L$  was accompanied by a corresponding increase in PL band-to-band radiative transition intensity as a function of distance from the GaN/sapphire interface. We attribute these observations in PL intensity and minority carrier diffusion length to a reduced carrier mobility and lifetime at the interface, and due to scattering at threading dislocations. The results of EBIC and PL measurements are in good agreement with the values for dislocation density, obtained using TEM, which we discussed earlier in this report.

Positron annihilation experiments have been conducted in HVPE films with varying thicknesses from 1 to 68  $\mu\text{m}$ . Other samples doped with Mg and bulk GaN samples grown at UNIPRESS were also investigated and the behavior of positron annihilation in Mg-doped samples established. Unlike in the Mg-doped samples, the positron lifetime in the HVPE samples under investigation increased as the lattice temperature was lowered. This was interpreted as meaning that the acceptors in these n-type samples are due to Ga-vacancies as opposed to relatively shallow acceptor impurities. The similarities in the behavior of these samples and those investigated in a previous study where the III/V ratio was changed also lend support to the Ga-vacancy argument. The previous investigation established that as the III/V is lowered by increasing the ammonia flow during the growth, the Ga-vacancy concentration increased. Using Mg-doped samples as standard, the vacancy concentration was determined to be about  $10^{17} \text{ cm}^{-3}$  near the surface for the layer with a thickness greater than 30  $\mu\text{m}$  (could be as high as 68  $\mu\text{m}$ ). Assuming that the growth parameters in

the set of layers with varying thicknesses that were investigated are the same, the Ga-vacancy concentration increases to mid  $10^{19} \text{ cm}^{-3}$  near the interface. Since the interfacial region is n-type and highly conductive, this region must also contain even larger concentrations of O and or N-vacancies with lead to n-type material. SIMS results already indicate mid  $10^{19} \text{ cm}^{-3}$  levels of O being present in this region. This has been attributed to O out-diffusion from sapphire as previously reported. Moreover, the preliminary data in sample LH1232, 2.6  $\mu\text{m}$  thick sample, suggest that this sample contains vacancy clusters instead of Ga vacancies.

FTIR, ODMR and EPR measurements have been made in both Lincoln and Samsung HVPE layers. In FTIR measurements, two absorption bands corresponding to binding energies of 30.9 and 33.9 meV were found. The former is of higher concentration than the latter and is attributed to Si donors. Splitting of the binding energies with magnetic field is consistent with an effective mass of 0.22  $m_0$ . Angular rotation studies were performed with the magnetic field oriented perpendicular and parallel to the c-axis to provide symmetry information. The ODMR in a 5-10  $\mu\text{m}$  thick GaN layer on the 2.2 eV peak, the notorious yellow emission, showed signatures of shallow donor (effective mass like) and deep defect centers with g-values of 1.95 and 1.99, respectively. The 3.27 eV peak with resolved LO phonon replicas, which is the blue peak observed in many GaN films grown by a variety of methods, is attributed to transitions involving shallow acceptors with  $g_{\parallel} \sim 2.1$  and  $g_{\perp} \sim 2.0$ . ODMR on the 2.4 eV "green" PL band from the Samsung free-standing layer also reveals evidence for shallow donors with a g-value of 1.95 and other deeper centers. The larger linewidth of the shallow donor signal from the Samsung sample, relative to that found for the Lincoln layers, is indicative of a lower concentration of this center, which leads to an increased hyperfine interaction. EPR studies confirmed the notable difference between the Lincoln and Samsung layers, particularly the larger linewidths in the Samsung material due to the lower concentration of shallow donors. Specifically, the Samsung free-standing sample has about  $6 \times 10^{15}$  uncompensated donors per  $\text{cm}^3$  while the Lincoln sample has a concentration about a factor of four higher.

Micro cathodoluminescence with scanning capability was used to probe optical transitions along the edge of the wafer extending from the surface into the substrate. Evolution of the GaN band edge and sapphire-related peaks were monitored. In addition to the commonly observed 2.2 eV peak which diminished toward the interface, an emission line at 2.9 eV and dopant-related near band edge emission emerged at the interface. The former may be correlated with Zn pretreatments of the growth template. The latter can be correlated with O diffusion, although underlying mechanisms are under investigation.

Calculations indicate that incorporation of Si has a negligible effect on the lattice constant, but O and Mg can lead to an observable expansion of the lattice. Since

values of the GaN lattice constant have often been based on bulk crystals that are now known to contain large concentrations of oxygen, the "true" GaN lattice constant is actually smaller than what has been measured for such crystals. Boron is an unintentional impurity that can be introduced during MBE growth. There has been speculation about whether B might act as an acceptor in GaN; this would require it to be incorporated on the nitrogen site. Our computations indicate that incorporating B on the N site is energetically unfavorable. Even if it did incorporate there, it would act as a *deep*, rather than a shallow acceptor. Formation energies of H in AlN and GaN have also been calculated. The behavior of H in AlN is very similar to GaN:  $\text{H}^+$  dominates in p-type, H in n-type. Surprisingly, H in InN behaves exclusively as a donor, i.e., it is *not* amphoteric as in GaN and AlN, but actually contributes to the n-type conductivity of the material.

Scanning thermal microscopy (SThM) has been applied to measure the local thermal conductivity of epitaxial GaN. Since the thermal conductivity is affected to a large extent by phonon scattering, a closer to the true value of this parameter can be obtained by a local measurement in areas of lower defect concentration such as those found in the wing regions of lateral epitaxially grown GaN. The method relies on a thermo-resistive tip forming one quadrant of a Winston bridge. The bridge is balanced with the tip heated followed by bringing the tip in contact with the sample under test which cools down due to thermal dissipation. However, the feedback circuit attempts to keep the thermo-resistance and thus the tip temperature the same. The square of the feedback voltage necessary for this is proportional to the thermal conductive. Accurate values can be obtained with calibration using known substrates such as GaSb, GaAs, InP, Si and Al metal. Using SThM, thermal conductivity,  $\kappa$ , values in the 2.0 – 2.1 W/cm-K in the wing regions of lateral epitaxially grown GaN, 1.70 – 1.75 W/cm-K in HVPE grown GaN, and 3.0 – 3.3 W/cm-K for free-standing AlN have been measured.

## Outline

### I. Introduction

#### II.1. Structural Analysis by TEM

#### II.2. Structural Analysis by Etching

#### II.3. Structural Analysis by X-ray Diffraction

### III. Impurities Determined by Secondary Ion Mass Spectroscopy

### IV. Transport Properties: Analysis of Hall Data and Mobility Fitting

### V. Point Defects

#### V.a. PL Dealing with Band Edge

#### V.b. PL Dealing with the Defect Region of the Spectrum

#### V.c. DLTS

#### V.d. Minority Carrier Lifetime

V.e. Positron Annihilation: Lincoln layers- Samsung layers? In Progress

V.f. EPR and ODMR

V.g. Scanning Micro-Cathodoluminescence Spectroscopy

## VI. Theory

## VII. Thermal Conductivity Measurements

## VIII. Conclusions

## I. Introduction

Semiconductor nitrides such as aluminum nitride (AlN), gallium nitride (GaN), and indium nitride (InN) are very promising materials for their potential use in optoelectronic devices (both emitters and detectors), and high power/temperature electronic devices as have been treated in length and reviewed recently<sup>1,2,3,4,5,6,7</sup>. These materials and their ternary and quaternary alloys cover an energy bandgap range of 1.9 to 6.2 eV, suitable for band-to-band light generation with colors ranging from red (potentially) to ultraviolet (UV) wavelengths. Specifically, nitrides are suitable for such applications as surface acoustic wave devices<sup>8</sup>, UV detectors<sup>9,10</sup>, Bragg reflectors<sup>11</sup>, waveguides, UV and visible light emitting diodes (LEDs)<sup>12,13,14</sup>, and laser diodes (LDs)<sup>15</sup> for digital data read-write applications. During the last several decades, lasers and LEDs have expanded remarkably both in terms of the range of emission wavelengths available and brightness. The nitride semiconductor-based LEDs have proven to be reliable in such applications as displays, lighting, indicator lights, advertisement, and traffic signs/signals. Additional possible applications include use in agriculture as light sources for accelerated photosynthesis, and in health care for diagnosis and treatment. Lasers, as coherent sources, are crucial for high-density optical read and write technologies. Because the diffraction-limited optical storage density increases approximately quadratically (the best case scenario) as the probe laser wavelength is reduced, nitride-based coherent sources at wavelengths down to UV are attracting a good deal of attention. Optical storage would enable the storage and retrieval of inordinate number of images and vast quantities of text with untold efficiency. Other equally attractive applications envisioned include printing and surgery.

When used as UV sensors in jet engines, automobiles, and furnaces (boilers), the devices would allow optimal fuel efficiency and control of effluents for a cleaner environment. Moreover, UV sensors that operate in the solar blind region (260 to 290 nm) would have high detectivity because the ozone layer absorbs solar radiation at those wavelengths, thus virtually eliminating the radiation noise. Consequently, these detectors are expected to play a pivotal role in threat recognition aimed against aircraft and other vehicles<sup>9,10,16</sup>. GaN photodiodes<sup>17</sup> exhibited zero-bias responsivities of about 0.21 A/W at 356 nm that decreased by more than three orders of magnitude for wavelengths longer than 390 nm. The noise equivalent power (NEP) at a reverse bias of 10

V is ( $f > 100$  Hz)  $6.6 \times 10^{-15}$  W/Hz<sup>1/2</sup> which is extremely small<sup>18</sup>. Detector speed while affected in terms of uniformity by the sheet resistance of the p-layer, which suffers from the notoriously low doping levels, is in the picosecond range<sup>19</sup>. Finally, the GaN based detectors with AlN mole fractions approaching the solar blind region of the spectrum has been fabricated into arrays for imaging. Detector arrays with pixel sizes of 32x32 have been fabricated and tested already<sup>20</sup>.

GaN's large bandgap, large dielectric breakdown field, fortuitously good electron transport properties<sup>21,22,23</sup> (an electron mobility possibly in excess of  $2,000 \text{ cm}^2 \text{ V}^{-1} \text{ s}^{-1}$  and a peak velocity approaching  $3 \times 10^7 \text{ cm s}^{-1}$  at room temperature), and good thermal conductivity are conducive high power/temperature electronic devices.<sup>24</sup> In one of the earlier reports on SiC substrates, Sheppard et al.<sup>25</sup> have reported that 0.45  $\mu\text{m}$  gate, high power modulation doped FETs (MODFETs) exhibited a power density of 6.8 W/mm in a 125  $\mu\text{m}$ -wide device and a total power of 4 W (with a power density of 2 W/mm) at 10 GHz. Other groups have also reported on the superior performance of GaN-based MODFETs on SiC and sapphire substrates with respect to competing materials, particularly at X band and higher frequencies.<sup>26,27,28,29</sup> What is astounding is that researchers at HRL Laboratories have recently demonstrated GaN/AlGaN MODFETs prepared by MBE on SiC substrates, which exhibited a total power level of 6.3 W at 10 GHz from a 1-mm wide device. What is more astounding is that the power level is not really thermally limited as the power density extrapolated from a 0.1-mm device is 6.5 W. Equally impressive is the noise figure of 0.85 dB at 10 GHz with an associated gain of 11 dB. The drain breakdown voltages in these quarter micron gate devices are about 60 V, which are in part responsible for such a record performance.<sup>30</sup>

Applications of high power GaN based MODFETs include in amplifiers operative at high power levels, high temperatures and in unfriendly environments such as radar, missiles, satellites as well as in low-cost compact amplifiers for wireless base stations. Much of these applications are currently met by pseudomorphic modulation doped FETs.<sup>31</sup>

Nitride semiconductors have been deposited by vapor phase epitaxy (i.e., both hydride VPE<sup>32</sup> [HVPE] which has been developed for thick GaN layers and organometallic VPE<sup>33</sup> [OMVPE] which has been developed for heterostructures), and in a vacuum by a slew of variants of molecular beam epitaxy (MBE).<sup>16</sup> All the high performance light emitters, which require high quality InGaN, have been produced OMVPE. On the other hand, MBE has been very successful in producing structures, which do not require InGaN. Some examples are FETs and detectors. With its innate refined control of growth parameters, *in-situ* monitoring capability, and uniformity, MBE is well suited for depositing heterostructures and gaining insight to deposition/incorporation mechanisms. MBE's control

over growth parameters is such that any structure can be grown in any sequence. The structures based on conventional compound semiconductors such as IR lasers for CD players, surface emitting vertical cavity lasers, and high-performance pseudomorphic MODFETs have all been produced very successfully, most of them commercially, by MBE. Nitride growth, however, requires much higher temperatures than those used in producing conventional Group III-V semiconductors for which the MBE systems were designed. With design improvements, such as handling relatively high substrate temperatures, having sources to function without self destruction in nitrogen environment, particularly ammonia, and RF nitrogen sources which are nearly ion free and clean, MBE begun to make a statement in that the highest mobility bulk and two dimensional electron gas mobilities are in its domain when grown on MOCVD and HVPE buffer layers. Even without MOCVD buffer layers, bulk and two dimensional electron gas (2DEG) mobilities are competitive as described below.

The room-temperature electron mobility values in bulk GaN grown with HVPE to a thickness of 60- $\mu\text{m}$  was reported to be reported for GaN was  $950 \text{ cm}^2/\text{Vs}$ .<sup>34</sup> Whereas that reported for Metal Organic Chemical Vapor Deposition (MOCVD) grown layers were also have in excess of  $900 \text{ cm}^2/\text{Vs}$ ,<sup>35</sup> though the temperature dependence of mobility in this particular sample was rather unique. Early MBE layers exhibited mobilities as high as  $580 \text{ cm}^2/\text{Vs}$  on SiC substrates, which at that were not as commonly used as in more recent times.<sup>36</sup> Typically, however, the MBE-grown films produce much lower mobility values of  $100\text{--}300 \text{ cm}^2/\text{Vs}$ .<sup>37</sup> The lower mobilities have been attributed to both high dislocation densities<sup>37,38,39</sup> and elevated levels of point defects<sup>40,41</sup> in the GaN films.

Dislocations are an important scattering mechanism in films having dislocation densities above  $1 \times 10^8 \text{ cm}^{-2}$ .<sup>37, 38</sup> Depending on the particulars of the growth and substrate preparation, GaN films grown by MBE typically have dislocation densities in the range of  $5 \times 10^9\text{--}5 \times 10^{10} \text{ cm}^{-2}$ .<sup>37</sup> With refined procedures, however, dislocation densities in the  $8 \times 10^8\text{--}2 \times 10^9 \text{ cm}^{-2}$  can be obtained when grown directly on sapphire substrates with AlN or GaN buffer layers. Dislocation reduction is really the key to achieving high mobility GaN which goes to the heart of buffer layer and or early stages of growth. Based on the premise that the [002] X-ray diffraction is affected by screw dislocations and the [104] peak by edge dislocations and the fact that RF-nitrogen grown MBE layers produce excellent [002] peaks (in the 40-120 arcsec range) while the [104] peaks are wider and weaker (in the 180 to 300 arcseconds) one can conclude that the majority of the dislocations in MBE layers are propagating edge type.

The strength of MBE that is producing 2D growth does not bode well in dislocation reduction as the edge dislocations which propagate along the c-axis go right through the sample, though the detailed picture is somewhat dependent on the particulars of the growth such

as pitted or pit free growth which depends on the group V/III ratio. Some sort of 3D growth at the early stages of the growth, as in the case of growth from vapor, followed by a smoothing layer would help reduce dislocations. The other option is to use HVPE or MOCVD buffer layers for MBE growth. This approach led to record or near record bulk ( $1,150 \text{ cm}^2/\text{Vs}$  RT)<sup>42</sup> and 2DEG ( $53,500$  at  $4.2 \text{ K}$ ) mobilities<sup>43</sup> It is clear that the buffer layers grown by the vapor phase epitaxy method helps eliminate the main problem associated with MBE, that is the poor quality of the buffer layer. The other long-standing obstacle for MBE, difficulties associated with sapphire and SiC substrate preparation, has been eliminated. In the case of sapphire, a high temperature anneal in  $\text{O}_2$  environment produces atomically smooth and damage free surface.<sup>44</sup> In the case of SiC, some form of  $\text{H}_2$  etching at elevated temperatures removes the surface damage caused by polishing<sup>45</sup> as in the case of sapphire. Controlling the Ga/N ratio and substrate temperature causes the dislocation density across the homoepitaxial interface to remain constant.<sup>46,47</sup> While the above two works are related to RF MBE, ammonia MBE has also produced very high electron mobilities (as high as  $70,000 \text{ cm}^2/\text{Vs}$  at few K) when grown on bulk GaN wafer grown under high pressure and temperature conditions.<sup>48</sup>

## II. Structural Analysis

Transmission electron microscopy, defect revealing etches in conjunction with Atomic Force Microscopy (AFM), and X-Ray diffraction analyses were used to analyze HVPE layers on sapphire substrates from Lincoln Laboratory and HVPE templates that have been laser-separated from sapphire. Details of the results are discussed below in the order mentioned above.

### II.1. Structural Analysis by TEM

#### II.1. LINCOLN LABORATORY SAMPLES

Hydride VPE samples grown at Lincoln Laboratories with  $1.5 \text{ m}$ , two with  $5.5 \text{ m}$  and  $55 \text{ m}$  thick were investigated for defects, and polarity which was found to be Ga-polarity, as expected, by convergent beam electron diffraction combined with simulations. The density of misfit dislocations at this interface was estimated to be on the order of  $10^{13} \text{ cm}^{-2}$  based on high-resolution electron microscopy images. Conventional TEM studies show that threading dislocations are dominant from the interface to the top surface. Similar densities of all three types of these dislocations (edge, screw and mixed) were found. The highest density of threading dislocations (of the order of  $10^{10} \text{ cm}^{-2}$  was found close the interface. Threading dislocation density decreased gradually with distance from the interface. For the  $55 \mu\text{m}$  sample, this density is about  $10^8 \text{ cm}^{-2}$  at the surface.

HVPE layers were grown on sapphire coated with ZnO in a chloride-transport HVPE vertical reactor.<sup>49, 50</sup> Four different samples cut from three different wafers were investigated for this particular investigation.<sup>51</sup> Specifically, one  $1.5 \text{ m}$ , two  $5.5 \text{ m}$  and one  $55 \text{ m}$  GaN samples were examined. Cross-sectional and plan-

view TEM specimens were prepared from all these four samples. However, the plan-view specimen from 55 nm thick layers could not be used due to breakage caused by the relaxation of the large stress accumulated at the interface. The stress was determined to be 400 MPa at the interface compared to the sample surface as determined by the micro-Raman method, courtesy of Dr. J. Ager of Lawrence Berkeley National Laboratory. For all samples, the cross-sectional TEM specimens were prepared in [2-1-10] and [1-100] zone axis orientations.

TEM specimens were prepared by a standard method of mechanical pre-thinning followed by Ar-ion milling down to electron transparency. Plan-view samples were thinned from the substrate side such that the region near the top surface of each layer could be examined. In case of 55 nm thick layer in order to obtain electron transparent areas from all thickness regions of the layer it was ion milled successively in a few steps.

All studied samples are shown in Table I. Their nominal thicknesses and measured thicknesses determined experimentally from TEM images are also listed.

#### II.1.a. TEM results

A well-established method "Convergent Beam Electron Diffraction (CBED)" was used to determine the polarity of HVPE GaN layers. Since GaN is a non-centrosymmetric crystal the difference in the intensity distribution within (0002) and (000-2) diffraction discs can be attributed to Ga and N distribution within the unit cell. However, this intensity distribution change depends also on sample thickness. Therefore, a comparison of experimental CBED patterns with patterns simulated for the thickness indicated by the pattern in the central disc indicates that these layers grow with Ga polarity (see Fig. 1 where such comparison is shown for diffraction pattern obtained from LH2661 (-7,3)G layer).

The density of misfit dislocations at the layer-substrate interface was investigated by High Resolution Electron Microscopy (HREM). The HREM images were filtered in Fourier space to cause the interfacial dislocations to stand out. An example of a HREM image taken for the LH2661 (-7,3)G layer before and after such filtering is shown in Fig. 2. This exercise led to a misfit dislocation density at the layer/substrate interface of about  $2 \times 10^{13} \text{ cm}^{-2}$ .

Conventional TEM studies indicate that the dominant defects present to be the threading dislocations. Bright field TEM images, recorded under multi-beam conditions in order to image all dislocations with different Burgers vectors, were used to estimate the density of these dislocations with resultant figures to be of the order of about  $10^{10} \text{ cm}^{-2}$  near the layer/substrate interface. The density of threading dislocations gradually decreased away from the interface and for the 55 nm thick layer it reached a value of about  $10^8 \text{ cm}^{-2}$  at the surface. Cross-sectional TEM images used for threading dislocation density determination are shown in Figs. 3-6.

Plan-view samples were used to determine the density of threading dislocations at the surface (Figs. 7 and 8). The density of dislocations determined from plan-view samples was in very good agreement with those extrapolated from cross-sectional samples. The threading dislocation densities are plotted as a function of distance from the interface in Fig. 9. A gradual decrease of density of these dislocations with increase of the distance from the substrate shown on this plot indicates a gradual improvement of layer quality with thickness.

We investigated the relative numbers of different types of threading dislocations (edge, screw and mixed) and recorded two types of dark field images – with (0002) and (-2110)-type reflections. In the first type of images, only the screw and mixed dislocations are visible whereas on the second one, only the edge and mixed dislocations are observed. Examples of such pairs of dark field images obtained for 1.5  $\mu\text{m}$  and 5.5  $\mu\text{m}$  thick samples are shown in Figs. 10-12. The results led to the conclusion that no specific type of threading dislocation dominate and that all three types of threading dislocations (edge, screw and mixed) are present in HVPE GaN layers in comparable densities.

In addition to threading dislocations, a high density of small pyramidal defects was observed in a band near the middle of the 1.5  $\mu\text{m}$  layer (LH1089 (1,-3)G) (Fig.13). This band was about 0.3  $\mu\text{m}$  wide and it was best visible in the dark field mode under two-beam (0,g) conditions where g was a (-2110)-type reflection. The band had an undulated character suggesting that the beginning of growth was rather three-dimensional and that this band was formed at a specific growth time and was then overgrown with nearly defect-free material. These defects are similar to those observed in GaN doped with Mg, Si, In or O. In cross-section projections these defects are triangles, but in plan-view they have a hexagonal shape. We suggest that these 3-D growth patterns which are augmented by high growth rates are necessary to reduce the defect concentration in the overlaying layers.

#### II.1.b. Free-standing HVPE layers

A 200  $\mu\text{m}$  thick laser separated and free-standing HVPE grown GaN template grown at Samsung was also characterized for its structural properties by transmission electron microscopy (TEM). Convergent Beam Electron Diffraction (CBED) was employed to determine the polarity of the free surface and the side juxtaposed to substrate before separation confirming the epitaxial surface to be of Ga-polarity. The substrate side was confirmed to be N-face. The density of dislocations near the N-face was determined to be, in order,  $3 \pm 1 \times 10^7$  and  $4 \pm 1 \times 10^7$  by cross-sectional TEM and plan-view TEM, respectively. Identical observations on the Ga-face revealed the defect concentration to be less than  $1 \times 10^7 \text{ cm}^{-2}$  by plan-view TEM and  $5 \times 10^5 \text{ cm}^{-2}$  by cross-sectional TEM.

The sample studied52 was obtained from Samsung and was grown by HVPE on sapphire substrate to a

thickness of 300  $\mu\text{m}$  and separated from the sapphire by laser induced lift off.<sup>53</sup> The GaN layer was then mechanically polished and dry etched on the Ga-face to obtain a smooth nearly epi-ready surface, whereas the N-face was only mechanically polished. Three specimens were prepared for TEM studies: one cross-sectional and two plan-view (from both template sides) samples. The cross-sectional specimen was prepared in such a way that [1100] zone axis would be later accessible during TEM observation. In order to prepare this sample a strip of the template was glued between two "dummy" silicon strips. This structure was then thinned down to electron transparency by a standard method of mechanical pre-thinning followed by Ar-ion milling. When electron transparent areas appeared in the sub-surface regions on both GaN template sides the ion milling was terminated. A similar method of mechanical thinning and Ar-ion milling was applied to prepare both, plan-view specimens. All three samples were investigated using a TOPCON 002B microscope, operated at 200 kV acceleration voltage.

Conventional TEM techniques were used to analyze defects present in these sample. Bright field images, recorded under multi-beam conditions (in order to image dislocations with different Burgers vectors), were used to estimate the density of dislocations.

In order to determine the polarity on the two sides of the GaN template the well-established method of convergent beam electron diffraction (CBED) was applied. Since GaN is non-centro-symmetric, the difference in the intensity distribution within (0002) and (000 $\bar{2}$ ) diffraction discs in the CBED pattern can be attributed to Ga and N distributions within the unit cell. However, this intensity distribution depends on sample thickness. Therefore, correct use of this method requires one to compare the experimental CBED patterns with patterns simulated for the thickness indicated by the pattern in the central, (0000) disc. To apply this method for our studies, we recorded several (for different thicknesses) [1100] zone axis CBED patterns on each side of the cross-sectional specimen and then compared them with simulated patterns.

#### II.1.b. TEM results

TEM study of cross-sectional specimen revealed that the surface of the side, which was juxtaposed to the substrate was of relatively poor quality as expected from the application of mechanical polishing only and to a lesser extent representing interfacial region between the GaN epitaxial layer and the sapphire substrate (Fig.14a). The roughness of this surface was about 0.1  $\mu\text{m}$ . Moreover, the sub-surface layer of about 0.2-0.3  $\mu\text{m}$  was severely damaged containing many defects.

The analysis of Convergent Beam Electron Diffraction (CBED) patterns obtained on the side previously next to the substrate indicates that it is of [0001], N-polarity which means that a long bond along the c-axis is from N to Ga (Fig.14). The polarity determination by CBED is consistent with chemical etching experiments in which the N-face etched very

rapidly in hot phosphoric acid ( $\text{H}_3\text{PO}_4$ ). In addition, Schottky barriers fabricated on this surface exhibited a much reduced Schottky barrier height (0.75 eV vs. 1.27 eV on the Ga-face), only after some 30-40  $\mu\text{m}$  of the material was removed by mechanical polishing followed by chemical etching to remove the damage caused by the first mechanical polish.<sup>54</sup>

First investigation of a plan-view specimen prepared for the N-face side revealed the presence of a very damaged surface, covered by a nearly amorphous layer. It is most likely that the surface was damaged during mechanical polishing as observed in cross-section (Fig.15a). An additional very short ion milling was performed in order to remove this highly defective sub-surface layer. Only after such a procedure, was the sample adequate for studying the defect distribution within the layer. A bright field image of this sample is shown in Fig.15a. Some dislocations (indicated by arrows) threading across the layer into the surface are visible edge-on. The density of these dislocations determined from the plan-view sample was estimated to be about  $4 \pm 1 \times 10^7 \text{ cm}^{-2}$ . These threading dislocations were observed also in cross-section. Few of them are clearly visible in bright field images as shown in Fig. 16. The density of these dislocations determined from cross-section was found to be about  $3 \pm 1 \times 10^7 \text{ cm}^{-2}$ . This value is in good agreement, within experimental error, with the value obtained from the plan-view sample. For comparison, a density of about  $1 \times 10^7 \text{ cm}^{-2}$  was obtained by etching the N-face in  $\text{H}_3\text{PO}_4$  for 15 seconds at 160°C followed by counting the etch pits on several Atomic Force Microscopy (AFM) images, details of which are discussed in the section entitled "Structural analysis by etching". The agreement between these two very different techniques lends confidence concerning the densities reported here. Most of these threading dislocations are of mixed Burger's vector because they are visible in bright field images with g-vector parallel and perpendicular to the c-axis (Fig. 16). However, one needs to be careful with such a conclusion because of the very low statistics (very few dislocations observed within the electron transparent area).

The intensity distribution within the CBED pattern measured on this face of the template indicates that it is of [0001] orientation, which implies a Ga-polarity, and means a long bond along the c-axis is from Ga to N direction. This is in agreement with wet chemical etching experiments in that etching rate in hot  $\text{H}_3\text{PO}_4$  was negligible. Additional confirmation was obtained from Schottky barriers formed on this surface with barrier heights of about 1.27 eV, as opposed to about 0.75 eV on the etched N-face.

TEM studies of a plan-view specimen prepared for the Ga-face side revealed a nearly defect-free surface. Very few dislocations were found on this surface. Two such dislocations marked by arrows are shown in Fig. 15b. Based on the plan-view study, the density of these dislocations was estimated to be less than  $1 \times 10^7 \text{ cm}^{-2}$ ,

however due to the very low statistics there is a relatively large uncertainty for this estimation. In cross-sectional study we could not find any threading dislocation within the electron transparent area and based on this information we estimated that density of these dislocations is less than about  $0.5 \times 10^6 \text{ cm}^{-2}$ .

The very low defect concentrations on the Ga-face of the sample necessitate application of another method for a more accurate determination of the dislocation count. To this end, we employed several defect revealing etches, such as hot  $\text{H}_3\text{PO}_4$  acid. Several AFM images, after etching, with large area scans, up to  $50 \mu\text{m} \times 50 \mu\text{m}$ , indicated a dislocation count of about  $5 \times 10^5 \text{ cm}^{-2}$ . It is remarkable that the cross-sectional TEM and hot  $\text{H}_3\text{PO}_4$  acid methods are in such good agreement.

Threading dislocations (mainly of mixed Burger's vectors) were found below the N-terminated surface. Their density determined from both plan-view and cross-sectional studies was about  $3 \div 4 \times 10^7 \text{ cm}^{-2}$ , which compares well with the value of about  $1 \times 10^7 \text{ cm}^{-2}$  obtained from defect revealing etches. Only occasional dislocations were found in the plan-view sample on the Ga-terminated surface. The density of the threading dislocations below this surface, estimated from cross-sectional studies, was less than  $5 \times 10^6 \text{ cm}^{-2}$ . Defect revealing chemical etches indicated a density of about  $5 \times 10^5 \text{ cm}^{-2}$ , which is in remarkable agreement with the figure estimated from cross-sectional TEM data considering the small statistical base in TEM. The significantly lower density of dislocations on the G-face side with respect to that near the N-face was probably due to dislocation interaction within the layer.

All our results showed a very low density (of the order of  $10^7 \text{ cm}^{-2}$ ) of threading dislocations in the present sample compared to values measured in standard HVPE GaN layers<sup>55,56</sup> indicating a very high structural quality of the free-standing GaN template under investigation.

In conclusion, a free-standing wafer of HVPE GaN was studied by various TEM methods. The standard method, based on analysis of the CBED pattern, was applied to determine layer polarity. It was found that the original, flat surface of the layer is Ga-terminated, whereas the rough surface (due to mechanical polishing), which was originally next to the interface with the substrate is N-terminated. This is consistent with other HVPE GaN layers. Threading dislocations (mainly of mixed Burger's vectors) were found below the N-terminated surface. Their density determined from both plan-view and cross-sectional studies was about  $3 \div 4 \times 10^7 \text{ cm}^{-2}$ , which compares well with the value of about  $1 \times 10^7 \text{ cm}^{-2}$  obtained from defect revealing etches. Only occasional dislocations were found in the plan-view sample on the Ga-terminated surface. The density of the threading dislocations below this surface, estimated from cross-sectional studies, was less than  $5 \times 10^6 \text{ cm}^{-2}$ . Defect revealing chemical etches indicated a density of about  $5 \times 10^5 \text{ cm}^{-2}$ , which is in remarkable agreement with the figure estimated from cross-sectional TEM data

considering the small statistical base in TEM. The significantly lower density of dislocations on the G-face side with respect to that near the N-face was probably due to dislocation interaction within the layer.

## II.2. Structural analysis by etching

Wet chemical etching is a quick and inexpensive method for surface and near-surface defect investigation. Hot phosphoric acid ( $\text{H}_3\text{PO}_4$ ), mixed  $\text{H}_3\text{PO}_4/\text{H}_2\text{SO}_4$  solution and molten potassium hydroxide (KOH) have been shown to etch pits at defect sites on the c-plane of GaN.<sup>57,58,59,60,61,62</sup> Kozawa et al.<sup>57</sup> found etch pits tentatively ascribed to dislocations using molten KOH to etch metalorganic chemical vapor deposition (MOCVD) GaN samples. However, the etch pit density (EPD) was  $2 \times 10^7 \text{ cm}^{-2}$ , while the dislocation density found by tunneling electron microscopy (TEM) was  $2 \times 10^8 \text{ cm}^{-2}$ . Hong et al.<sup>58,59</sup> related the hexagonal-shaped etch pits formed by  $\text{H}_3\text{PO}_4$  etching on MOCVD GaN samples to nano-pipes (open-core screw dislocations). No etch pits were reported to have formed at both screw and edge dislocations. Shiojima et al.<sup>60</sup> investigated etch pits formed on MOCVD GaN samples by molten KOH etching. By atomic force microscopy (AFM) and TEM analyses, they attributed the origin of etch pits to mixed dislocations. Admittedly, the origin of etch pits is still controversial and the obtained EPD (in the range  $4 \times 10^5$ – $1 \times 10^8 \text{ cm}^{-2}$ ) is lower than the dislocation density ( $10^8$ – $10^{10} \text{ cm}^{-2}$ ) found by TEM. Along the lines of wet chemistry, Youtsey et al.<sup>63,64</sup> showed the utility of KOH based photoenhanced electrical chemical (PEC) etching for dislocation-density estimation in n-type GaN films. After etching, nanometer-scale "whiskers-like" features were obtained which were attributed to pure edge and mixed pure-screw dislocations through a cross-sectional TEM analysis. In this subsection, the analyses of both HVPE layers and GaN templates by wet chemistry in an effort to determine the defect concentration will be summarized.

### II.2.a. Lincoln Samples

Defects in GaN layers grown by HVPE at Lincoln Laboratory have been investigated by photo electrochemical (PEC) etching, and by wet etching in hot  $\text{H}_3\text{PO}_4$  acid and molten KOH. Threading vertical wires (i.e. whiskers) and hexagonal-shaped etch pits are formed on the etched sample surfaces by PEC and wet etching, respectively. Using atomic force microscopy, we find the density of "whisker-like" features to be  $2 \times 10^9 \text{ cm}^{-2}$ , the same value found for the etch pit density on samples etched with both  $\text{H}_3\text{PO}_4$  and molten KOH. This value is comparable to the dislocation density obtained in similar samples with TEM, and is also consistent with the results of Youtsey et al.

The samples investigated for this segment of study 65 consisted of intentionally Si-doped n-type ( $n \sim 2 \times 10^{18}$ ) GaN layers grown by hydride vapor phase epitaxy (HVPE) at Lincoln Laboratories on sapphire.<sup>66,67</sup> The thickness of the nitride films is about  $9 \mu\text{m}$ . A tapping-mode Digital AFM was used to investigate the as-grown and etched

surface morphology of GaN samples. AFM image of the as-grown GaN surface reveals few point defects (pits) positioned at surface step terminations (Fig.17). These pits have been reported previously to correspond to the surface termination of pure screw or mixed dislocations.<sup>68, 69</sup> Armed with these TEM based reports, AFM can be used to estimate defect density on atomically smooth surfaces with a high degree of ordering.

The PEC etching of GaN samples was carried out in a standard electrochemical cell at room temperature using an unstirred 0.02 molar KOH solution and a He-Cd laser (325 nm) as a source of the UV illumination. A 100nm-thick Ti mask was patterned, around the periphery of the sample with a standard lift-off process. The Ti contact served to assist photocurrent conduction. No additional bias was applied between the sample and the cathode during etching. Moderate illumination density (10-100 mW/cm<sup>2</sup>) was used to etch crystalline GaN material selectively, leaving threading vertical wires on the surface. At higher excitation densities, the PEC etching process left a smooth surface with no freestanding pillars. This is due to surface reaction being limited by reactants in the solution rather than holes. The abundance of holes on the surface leads to etching of GaN in the dislocation sites as well.

Fig. 18 illustrates an AFM image of the etched surface morphology produced by the PEC process after 60 minutes of etching. We have estimated the height of the "whisker-like" features to be about 700 nm and the lateral size of the order of 100 nm. The density is approximately  $2 \times 10^9 \text{ cm}^{-2}$  and according to the TEM analysis<sup>66</sup> this value is quite close to the effective density of dislocations and is consistent with the results of Youtsey et al.<sup>63,64</sup> obtained in a similar sample. In order to clarify further the relation between EPD and dislocation density in GaN and look for any consistency among the various chemical etches, we have used H<sub>3</sub>PO<sub>4</sub> and molten KOH as defect etchants in GaN, which produce hexagonal-shaped etch pits. By varying the time and temperature, we were able to optimize the etching process to produce a pitted surface that clearly reveals the size and density of the pits.

The AFM image of the GaN sample etched by molten KOH for 2 minutes at 210 °C is shown in Fig.19a. The etch pits, with density of about  $1 \times 10^9 \text{ cm}^{-2}$ , are of hexagonal shape and their size ranges from 40 to 100 nm in diameter and from 10 to 30 nm in depth. Most etch pits terminated surface steps, that is consistent with high concentration of pure screw or mixed screw-edge dislocations found in HVPE GaN samples by TEM study.<sup>66</sup>

Fig.19 b shows the surface morphology of the GaN sample etched in H<sub>3</sub>PO<sub>4</sub> for 6 minutes at 160 °C. The EPD is the same as that found for the KOH etched sample,  $1 \times 10^9 \text{ cm}^{-2}$ . The size of the etch pits ranges from 25 to 70 nm in diameter and from 8 to 20 nm in depth. By careful adjustment of the etching parameters, we obtain similarly pitted surface morphologies with the same value of EPD using both molten KOH and H<sub>3</sub>PO<sub>4</sub> etching. During the

etching process, a careful balance must be struck to ensure that every defect is etched to a point where it can be distinguished, but not over etched to the point where they begin to merge together. When the latter occurs, the density of defects is underestimated. To elucidate this further, we show in Fig. 20 a  $15 \times 15 \mu\text{m}^2$  AFM scan of a GaN surface etched for 10 min at 200 °C in H<sub>3</sub>PO<sub>4</sub>. Two different types of etch pits with different sizes are revealed on the etched surface. Larger pits have diameters more than 1  $\mu\text{m}$  and depth of ~450 nm (lower limit) whereas smaller pits are ~250 nm in diameter and around 70 nm (lower limit) in depth. Altogether we estimate the EPD to be  $1 \times 10^8 \text{ cm}^{-2}$ , an order of magnitude less than the correct value obtained earlier due to over-etching.

In summary, PEC and both H<sub>3</sub>PO<sub>4</sub> and molten KOH chemical etching were carried out on HVPE GaN samples to investigate the density of defects. Employing atomic force microscopy (AFM), we have found that the density ( $2 \times 10^9 \text{ cm}^{-2}$ ) of the "whisker-like" features on PEC etched samples is very close to the EPD (as high as  $1 \times 10^9 \text{ cm}^{-2}$ ) obtained on samples etched with both H<sub>3</sub>PO<sub>4</sub> and molten KOH. Future studies will include plane-view and cross-sectional TEM analysis on etched samples to relate in detail the etch pits to the nature of dislocations in the GaN material.

## II.2.b. Samsung free-standing GaN by HVPE

A free standing 300  $\mu\text{m}$  thick GaN template grown by hydride vapor phase epitaxy (HVPE), which has been reduced to 200  $\mu\text{m}$  by lapping and polishing, has been characterized for its structural and optical properties using X-ray diffraction, defect delineation etch followed by imaging with atomic force microscopy (AFM). The Ga-face and the N-face of the c-plane GaN exhibited a wide variation in terms of the defect density. The defect concentrations on Ga and N-faces were about  $5 \times 10^5 \text{ cm}^{-2}$  for the former and about  $1 \times 10^7 \text{ cm}^{-2}$  for the latter.

The samples were grown by hydride vapor phase epitaxy (HVPE) on sapphire substrates to a thickness of 300  $\mu\text{m}$ . In order to obtain a free standing GaN substrate, the thick GaN layer was separated from the sapphire by laser induced lift off.<sup>70</sup> The GaN wafers were then mechanically polished and dry etched on the Ga-face to obtain a smooth epi-ready surface, whereas the N-face was only mechanical-chemically polished. Both the Ga and N-faces were independently etched in hot H<sub>3</sub>PO<sub>4</sub> to reveal the defects as examined by AFM imaging.<sup>71</sup>

Before the defect revealing process, as received surfaces of GaN were examined by AFM imaging. The morphology of the Ga-face is shown in atomic force microscopy (AFM) image in Fig 21(a). Here, the scratches from the mechanical-chemical polishing are visible across the surface. The indicated scratch is 2 nm in depth and 150 nm wide. The root mean squared (rms) roughness of the surface is 0.44 nm. Figure 21(b) shows an AFM image of the as-grown N-face of the GaN substrate. Because the N-face was not dry etched, the rms roughness (6.1 nm) is much higher than that of the Ga-

face. Again, lines from the mechanical polishing are still visible on the surface, though to a lesser degree than on the Ga surface.

It has been reported that hot phosphoric acid ( $\text{H}_3\text{PO}_4$ ) etches defect sites on the surface of GaN, producing etch pits that reveal the location, and therefore density, of extended defects that form in GaN.<sup>57,58</sup> Two faces of the sample were etched in  $\text{H}_3\text{PO}_4$  at 160°C with this in mind until the defects on the surface were clearly revealed. The N-face was etched in  $\text{H}_3\text{PO}_4$  for 15 seconds at 160°C, and the etched surface is shown in the AFM image of Fig. 22. After the etching, the rough and disordered surface found in Fig. 21 has been smoothed (rms roughness = 1.9 nm), and the defect sites have been etched, revealing hexagonal pits. By counting the etch pits on several images, we ascertain that the density on the N-face is about  $1 \times 10^7 \text{ cm}^{-2}$ . The deep etch pits on the surface marked (a), (b), and (c) are 2.1  $\mu\text{m}$ , 1.2  $\mu\text{m}$ , and 1.5  $\mu\text{m}$  wide by 6 nm, 4.7 nm, and 8 nm deep, respectively. Also visible on the surface are terraces that have formed, many of which terminate at dislocation sites. The density figure is comparable to  $3 \pm 1 \times 10^7$ ,  $4 \pm 1 \times 10^7 \text{ cm}^{-2}$  obtained by cross-sectional and plan-view TEM analysis.

It is well known that  $\text{H}_3\text{PO}_4$  strongly attacks the N-face of GaN, and that the etch rate for the Ga-face is considerably lower. This creates a problem when etching the Ga-face in that it is possible to etch through the sample from the N-face while trying to form etch pits on the Ga-face. This is especially a problem when the sample is of high quality, as it will often take considerable time to etch defect sites on the Ga-side to a point where they are visible with AFM imaging. To solve this problem we used the surface tension of the acid to float the sample with the Ga-face down, minimizing the effects of the acid on the N-face. Note, however, that even this method has limits, as the vapor of the acid will slowly etch the N-face. The morphology of the Ga-face etched with this method for 50 min is depicted in Fig. 23. Still visible on the surface are the scratch lines that resulted from the mechanical polishing process, indicating that the non-defective c-plane GaN has not been significantly etched by hot  $\text{H}_3\text{PO}_4$  acid. The inset of the figure is a zoom into the region indicated by the white box, and shows that the black dot barely visible in the larger image is in fact a small hexagonal etch pit that has formed on the surface. We found three distinct sizes of etch pits. These pits, termed (for simplicity) small, medium, and large can be seen in Fig. 23. The small pit, visible in the inset, has a width of 215 nm and a depth of 10 nm. The medium etch pit can be seen in the upper left corner of the image and is 800 nm wide by 13 nm deep. The large etch pits are  $\sim 1.5 \mu\text{m}$  in width and  $\sim 300 \text{ nm}$  deep. The density compares with  $< 1 \times 10^7 \text{ cm}^{-2}$  by plan-view and  $5 \times 10^5 \text{ cm}^{-2}$  by cross-sectional TEM analyses. The total density of etch pits on the Ga-face is  $4.3 \times 10^5 \text{ cm}^{-2}$ , a value that is more than one order of magnitude lower than that found on the N-face.

### II.3. Structural evaluation by X-ray diffraction

High resolution X-ray rocking curves (omega scan) were measured by a Philips X'Pert MRD system equipped with four-crystal Ge monochromator in Lincoln layers and Samsung templates. The instrument resolution is verified to be better than 10 arcsec under this diffraction geometry where Cu  $\text{K}\alpha_1$  line of X-ray source is used. The [002] symmetric and [104] asymmetric peaks in 10  $\mu\text{m}$  thick HVPE films by Lincoln Labs had FWHM values between 5.8 and 7.9, and 3.9 and 5.2, respectively. The Samsung template investigated had wide diffraction peaks (20.6 and 24 arcmin for [002] and [104] diffractions, respectively) on the Ga-face when a 2 mm slit size was used. When the slit size was reduced to 0.02 mm, the Ga and N-face [002] peaks reduced to 69 and 160 arcseconds. This may indicate that the sample may have been bowed since the dislocation density is low and can not account for the observed broadening. Using the particular geometry of the X-ray diffraction system in terms of the area covered by the incident beam, a bowing radius of 1.2 m was calculated. In short, the [104] asymmetric peak half widths HVPE samples by Lincoln Labs are respectable, and both [002] and [104] peaks for the Samsung template are very good.

A total of 10 samples were obtained from Dr. Molnar and analyzed for their symmetric and asymmetric X-ray peaks. Samples VGaN ..... were heavily Si-doped whereas the Samples VGaN ..... were Zn doped for obtaining high resistivity. Samples VGaN ..... were unintentionally doped. The data obtained in all of the samples are tabulated in Table II.

A crystallographic analysis by high-resolution x-ray diffraction rocking curves (omega scans) with different slit widths of a Samsung template<sup>72</sup> is illustrated in Fig. 24. Both rocking curves from the Ga-face and N-face are presented in the plot, for (a) c-plane symmetric (0002) direction and (b) a-plane asymmetric (10-14) direction. A very narrow FWHM was measured on the Ga-face, down to 69 arcsec for (0002) reflection (at a slit width of 20  $\mu\text{m}$ ), and 103 arcsec for (10-14) (at a slit width of 100  $\mu\text{m}$  as the signal gets to be very small for smaller slit widths and much longer data collection times are required). The FWHM for the N-face is 160 arcsec for (0002) direction (at a slit width of 20  $\mu\text{m}$ ) and 140 arcsec for (10-14) direction (at a slit width of 100  $\mu\text{m}$ ). The superior quality of the Ga-face over that of the N-face agrees well with the large deviation of extended defect density as determined from our etching experiments. It is believed that lattice distortions from dislocations with screw component would contribute to the broadening of (0002) peak, and the lattice distortions from the edge dislocations contribute to the width of the asymmetric peak.<sup>73, 74</sup> Comparing with the reported x-ray data<sup>66, 75</sup> of HVPE GaN, the FWHMs of which are typically in the range of 5-7 arcmin for the (0002) peak and 10-12 arcmin for the (10-12) peak (less than 10 arcmin for the samples that we have obtained from Dr. Molnar), we suggest that the density of both type of dislocations are dramatically reduced in the free-standing GaN template.

With the increase of the slit width, not only the FWHM is increased, as shown in Fig. 24, but also a non-gaussian multi-peak feature emerges. The dependence of FWHM on the slit aperture is tabulated in Table III. Specifically, when the slit size is increased from 0.02 mm to 2 mm, the FWHM of the (0002) peak on the Ga-face increases from 69 arcsec to 20.6 arcmin; when the slit size is increased from 0.1 mm to 2 mm, the FWHM of the (10-14) peak increased from 103 arcsec to 24 arcmin.

This sort of broadening has been attributed to the tilt and twist,<sup>74</sup> which result in sub-millimeter scale mosaic spread and cause the observed dependence on the slit size. This seem at first plausible as our X-ray diffraction system uses a highly collimated Cu K $\alpha_1$  point source. However, the low defect concentration observed in TEM and etching experiments point to another source, which we believe to be bowing<sup>76</sup> even though GaN was removed from sapphire and a casual observed could indeed make the assumption that it is relaxed with no cause for bowing. Perhaps a more likely cause for bowing is the surface mechanical polish which affects both the Ga- and N-faces. By assuming the FWHM at beam width of 0.02 mm to be the intrinsic broadening of GaN, we can estimate the upper limit of the bowing to be with a bowing radius of 1.20 m or larger. It has been reported<sup>53</sup> that a bowing radius of about 0.8 m was found in the HVPE grown GaN thick films (~275 $\mu$ m) before separation from sapphire substrate, and a bowing radius of about 4 m after separation. As mentioned above, our sample underwent a mechanical polishing process, which could be the reason for the relatively large bowing.

### III. Impurities determined by Secondary Ion Mass Spectroscopy

Secondary-ion-mass-spectroscopy (SIMS) measurements demonstrate that it is difficult to reduce common impurities such as C, Si, and O, much below the  $10^{17}$ -cm<sup>-3</sup> level in thick GaN layers,  $10^{16}$ -cm<sup>-3</sup> in free-standing templates, and somewhat worse in thin epitaxial layers grown directly on lattice mismatched substrates. Specific impurities probed by SIMS as part of this investigation were nominally O, C, and Si. In the HVPE layer studied, both O and Si concentrations drop rapidly away from the surface into the sample- mainly due in part to the artifact of the technique and in part due to condensates on the surface of the sample, down to about  $10^{17}$  cm<sup>-3</sup> for Si and high  $10^{16}$  cm<sup>-3</sup> for O. The Ga-face profile in the Samsung template indicates levels below mid  $10^{16}$  cm<sup>-3</sup> for all three of the impurities. The picture is different for the N-side, however, as this side was juxtaposed to the substrate during growth and was mechanically polished after laser separation. The impurity concentration is some 1-3 orders of magnitude higher than the case for the Ga-face. Particularly the concentration of O and C is high, albeit some drop occurs as one goes deeper into the film. This should be re-examined in a sample where the N-surface is etched some.

Semiconductor materials have always grappled with intentional and unintentional impurities. These impurities

may be imported on the surface of the substrate with their genesis in the chemicals used and introduced during the deposition process. The latter may be due to the environment in which the deposition takes place and impurities present in the source material used. GaN is no exception and what exacerbates the situation is that there are many structural and point defects present. The lack of extremely high crystalline quality takes away the intrinsic resistance against incorporation of impurities. Among the chemical impurities are elements such as O, Si and C, and Si among the ones that have gotten a good deal of attention. The former two in GaN form shallow donors while the latter is a deep level with acceptor tendencies.

While oxygen and silicon have received a great deal of attention as the main source of unintentional impurities. The role of carbon is not well understood. This is despite the fact that there is a massive amount of carbon present in MOCVD. Computations predict carbon to be a deep acceptor -- but its behavior could be significantly affected by complexing with other impurities or defects. This could come to light when MOCVD buffer layers are employed and is relevant in cases when this method is used for the production of electronic devices. In addition to being substitutional and well behaved impurities, these species can also form complexes with native defects, complicating the analyses. Since the conductivity is of paramount importance for devices, it is imperative that impurity incorporation in GaN is examined.

Unwanted impurities impede efforts to attain high performance electronic device operation. Secondary-ion-mass-spectroscopy (SIMS) measurements demonstrate that it is difficult to reduce common impurities such as C, Si, and O, much below the  $10^{17}$ -cm<sup>-3</sup> level in thick GaN layers,  $10^{16}$ -cm<sup>-3</sup> in free-standing templates, and somewhat worse in thin epitaxial layers grown directly on lattice mismatched substrates. The picture is somewhat better in films grown by MBE on MOCVD and HVPE templates. The SIMS data can shed light on whether the measured donor and acceptor concentrations, by Hall, are due to impurities or native defects or both. An excellent example for why control of point defects and impurities is important is the GaN/AlGaIn structures which is used to form Modulation doped FETs. First of all, it is clear that in order to get high mobilities, the concentration of defects and impurities on the GaN side has to be reduced. Second, there is the issue of where the electrons in the 2DEG actually come from. The AlGaIn layer on top is "nominally undoped", but is likely to contain significant levels of donor like states, probably due to unintentional incorporation of oxygen and other native defects. Donors in this layer thus probably significantly contribute to the electron density in the 2DEG along with those from surface states. In a device with contacts, those electrons can also be supplied by ohmic contacts. Reproducible and reliable device fabrication will require strict control of impurity incorporation.

As mentioned above, chemical impurities can best be probed with Secondary Ion Mass Spectroscopy (SIMS).

The technique is refined and calibrated to the point where chemical impurity concentrations down to about  $10^{15} \text{ cm}^{-3}$  can be quantitatively determined. Since there are issues surrounding GaN being doped with residual oxygen in substitutional or interstitial sites next to a vacancy for example, SIMS method will be a really important player. In Fig. 25 and 26, we show the SIMS profiles in an HVPE layer on sapphire substrate and an free-standing GaN template. For the latter, profiles from both the Ga- and N-faces are shown. Specific impurities probed were nominally O, C, and Si. In the HVPE layer, both O and Si concentrations drop rapidly once away from the surface—mainly due in part to the artifact of the technique and in part due to condensates on the surface, down to about  $10^{17} \text{ cm}^{-3}$  for Si and high  $10^{16} \text{ cm}^{-3}$  for O. The Ga-face profile in the Samsung template indicates levels below mid  $10^{16} \text{ cm}^{-3}$  for all three of the impurities. The picture is different for the N-side, however, as this side was juxtaposed to the substrate during growth and was mechanically polished after laser separation. The impurity concentration is some 1-3 orders of magnitude higher than the case for the Ga-face. Particularly the concentration of O and C is high, albeit some drop occurs as one goes deeper into the film. This should be re-examined in a sample where the N-surface is etched some amount. Since, the same GaN template is under investigation, it can be concluded that impurity incorporation is dependent on the structural quality of the film.

#### IV. Transport Properties: Analysis of Hall data and mobility fitting

Detailed transport measurements were undertaken in both Lincoln (AFRL) and Samsung HVPE (AFRL and VCU) materials in an effort to gain insight to impurities and defect including their depth profiles, and scattering events. In GaN grown on foreign substrates such as sapphire, regardless of the growth method, there exist a about  $0.2 \mu\text{m}$  region at the interface that is highly doped and exhibits nearly temperature independent carrier transport. Such layer complicates efforts, which utilize temperature activated processes occurring in the film to extract useful information such as accurate electrically active impurity concentrations and donor activation energies in n-type samples. Extraction of the effect of this layer has been dealt with in a variety of ways including detailed Hall measurements at high magnetic fields, differential Hall measurements involving sequential etching and measurements, and modeling. By investigating the films properties as a function of the layer thickness ranging from about 1 to  $68 \mu\text{m}$ , all the other parameters were kept the same, we determined the critical parameters as they evolve from the sapphire-GaN interface and up. A strong dependence on distance from the interface was observed with the averaged mobility figures increasing from  $190 \text{ cm}^2 \text{ V}^{-1} \text{ s}^{-1}$  in the  $5 \mu\text{m}$  film to  $740 \text{ cm}^2 \text{ V}^{-1} \text{ s}^{-1}$  in the  $68 \mu\text{m}$  film. The preliminary differential Hall measurements indicate that the mobility at the surface of the thick layer is about  $1200 \text{ cm}^2 \text{ V}^{-1} \text{ s}^{-1}$ .

The Samsung free-standing GaN template made it possible for us to remove some  $30 \mu\text{m}$  of what would have been the interfacial layer, before laser separation, to make sure that the measurements are not affected by it. In addition, Raman measurements were made in the sample used for Hall measurement to accurately determine the vibration mode frequencies for an accurate determination of the high frequency dielectric constant from the low frequency dielectric constant. Electron mobilities in this material were  $1425 \text{ cm}^2/\text{Vs}$  at  $T=273 \text{ K}$  and  $7385 \text{ cm}^2/\text{V}\cdot\text{s}$  at  $48.2 \text{ K}$ . By using the most recent unscreened acoustic deformation potential and allowing only the acceptor concentration to vary, we obtained an excellent fit to the measured mobility in the temperature range of  $30 - 273 \text{ K}$  by using an iterative BTE method. In addition, an excellent fit for the temperature dependence of the electron concentration was also obtained utilizing the acceptor concentration determined from the fit to the Hall data ( $2.4 \times 10^{15} \text{ cm}^{-3}$ ), and the charge balance equation. This led to a donor concentration of  $1.6 \times 10^{16} \text{ cm}^{-3}$ , and an activation energy of  $26 \text{ meV}$ , the latter being the highest reported in the literature for GaN.

Both the Lincoln and Samsung layers, unintentionally doped, were characterized by variable temperature Hall measurements, in some cases in the form of differential Hall measurements, coupled with calculations of the temperature dependent mobility and SIMS measurements in an attempt to determine the acceptor and donor concentrations and likely causes for those impurities. A highly conductive layer at the original sapphire-GaN interface is commonly observed in HVPE layers,<sup>77</sup> perhaps even other forms of growth. This layer can be dealt with by either assuming a two-layer conduction in the model calculations or by removing the suspect region by etching. More accurate results can be obtain by extending the two-layer approach to successive Hall measurement at each step of certain amount of the layer removal, as will be discussed below. Since the Samsung template was a free-standing one, we chose to remove some  $30 \mu\text{m}$  material from the N-face, which represents the original epi-substrate interface. The additional benefit of such etching is that the damage caused during mechanical polishing can be removed.

In Hydride vapor phase epitaxial (HVPE) GaN grown on  $\text{Al}_2\text{O}_3$ , after a few microns of growth, excellent quality may be obtained; however, the interface region is known to be highly defected, and highly conductive, and will thus have a strong influence on the measured electrical properties.<sup>77</sup> This situation is schematically depicted in Fig. 27, which also illustrates the various donors and acceptors expected in the bulk region, above the interface. In the last three years, several schemes have been proposed to study the bulk electrical properties independently of the interface properties. The first model<sup>77</sup> treated the interface region as a well-defined temperature-independent degenerate gas. A two-layer Hall analysis can then be used to determine the electron concentration of the layer away from the interface, the results of which are illustrated in Fig. 28. Note that the raw data give a

completely misleading picture, while the corrected data are very reasonable even though underlying assumptions are not well tested. The corrected mobility in a ~68  $\mu\text{m}$  thick HVPE layer, i.e. the mobility for the portion of the layer excluding the interfacial region, in the form of temperature dependent data is shown in Fig. 29, where the uncorrected data are also shown. To gain a better insight, the electrochemical capacitance-voltage method was employed to study the interfacial region.<sup>78</sup> In this method the charge depth profile near the surface is successively performed while the epilayer is progressively etched away. When used in conjunction with SIMS analysis, it becomes evident that O, and not Si, is the dominant donor in the interfacial region as shown in Fig. 30. However, this technique suffers from the influence of persistent photoconductivity, and thus must itself be regarded in that light.

The magnetic-field dependencies of the conductivity and Hall coefficient can be used to deal with multi-layer conduction. However, very high magnetic fields ( $> 10$  T) are needed for an accurate determination of the mobility and carrier concentration.<sup>83</sup> Yet another method, "differential Hall measurement" can be used to tackle multi-layer conduction.<sup>79</sup> In this approach, as illustrated in Fig. 31, thin layers of thickness  $\delta d$ , are successively removed from the sample, by reactive ion etching (RIE), and Hall-effect measurements are then carried after each RIE step. Needless to say, an accurate knowledge of the removed material or remaining thickness of the layer after each step is needed. This was attained by making profilometer measurements through a small hole, ion-milled down to the  $\text{Al}_2\text{O}_3$  substrate. (Note that the  $\text{Al}_2\text{O}_3$  is not affected by the particular chemistry used in Reactive Ion Etching). One can then use the following expression:

$$\mu_{\delta d} = [\mu_d^2 n_d - \mu_{d-\delta d}^2 n_{d-\delta d}] / [\mu_d n_d - \mu_{d-\delta d} n_{d-\delta d}]$$

$$n_{\delta d} = [\mu_d n_d - \mu_{d-\delta d} n_{d-\delta d}]^2 / \delta d [\mu_d^2 n_d - \mu_{d-\delta d}^2 n_{d-\delta d}]$$

to determine the mobility  $\mu$  and carrier concentration  $n$  in each thin layer. Preliminary results for  $n$ , along with SIMS impurity profiles, are shown in Fig. 24. Note that simple Hall measurements would produce the "average  $n$ " curve, which is much too high because it is strongly influenced by the interfacial region. However, the "true  $n$ " curve, determined by differential Hall measurements follows the impurity profiles very well, and the magnitude of  $n$  is what would be expected with about 50% compensation of the O and Si donors. Efforts are underway to extend the electron concentration profiles into the interfacial region, along with attempts to obtain good mobility profiles.

For the case of the Samsung material, after removing some 30  $\mu\text{m}$  material from the back N-face, high electron mobilities both at room temperature ( $\mu = 1425 \text{ cm}^2/\text{Vs}$  at  $T=273 \text{ K}$ ) and below were measured ( $\mu = 7385 \text{ cm}^2/\text{Vs}$  at  $48.2 \text{ K}$ ). The temperature dependencies of both the Hall mobility and electron concentration pointed to the absence of such a second conducting layer after etching. Therefore, the analysis was based on a single layer model with a single donor level.<sup>72,80</sup>

The temperature dependence of the calculated electron mobility, by Boltzmann Transport Equation (BTE) based theory,<sup>81</sup> was fitted to the experiments in concert with the temperature dependence of the electron concentration and charge neutrality. For accuracy, Raman modes were measured and the recent unscreened acoustic deformation potential used. The latter was obtained from samples with very high low temperature 2DEG mobilities where the acoustic phonon scattering is prominent. Excellent fitting of the mobility in the Samsung template in the entire temperature range measured was obtained which resulted in ionized donor and total acceptor concentrations of  $1.48 \times 10^{16} \text{ cm}^{-3}$  and  $2.4 \times 10^{15} \text{ cm}^{-3}$ , respectively. As mentioned previously, we assumed singly ionized acceptor.

An accurate calculation of the mobility requires e.g., the numerical iterative solution of the Boltzmann transport equation (BTE).<sup>81</sup> For simplicity, one can use an alternative approach by considering the limiting effect of each scattering mechanism on mobility as if they are independent of each other. Assuming that scattering events are independent of each other, the total mobility can be approximated by the Matthiessen's rule in the form of  $1/\mu = \sum (1/\mu_i)$ . The mobility limited by ionized impurity scattering takes into account the screening by free carriers. The donor impurity concentration ( $N_D$ ) and the acceptor concentration ( $N_A$ ) are important fitting parameters.<sup>82,83</sup> Scattering by polar optical phonons is inelastic in nature so a quasi-analytical treatment has been derived<sup>84</sup> for reducing the complexity of calculations. The mobilities limited by acoustic-mode deformation potential scattering and by piezoelectric scattering can be expressed<sup>85</sup> with the acoustic deformation potential and piezoelectric constant in wurtzite GaN. All material parameters of GaN used for the calculations are tabulated in a book by Morkoç<sup>1</sup>, but with exact phonon frequencies measured for the sample under investigation and recently confirmed unscreened acoustic deformation potential.<sup>86</sup> All the pertinent parameters for GaN are tabulated in Table IV. The mobilities limited by polar optical phonon scattering, acoustic phonon scattering and piezoelectric effects are independent of impurity levels, so their temperature dependence is universal for GaN. The impurity scattering, on the other hand, is very sensitive to ionized impurity concentration, especially in the low temperature range. This is because acceptors are completely ionized, while scattering related to lattice vibrations are frozen out at low temperatures. The mobility limited by neutral impurities ( $N_D - N_A - n$ ) is also counted in the total mobility by using the Erginsoy's expression.<sup>87</sup> The details of this treatment for the Samsung material can be found in a paper by Yun et al.<sup>72</sup> Here we will report on the exact calculation by BTE with more refined and accurately measured Hall data.

In Table IV, the GaN parameters used are tabulated. Extreme care was taken for the accuracy of the experimental conditions such as the magnetic field, current and the sample temperature.<sup>80</sup> The measurements were performed in the same Hall sample, in the form of a van der Pauw pattern with Ti/Al based ohmic contacts,<sup>88</sup>

both at VCU and at the University of Michigan by Lee Adrienne Farina and Prof. C. Kurdak. The iterative BTE simulations were performed by Prof. D. L. Rode at Washington University. The Raman measurements for both the A and E phonons in  $Z(X,X)Z\text{-bar}$  and  $A(Z,X)Y$  backscattering scattering geometries were performed by Prof. K. T. Tsen at ASU. A good deal of helpful discussions was carried out with Dr. Wlodek Walukiewicz of Lawrence Berkeley Laboratory and Prof. W. Lambrecht of Case Western regarding the acoustic deformation potential in GaN. Though the data that we are about to present are based on the above collaborative effort, similar experiments particularly those based on elimination of the effect of the interfacial layer by high magnetic fields measurements were also undertaken at AFRL at Wright Patterson AFB by Drs. A. Saxler and D. Look in a different Samsung sample. The measurements in this particular case were performed with the N-face of the sample in the as received form and its highly conductive effect was taken into consideration in the analysis in form of a two-layer conduction mechanism. The results of this effort is similar to the VCU and collaborators' effort and thus will not be repeated here.

Using  $E_{ds} = 8.54$  eV without screening. If screening is included, a value of 12 is better but is not applicable here. This is a controversial in that the low temperature mobility of the 2DEG GaN/AlGaIn system is considered affected by screening. To fit the experimental and the calculated mobility, screened mobility is used which causes the deformation potential to go up to 12 eV. In our case, we have three-dimensional system with low electron concentration. Therefore, the deformation potential without screening which is about 8.54 eV has been used in our simulations as a fixed parameter. The phonon energies used were measured in this sample as  $A_1(LO) = 737.0 \text{ cm}^{-1}$ ;  $A_1(TO) = 532.5 \text{ cm}^{-1}$ ;  $E_1(LO) = 745.0 \text{ cm}^{-1}$ ;  $E_1(TO) = 558.5 \text{ cm}^{-1}$ . The high frequency dielectric constant was calculated using the Lyddane-Sachs-Teller relation expression  $\epsilon_0 = \epsilon_\infty (\omega_{LO} / \omega_{TO})^2$ . The Debye temperature was also calculated. The other parameters were kept the same as those reported previously. For completeness, the new parameter set is listed in Table IV.

Experimental and calculated, through Rode's iterative BTE method, mobilities as a function of temperature are shown in Fig. 32. The calculations are shown for three different values of the acceptor concentrations for elucidating sensitivity of the mobility to the acceptor concentration. The best fit is  $2.4 \times 10^{15} \text{ cm}^{-3}$  giving the best fit with an accuracy of  $0.5 \times 10^{15} \text{ cm}^{-3}$ . We should remark here that no fitting parameters were used and the excellent fit attest to the validity of the parameters of Table IV as well the accuracy of the measurements as well as the iterative BTE method itself. We can also argue that the unscreened acoustic deformation potential fits well for the bulk sample investigated.

The temperature dependent electron concentration was also fit with one donor model, using an acceptor concentration of  $2.4 \times 10^{15} \text{ cm}^{-3}$ , as shown in Fig. 33. The

quality of the fit over the entire temperature range indicates that the one donor model is quite satisfactory. It is important that the measurements are made at very low temperatures to obtain a good and reliable fit. Previous efforts were frustrated because of highly conductive interfacial layer, which is nearly temperature independent. Since the N-face was etched sufficiently to remove the conductive layer, the measurements represented the actual picture in the bulk.

The donor activation energy as well as the donor concentration can be determined from the fit using the expression, assuming a single donor:

$$\frac{N_D^+}{N_D} = 1 - \frac{1}{1 + \frac{1}{g_d} \exp\left(\frac{E_D - E_F}{kT}\right)}$$

where  $N_D$  and  $N_D^+$  represent the total and ionized donor densities. The degeneracy factor,  $g_d$  is two reflecting a single band in which electrons can have spin up and down. The acceptors in the n-type semiconductor under study are all ionized and negatively charged. The charge balance requires that the total positive charge which is just the ionized donor concentration be equal to the total negative charge which is the sum of the total acceptor concentration, since all are ionized, and the electron concentration. The charge neutrality must be satisfied at all temperatures. Consideration of the above led to a donor concentration of  $1.55 \times 10^{16} \text{ cm}^{-3}$  and a donor ionization (binding) energy of 25.5 meV. The value of the donor activation energy is the screened value. The donor binding energy determined from the above fitting corresponds to the screened binding energy which is related to the binding energy in a dilute semiconductor through  $E_D = E_D^0 - \alpha N_D^{1/3}$ . Here  $E_D^0$  is the binding energy in the dilute limit and  $\alpha$  is an empirical screening parameter, which is dependent on the semiconductor. Assuming the value<sup>1,80</sup> of  $\alpha$  to be  $\alpha = 2.1 \times 10^{-8} \text{ meV}\cdot\text{cm}$ , the unscreened donor binding energy for intrinsic GaN should be about 30.7 meV. The value of 25.5 meV is consistent with the above expression and represents the highest value for the measured donor binding energy in any GaN reported thus far.

## V. Point defects

Semiconductor GaN contains many structural and point defects to a large extent promoted by lattice and stacking mismatch substrates. Even though, GaN broke the long standing paradigm and made it to the market place with LEDs, the point defects have taken the center stages as they exacerbate efforts to increase efficiency of emitters, increase laser operation lifetime, and anomalies observed in electronic devices. Wide-bandgap semiconductors exhibit self-compensation, in which defects are formed to compensate the dopant effects. For example, when Si donor is added to GaN, the lattice may attempt to create Ga vacancies  $V_{Ga}$ , which are acceptors, in order to reduce the total energy. This is one way in which point defects, i.e., vacancies, interstitials, and/or

antisites, are formed. Another way is through defective or incomplete kinetic processes on the growing surface of an epitaxial layer. For example, insufficient N flux at the growing surface could result in N vacancies,  $V_N$ . Another driving force for the creation of point defects may be the polarization fields that are always present in nitrides. Even in the absence of strain (which leads to piezoelectric fields), spontaneous polarization is present, which can give rise to significant fields. Ultimately, these fields need to be screened in macroscopic samples, but one may wonder whether on microscopic length scales the fields could provide a driving force for defect creation. Point defects in GaN, which have been tentatively identified, include  $V_N$ ,  $V_{Ga}$ , and  $Ga_i$ . A wide range of analysis tools has been brought to bear to investigate the point defects and their impact on physical properties of GaN. Among the techniques employed are Photo Luminescence, Deep Level Transient Spectroscopy, minority carrier lifetime measurements, Positron Annihilation Electron Paramagnetic Resonance (EPR), and Optically Detected Magnetic Resonance (ODMR). The results obtained from the aforementioned methods as well as their analyses will be reported next.

#### V.a. PL dealing with band edge, but particularly the defect region of the spectrum

In the Samsung material, the  $\Gamma_5$  and  $\Gamma_6$  free excitons have been identified from emission measurements by utilizing polarization geometries where the E field is perpendicular to the c axis, favoring the  $\Gamma_5$  exciton and E field parallel to the c-axis favoring the  $\Gamma_6$  exciton. In the latter geometry the light is coupled from the side of the sample which is rendered possible due to free-standing thick sample. Focusing on the defect region of the PL spectrum, the N-face of the sample exhibited the usual yellow line. However, the Ga-face exhibited a broad band encompassing both yellow and green bands. Upon increased below gap radiation, the yellow band saturated while the green continued to grow. It is suggested that the green line is due to Ga vacancy, whereas the yellow band may be due to the same vacancy complexed with dislocations which are more abundant on the N-face than on the Ga-face.

For deeper transitions associated with defects, experiments with variable excitation intensity and excitation energy showed two bands with maxima at about 2.15 eV (yellow luminescence) and 2.43 eV (green luminescence). Unlike in RMBE, RF-MBE and MOCVD and other HVPE grown GaN samples, the yellow luminescence in the free-standing template is weak and can be easily saturated. In contrast, the green luminescence is dominant and is attributed to the isolated defect involving gallium vacancy, whereas the yellow luminescence is related to the same defect bound to dislocation or surface bound structural defect.

Optical measurements, such as photoluminescence, can be used to discern information regarding transitions

involving intrinsic processes such as free excitons, impurities such as impurity bound excitons and donor acceptor transitions, and defect related transitions. Free excitons appear in high quality material, and detailed excitonic structure can be used to discern information not only about the underlying physics, but also on the quality of the sample. As such PL is a very powerful technique for analyzing the position of defect states within the bandgap and to some extent their nature, particularly when combined with systematic and well controlled growth and other allied experiments.

Excitons in wurtzite GaN take on a special meaning in that the valence band is not degenerate due to the crystal field and spin-orbit interactions at the  $\Gamma$  point. The zone center conduction band is made up of the s states of Ga with  $\Gamma_7$  symmetry. The valence band is made up of the p states of N and is split into three doubly degenerate bands, caused by spin-orbit and crystal-field interactions. The three emerging valence band states are termed  $\Gamma_9^V$ , upper  $\Gamma_7^V$ , and lower  $\Gamma_7^V$ . The related free exciton transitions from the conduction band to these three valence bands are termed A, B and C excitons. In terms of symbols, they are:  $A \equiv \Gamma_7^C \rightarrow \Gamma_9^V$  (also referred to as the heavy hole state),  $B \equiv \Gamma_7^C \rightarrow \Gamma_7^V$  upper (also referred to as the light hole state), and  $C \equiv \Gamma_7^C \rightarrow \Gamma_7^V$  lower (also referred to as the crystal field split band). In an ideal wurtzitic crystal, excitons associated with all three bands are allowed in the  $\alpha$  polarization ( $E \perp c$  and  $k \parallel c$ ). In the  $\sigma$  polarization ( $E \perp c$  and  $k \perp c$ ), A and B excitons are observable with C exciton being very weak. In the  $\pi$  polarization, the ( $E \parallel c$  and  $k \perp c$ ), A and C excitons are observable with B exciton being weak. Carrier population is such that A exciton is predominant and has an interesting character.

The top valence band, A, has  $\Gamma_9$  symmetry while the two lower valence bands, B and C, have  $\Gamma_7$  symmetry. From group theory arguments and the direct product of the group representations of the band symmetries, the following intrinsic excitons are obtained:<sup>89</sup>

$$\Gamma_7 \times \Gamma_9 \rightarrow \Gamma_5 + \Gamma_6$$

The  $\Gamma_5$  and  $\Gamma_6$  excitons are both doubly degenerate; the  $\Gamma_5$  exciton is allowed, the  $\Gamma_6$  exciton is forbidden. The  $\Gamma_5$  exciton has antiparallel electron and hole spins, whereas the  $\Gamma_6$  exciton has parallel spins. In polarization experiments the  $\Gamma_5$  exciton is allowed for  $E \perp c$ , while the  $\Gamma_6$  exciton is forbidden in both modes of polarization. However, the  $\Gamma_6$  exciton quite often appears, possibly due to the finite momentum of the photon.<sup>90</sup> It may also

appear if strain is present, which relaxes the selection rules.<sup>91</sup> The  $\Gamma_6$  emission is preferentially polarized  $E||c$ .

Turning to the analysis of defects, the method takes advantage of the fact that most point defects emit light with specific photon energies after they capture nonequilibrium carriers. The intensity of PL from different defects depends on concentration of the particular defect and its capture cross-section. Thus, in n-type semiconductor nonequilibrium holes (which are minority carriers) are captured by acceptors with the rate proportional to the acceptor concentration and its hole cross-section. Since the capture rate is typically much faster than the recombination rate, PL intensity is proportional to the capture rate. The "lifetime" of PL may be found from transient PL measurements.

*Capture cross-section* can be estimated from the temperature dependence of the PL intensity since the quenching of PL with temperature, which is related to thermal escape of holes to the valence band (in n-type), depends on the holes capture cross-section and position of the defect energy level. *Concentration* of the defect may be estimated from the dependence of PL intensity on excitation rate. Indeed, PL intensity increases linearly with excitation rate until the product of the capture rate (which in turn is the product of excitation rate by the quantum efficiency of the PL via chosen defect) and the PL lifetime exceeds concentration of the defect. At a higher excitation rate PL intensity saturates.

The shape of the defect photoluminescence (PL) spectrum depends on the position of the defect energy level in the gap as well as on the strength of coupling with different phonon modes. Usually, the deeper the defect the stronger electron-phonon interaction. The strength of the coupling (which is characterized by the Huang-Rhys factor) and energies of the vibrational modes can be found from analysis of the PL band shape and its variation with temperature. Among vibrational modes, the lattice or defect modes may dominate. Practical issue is that interaction of the defect with phonons should not depend on the sample history. Therefore, the shape of the defect PL band including phonon replicas is the identification card of the defect. Besides, defects with the strong electron-phonon interaction are characterized by different equilibrium position in the lattice when they bind a carrier and loose it. As a result, position of the energy level of such defect relative to the conduction or the valence bands is different in different experiments (optical and thermal). The configuration coordinate diagrams for the defect can be constructed from the results of PL and PL excitation spectra data. These diagrams can explain many properties of defects including their metastable behavior.

Critical information can be obtained from PL behavior under application of hydrostatic or uniaxial pressure to the crystal. The shift of the PL band with the pressure depends on deformational constants, which are different for different defects. The pressure experiments are able to reveal the DX-type centers. Uniaxial pressure

PL is a powerful tool for study of anisotropic defects, which can reorient with application of external fields. Also useful in analyzing the optical signature of defects are methods which employ resonant excitation of defects by polarized light (polarization diagrams method).

Some of the PL bands arise from the donor-acceptor pairs (DAP) type transitions. Peculiarities of DAP type transitions (characteristic shifts of the DAP-type bands with excitation intensity and with temperature) help to identify the nature of defects and find energy positions of the defect levels without the Coulomb interaction which may change them dramatically. Another issue to be cognizant of is that a high concentration of defects (when semiconductor is intentionally doped) often leads to large potential fluctuations, which greatly affect the properties of the semiconductor under investigation. PL is also an efficient tool for revealing and describing these fluctuations.

#### **HVPE samples: Before and after PEC etching**

The PL spectrum of an as grown Lincoln HVPE sample is shown in Fig. 34. Superimposed on the figure is the spectrum after PEC etching which has implications to surface defects as will be discussed following the discussion of the as grown samples.

The as-grown sample has quite high internal quantum efficiency – about 4 %. Most of emission intensity resulted from the exciton-related transitions. The main peak at photon energy of 3.471 eV with the full width at half maximum (FWHM) of about 7 meV has been attributed to an exciton bound to a neutral shallow donor. Two next sharp peaks are LO phonon replicas of the main exciton peak. The shallow DAP band possibly contributes in the peak at about 3.285 eV and the peak at about 3.18 eV is its LO phonon replica. The spectrum contains also two broad bands related to deep acceptors: a blue band with the maximum at about 2.9 eV and a yellow band with the maximum at about 2.25 eV

We have studied the effect of photo-enhanced chemical (PEC) etching and hot wet etching on low-temperature photoluminescence (PL) of HVPE and other GaN layers which turned out to have implications in regard to surface defects.<sup>92,93</sup> The samples were Si-doped ( $n \sim 2 \times 10^{18} \text{ cm}^{-3}$ ) GaN layers grown by hydride vapor phase epitaxy (HVPE) on sapphire. The thickness of the GaN layer was about 10  $\mu\text{m}$ . The PEC etching of GaN samples was carried out in a standard electrochemical cell at room temperature using an unstirred 0.02 molar KOH solution and a He-Cd laser (325 nm) as a source of the UV illumination.<sup>65</sup> As a result of PEC etching, the whiskers were formed at dislocations.<sup>63</sup> The whiskers represented vertical wires with diameter of about 100 nm and about 1  $\mu\text{m}$  height, as was established by atomic force microscopy (AFM). The area around dislocations was etched to the same depth. An alternative etching utilized hot  $\text{H}_3\text{PO}_4$  or molten KOH. Typical temperature of wet etching was 160 °C and the etching time was varied from 2 to 10 minutes. AFM study showed that in these etching conditions only

etch pits are formed at dislocation sites and the etching of the main layer is negligible.

Figure 34 also serves to compare the PL spectrum before and after PEC etching. After PEC etching, the integrated intensity increased two times. Nearly the same increase can be observed for the exciton peaks, yellow and blue bands, however an increase of the shallow DAP emission is much larger – about ten times. These results evidence that concentration of nonradiative defects decreased and concentration of shallow acceptors increased. The first conclusion follows from increase of radiative recombination and in particular exciton emission after PEC etching. The second conclusion can be supported by consideration of the balance of carriers in n-type GaN. The low-temperature PL via considered defects might involve DAP-type transitions (from a shallow donor to an acceptor) or eA-type transitions (from the conduction band to an acceptor). In both cases, the rate of radiative recombination is determined by the rate of hole-capture by the acceptors since the radiative lifetime is much longer than the hole-capture time. We assume that the nonradiative defects present mostly at the surface and etching changes the surface condition reducing the nonradiative defect concentration. Possibly the shallow acceptor is a native defect (such as gallium vacancy or its complex with a shallow donor) which can be bound to dislocation. In this case the reducing of dislocation-free volume by PEC etching results in relative increase of the PL related to defects bound to dislocations. The above assumptions are supported by the results of hot wet etching, see Fig. 35.

The Samsung material was investigated by AFRL, NRL and VCU teams. In what follows, the details of the PL observations in relation the band edge emission are discussed. First, the PL focusing in on the A exciton by D. C. Reynolds et al.<sup>94</sup> will be discussed followed by additional measurements dealing with both the Ga and N-face, the latter before and after etching. Moreover, the defect region, namely the yellow-green, of the PL spectrum is discussed with important implications about the genesis of these transitions.

For propagation vector  $k||c$ , the  $E$  vector is normal to the  $c$  axis ( $E \perp c$ ) and the resultant emission is shown in shown in Fig. 36 as the solid line. The dashed line shows the reflection spectra. The emission peak at 3.4809 eV is the free exciton associated with the A valence band, while the peak at 3.4748 eV is the  $D^0, X$  peak. Two reflection minima are observed. The lowest energy minimum is associated with the A valence band and correlates with the free exciton emission peak. The higher energy minimum is associated with the B valence band.

When the crystal is rotated 90°, such that  $k \perp c$ , the  $E$  vector can now take the form  $E \perp c$  or  $E || c$ . The emission for the  $E \perp c$  polarization is shown as the solid line in Fig. 37 where the  $\Gamma_5$  emission is observed along with a weak  $\Gamma_6$  emission. For  $E || c$  polarization, the dashed line is

obtained in Fig. 37. The dominant emission is now the  $\Gamma_6$  exciton (3.4785 eV). Since, the  $\Gamma_5$  (3.4814 eV) and  $D^0, X$  emissions are polarized with  $E \perp c$ , their intensity is greatly reduced.

The emission peak at 3.4857 eV for the  $E || c$  polarization, not observed for the  $E \perp c$  polarization, is most likely the longitudinal exciton previously reported by Hopfield and Thomas<sup>95</sup> in CdS. They report that the longitudinal exciton is coupled to the  $\Gamma_5$  exciton (transverse) due to a slight misalignment, which causes a small component of the  $E$  vector to be resolved in the  $E \perp c$  direction. They also reported that as the crystal is rotated, the longitudinal emission line should converge onto the transverse ( $\Gamma_5$ ) emission line. This was not observed, due to the rapid broadening of the longitudinal line as the crystal is rotated. Such a broadening is observed in Fig. 4 (dashed line), even though the rotation was only slight. The solid curve shows the emission when the polarizer is oriented  $E \perp c$ , while the dashed curve shows the emission when the crystal is slightly rotated about the "c" axis. The broadening of the longitudinal line at 3.4853 eV is clearly observed.

Turning our attention to PL on both faces of the Samsung material, the PL from the Ga-face after mechanical-chemical polishing and followed by chemical etch was taken. The Ga-face PL was similar before and after the chemical etch and demonstrated very sharp lines in the excitonic region. The peaks observed at 3.4710 eV and 3.4778 eV are attributed to exciton bound to a neutral shallow donor (BDE) and free exciton (FE), respectively. The FWHM of these peaks at 10 K are 1.1 and about 2.5 meV, respectively. A small peak between BDE and FE peaks (at 3.4748 eV) is not identified. Instead of the typical exciton bound to a shallow acceptor peak occurring at 3.465-3.466 eV,<sup>96</sup> we have observed a set of sharp peaks in the range 3.440 – 3.455 eV with the largest peak being at 3.4465 eV. We attribute this peak to exciton bound to some deep acceptor (BAE). In the range 3.0 – 3.4 eV one can find peaks related to exciton transitions involving one to three LO phonons, as well as weak peaks due to shallow donor-acceptor transitions (the main peak at 3.257 eV is followed by few LO phonon replicas). Instead the commonly observed yellow luminescence centered at about 2.2-2.3 eV in our MOCVD and MBE grown samples, a broad green band with the maximum at 2.44 eV and FWHM about 370 meV was observed from the Ga-face.

Low-temperature PL from the N-face, which was originally only mechanical-chemically polished and cleaned, essentially revealed broadened exciton peak with the maximum at about 3.47 eV and FWHM about 20 meV. Contrary to the Ga-face, a yellow luminescence band centered at about 2.3 eV has been observed. After a chemical etch, the PL spectrum from the N-face became nearly identical to that of the original Ga-face. The

FWHM of the main exciton peak at 3.471 eV decreased down to about 1.0 meV. The transformation of the spectrum is most likely due to the removal of the surface damage. More detailed investigations as to the identity of several shallow peaks which have not heretofore been reported in the literature are underway.

#### Vb. PL dealing with the defect region of the spectrum

Photoluminescence is a powerful tool to investigate deeper extrinsic transitions as well. By detailed experiments, and particularly in conjunction with observation in regard to other supporting experiments, a good deal of knowledge about the nature of these transitions can be garnered. One such transition in GaN is the omnipresent 2.2-2.3 eV yellow band which has been with GaN from nearly its inception and the present Samsung GaN templates are no exception except that the yellow PL on the Ga-face was saturable and gave way to green PL. Both steady-state<sup>97</sup> and transient<sup>98</sup> luminescent properties of these deep bands on Ga and N-faces have been investigated.

Although the yellow (YL) emission in GaN was attributed to deep donor-to-shallow acceptor transitions,<sup>99</sup> most investigators are now in agreement that YL is due to transitions from the conduction band or a shallow donor to a deep acceptor.<sup>100-101-102-103</sup> The issue of whether the YL is related to a point defect or to a distribution of states in the gap is still an open question. Using photoluminescence (PL) and the surface photovoltage spectroscopy (SPS), Shalish et al.<sup>104</sup> suggested that a broad distribution of the acceptor-like surface states is responsible for the YL band.<sup>104</sup> The red shift of the YL band with decreasing - energy of the below-gap excitation may also indicate that the broadening of the YL band is due to emission from several closely spaced traps.<sup>105</sup> On the other hand, the temperature-related behavior and the PL excitation spectrum has been quantitatively explained in the configuration-coordinate model, that attributes the broad band to a point defect with strong electron-phonon interaction.<sup>100-106</sup> On the structural side, the YL band is commonly attributed to gallium vacancies ( $V_{Ga}$ ).<sup>100-101-102-103</sup> Theory predicts a low formation energy and deep levels for the isolated  $V_{Ga}$  and its complexes with shallow donors such as  $V_{Ga}Si_{Ga}$  and  $V_{Ga}O_N$ .<sup>102-103</sup> It has also been demonstrated that the formation of these defects is much more favorable at the threading-edge dislocations.<sup>107</sup>

We now discuss our investigation of the YL band in the high-purity freestanding template grown by hydride vapor phase epitaxy (HVPE) method. The position of the so called YL band changes from 2.15 eV (yellow emission) to 2.43 eV (green emission) depending on experimental conditions. We account for our results on the basis that two point defects are present in the form of an isolated defect involving  $V_{Ga}$  and the same defect bound to a structural defect.

As discussed under structural investigations, the defect delineation etching demonstrated very low density

of dislocations in this sample:  $5 \times 10^5 \text{ cm}^{-2}$  and  $1 \times 10^7 \text{ cm}^{-2}$  on the Ga- and N-face, respectively.<sup>108</sup> From the fitting of the Hall effect data in the temperature range 50-300 K, we have estimated that the total concentration of acceptors in this sample is  $2.4 \times 10^{15} \text{ cm}^{-3}$ , whereas the concentration of the shallow donor is  $1.55 \times 10^{16} \text{ cm}^{-3}$ .<sup>72,80</sup> The PL for this study was excited either with a continuous-wave above-gap He-Cd laser (3.81 eV) or a below-gap second harmonic of the Ti/sapphire "Tsunami" pulse laser (in the range 3.1-3.4 eV). The excitation density was varied from  $10^{-4}$  to  $100 \text{ W/cm}^2$ . A closed cycle cryostat was used for measurements from room temperature down to 10 K.

Low temperature PL spectra from both sides of the sample are shown in Fig. 38. The spectrum from the Ga-face demonstrates sharp peaks in the photon range of 3.28 - 3.5 eV, that are related to excitonic transitions. The full width at half maximum (FWHM) of the highest peak at 3.471 eV, attributed to exciton bound to neutral shallow donor, is 1.0 meV. The excitonic spectrum from the as received N-face is nearly featureless with the FWHM of the main peak being about 20 meV. After etching the N-face in hot  $H_3PO_4$  for very short time to remove the mechanical polish induced damage, the spectrum approached to that from the Ga-face. Therefore, the broadening of the spectrum from N-face before etching is due to the surface damage caused by mechanical polishing.<sup>108</sup>

The unique feature of the PL scans is that the broad defect-related band dominating at photon energies 1.5-2.8 eV has a different shape and position when different faces of the sample are illuminated. The Ga-face emission is green (maximum at about 2.4 eV), whereas the N-face emission is yellow (maximum at about 2.2 eV) for an excitation density,  $P_{exc}$ , is about  $0.1 \text{ W/cm}^2$  covering a large area with unfocused laser beam. At a first glance it would appear that the yellow luminescence (YL) is related to the structural defects near the surface while the green luminescence (GL) is related to defects in the bulk of the material. To shed light on the matter, we have studied the effect of excitation intensity on the position of the defect-related PL band. It is well established that both at low and room temperature, the band blue-shifts with increasing excitation intensity, which is likely to be a donor acceptor transition. Similarly, the PL band maximum shifts from about 2.2 to 2.3 eV for the N-face and from about 2.3 to 2.43 eV for the Ga-face when the excitation density is increased from  $10^{-3}$  to  $100 \text{ W/cm}^2$  (Fig. 39)

A large shift of the PL band with excitation intensity is typical for deep donor-acceptor pairs or in a semiconductor with large potential fluctuations.<sup>109</sup> However this rationale can be excluded for the studied sample because the total concentration of acceptors is about  $2.4 \times 10^{15} \text{ cm}^{-3}$ <sup>80</sup> and the possible concentration of deep donors is about  $1.55 \times 10^{16} \text{ cm}^{-3}$ .<sup>110</sup> Such low concentration of deep defects cannot result in an intense PL caused by transitions from a deep donor to a deep acceptor due to the extremely small overlap of the corresponding wave-functions.<sup>111</sup> Moreover, our

tentative measurements of transient PL demonstrated that at room temperature the PL decay is exponential which suggests that the transitions from the conduction band to a deep acceptor are involved.<sup>112</sup> Potential fluctuations can also be neglected due to the low compensation in the studied sample.<sup>80</sup> Instead we suggest that the shift of the band with excitation intensity is related to a competition between two deep acceptors. At a low excitation density, the YL-related defect dominates, while at a high excitation density the yellow PL saturates giving the way to the GL. To verify this conclusion further, we performed resonant (below-band-gap) excitation at room temperature as discussed below.

Figure 40 shows the PL spectrum in the defect-related region for various excitation energies. The broad band gradually shifts with increasing excitation energy from about 2.2 eV (yellow emission) to 2.43 eV (green emission). In Fig. 41, we have plotted the variation of the position of the band maximum and the band FWHM as a function of the excitation energy,  $\hbar\omega_{exc}$ . In the same figure, the variation of the transparency of the sample is also shown. The variation of the shape and position of the band strongly correlates with the transparency curve. At  $\hbar\omega_{exc} < 3.26$  eV, where the absorption coefficient is of the order of 10, the position of band maximum saturates at about 2.2 eV and the band FWHM is about 590 meV. At  $\hbar\omega_{exc} < 3.35$  eV, where the absorption coefficient is more than  $\sim 10^3$ , the position of band maximum saturates at about 2.43 eV and the band FWHM is about 500 meV.

Our observations may be explained by assuming that the YL-related defect has relatively high concentration in the first 1  $\mu$ m from the surface, whereas the GL-related defect is distributed uniformly throughout the bulk. To explain the predominance of the YL at excitation photon energies below 3.3 eV, we suggest that the optical cross-section for the YL-related defect is much larger than that for the GL-related defect. In this case, the photons with  $\hbar\omega_{exc} < 3.3$  eV excite resonantly only the YL-related defects. It is possible that in the excitation photon range  $\hbar\omega_{exc} = 3.3 - 3.43$  eV, a two-step excitation takes place: first the photons excite resonantly the shallow acceptors and after their thermal ionization the holes are captured by the deep defects. In this case, not optical but non-radiative cross-section of deep defect dictates the defect-related emission and the GL may dominate due to its larger concentration and/or larger non-radiative capture cross-section. In the intermediate region ( $\hbar\omega_{exc} = 3.25 - 3.35$  eV), both mechanisms, resonant and non-radiative excitations, compete.

In short, we conclude that two deep defects contribute to the broad yellow-green band, namely the 2.15 eV (YL) and 2.43 (GL) bands. The defect causing the YL line prevails at the N-surface of the sample, and can be easily saturated by nonequilibrium holes due to very low concentration of this defect. The defect causing the GL line is uniformly distributed in the bulk GaN. We attribute

the GL and YL to isolated native defects ( $V_{Ga}$  or  $V_{Ga}$ -donor complex) and to the same defect bound to structural imperfection, respectively.

### V.c. Deep Level Transient Spectroscopy of n-type GaN

Deep centers in n-GaN have been characterized by DLTS in HVPE-grown GaN of different thickness and dislocation densities, and Samsung templates. A collation of all the deep centers and their known characteristics are shown in Table V in the text. Centers  $A_1$  and  $E_1$  found in as-grown and thin HVPE-GaN are very similar to the centers  $A_2$  and  $E$  induced by electron-irradiation, indicating their point-defect nature. The main deep centers in n-GaN, such as  $A_1$ ,  $B$ , and  $D$ , show higher concentrations in thinner samples, which suggests a connection with the high dislocation densities. Based on the anti-correlation between  $A_1$  and  $B$ , which can be observed in thin HVPE-GaN layers, the defect  $B$  is tentatively assigned to  $N_{Ga}$ . Centers  $A$ ,  $C$ , and  $D$  are not affected by 1-MeV electron-irradiation, thus ruling out the possibility of these centers being identical to any EI-induced centers; however, their nature remains unknown. 1-MeV electron irradiation creates  $V_N$ -related centers with thermal activation energies of 0.06 eV, and a center with  $E_T=0.85$  eV, which might be related to  $N_i$ . To shed light on the spatial distribution of defects away from the interface, HVPE-grown n-GaN layers with different thicknesses have been characterized by DLTS and TEM. The TEM results were discussed under the "TEM" section already. As the layer thickness decreases, an increase of deep centers, both in species and concentrations, was clearly observed, which is believed to be closely associated with the significant increase of threading dislocations in the regions near the GaN/sapphire interface. Based on a comparison with EI-induced centers and an observation of anti-correlation,  $A_1$  is tentatively assigned to  $N_i$ , and  $B$  to  $N_{Ga}$ . The Samsung template exhibited a new trap  $B'$ , with parameters  $E_T=0.53$  eV and  $\sigma_T=1.5 \times 10^{-15}$  cm<sup>2</sup> on the Ga-face, in addition to the four traps commonly observed in various epitaxial GaN layers. For the N-face sample, a N-vacancy related trap  $E_1$ , with  $E_T=0.18$  eV and  $\sigma_T=4 \times 10^{-17}$  cm<sup>2</sup>, was observed. On the other hand, the Ga-face sample contained trap  $C$ , with  $E_T=0.35$  eV and  $\sigma_T=1.6 \times 10^{-15}$  cm<sup>2</sup>. This trap may be related to surface damage caused by the RIE process employed. A new sample for which the damaged region is removed is under investigation. A Side benefit of the DLTS investigations is that the barrier heights of Ni/Au Schottky contacts were determined to be 1.27 eV and 0.75 eV for the Ga face and N face, respectively.

Deep Level Transient Spectroscopy (DLTS) is a powerful technique to determine the presence, concentration and capture-cross section of deep level if electrons or holes can be thermally excited out of the traps in conjunction with band bending caused by the reverse bias applied. In the case of much deeper defects, optically augmented DLTS and or conductance vs. the wavelength of the below the gap excitation source can be used to discern similar information, albeit the activation energies

in this case will be optical ones and are different from the thermally activated energies. The shortcoming of DLTS is that it is capable of giving local information about the defect centers. These can be assuaged to some extent if DLTS is accompanied with systematic studies, such as irradiation damage and measurements under pressure.

In DLTS, a p-n junction or a Schottky barrier structure is biased into depletion which causes the defects above the Fermi level (for n-type samples) to release their electrons. A charging pulse, which reduces the reverse bias across the junction, is applied to fill some of the previously emptied traps increasing the junction capacitance. Upon the removal of the charging pulse, the electrons trapped at the deep level(s) would be freed at a rate, which depends on the energy level of the trap. This is also related to the rate at which the capacitance would return to its equilibrium value. In DLTS, the change in capacitance in an appropriate time window is plotted as a function of sample temperature from which the activation energy of the trap is determined. Alternatively, the time rate of change in the capacitance as the traps empty can be plotted versus time from which pertinent information about the nature of the centers can be deduced. This technique is called the Isothermal Capacitance Transient Spectroscopy (ICTS), which has also been employed for analyzing nitrides.<sup>113</sup>

The HVPE GaN layers used in the DLTS study were grown on ZnO-pretreated sapphire in a chloride-transport HVPE vertical reactor at thicknesses of 5, 11, 15, 39, and 68  $\mu\text{m}$ . Details of the GaN growth and the sapphire pretreatment techniques are described elsewhere.<sup>114</sup> Ni/Au Schottky contacts with a diameter of 250  $\mu\text{m}$ , surrounded by large-area Ti/Al/Ti/Au ohmic contacts, were fabricated at Virginia Commonwealth University. A Bio-Rad DL4600 system with a 100-mV test signal at 1 MHz was used to take C-V and DLTS data at Wright State University. To determine the activation energy  $E_T$  of the deep centers, the DLTS spectra were taken at different rate windows, from 0.8 to 200  $\text{s}^{-1}$ , and were analyzed by the standard Arrhenius technique. For TEM studies, undertaken at Lawrence Berkeley National Laboratory, two samples with nominal thicknesses of 5  $\mu\text{m}$  and 68  $\mu\text{m}$  were selected, and cross-sectional specimens were prepared.

Carrier concentrations in the top regions of the five samples, determined by C-V measurements, were found to be in the  $10^{17}\text{-cm}^{-3}$  range; these results are similar to those found by Hall-effect measurements, corrected for the degenerate interface layer.<sup>77</sup> As the sample thickness decreased from 68 to 5  $\mu\text{m}$ , the apparent (average) mobility dropped from 740 to 190  $\text{cm}^2/\text{V s}$ . For the three thickest samples (68-13  $\mu\text{m}$ ), the apparent carrier concentrations were found to increase from  $1.3 \times 10^{17}\text{ cm}^{-3}$  to  $2.6 \times 10^{17}\text{ cm}^{-3}$ . As for the Schottky barriers, the reverse leakage current is significantly reduced, by almost three orders of magnitude, as the layer thickness is increased from 5 to 68  $\mu\text{m}$ . The soft breakdown and increased leakage current in thin films is most likely caused by

carrier tunneling or hopping through defect states associated with threading dislocations. The ideality factor also was indicative of the enhanced quality of the films in that it approached unity for the thickest layer.

Typical DLTS spectra for all five samples are presented in Fig. 42. Note that the spectra in the figure have different base lines, separated by  $0.5 \times 10^{14}\text{ cm}^{-3}$ . Salient features are that: i) the dominant centers are  $A_x$  ( $E_T=0.72\text{ eV}$ ), A ( $E_T=0.67\text{ eV}$ ), and B ( $E_T=0.61\text{ eV}$ ), with concentrations in the  $10^{13}\text{-}10^{14}\text{ cm}^{-3}$  range for the two thickest samples (see curves a and b); ii) for the 15- $\mu\text{m}$  sample (see curve c), a center with  $E_T=0.20\text{ eV}$  (labeled as D) appears at low temperatures; iii) for the 11- $\mu\text{m}$  sample (see curve d), in addition to a center with  $E_T=0.17\text{ eV}$  (also labeled as D) at low temperatures, the center  $A_1$  ( $E_T=0.89\text{ eV}$ ), with a higher concentration in the  $10^{14}\text{-}10^{15}\text{ cm}^{-3}$  range, arises; and iv) for the 5- $\mu\text{m}$  sample (see curve e), B becomes a prominent center and  $A_1$  drops significantly, as compared to its value in the 11- $\mu\text{m}$  sample, and the other observed centers are A, C ( $E_T=0.41\text{ eV}$ ), and D ( $E_T=0.23\text{ eV}$ ). Thus, we can state that as the HVPE-GaN samples become thinner, both the species and concentrations of the deep centers increase. Interestingly, most of deep centers found in HVPE-GaN have been also observed by us in n-GaN grown by other techniques, such as metalorganic chemical-vapor deposition (MOCVD) and reactive molecular beam epitaxy (RMBE). Depending on the material parameters such as the layer thickness, electron mobility and dislocation density, the concentrations of these deep centers can be as low as  $10^{13}\text{-}10^{14}\text{ cm}^{-3}$  for a 4.5- $\mu\text{m}$ -thick MOCVD-GaN, with an electron mobility of 765  $\text{cm}^2/\text{V s}$  and an estimated dislocation density of low- $10^8\text{ cm}^{-2}$ . They can be as high as  $10^{15}\text{-}10^{16}\text{ cm}^{-3}$  for 0.5- $\mu\text{m}$ -thick RMBE-GaN layers, with electron mobilities below 250  $\text{cm}^2/\text{V s}$  and dislocation densities in the  $10^9\text{-}10^{10}\text{ cm}^{-2}$  range.<sup>129</sup>

Free-standing Samsung GaN templates were also investigated by DLTS both on Ga-face and N-face.<sup>115</sup> The Schottky barrier were fabricated at VCU under identical conditions to those used for the Lincoln HVPE layers. Due to large defect concentration by virtue of growth and mechanical polish only, it was necessary to remove some 30  $\mu\text{m}$  of the material by chemical etching. This amount was found sufficient based on the Hall measurements performed at VCU. On the other hand, the Ga-face was just simply cleaned before fabrications. As will be described in detail below, this surface exhibited defects which are generally attributed to plasma damage such as that caused the RIE etching performed. DLTS experiments are underway for the Ga-face sample that underwent chemical etching to remove the damage. Judging from the reduced reverse bias leakage current and preliminary DLTS spectra, we believe that the damage caused by RIE has been eliminated.

Typical DLTS spectra for a SBD obtained from the Ga-face sample, measured as a function of temperature for a series of filling pulse widths ( $W_f$ ) and 0 bias and -8 V reverse bias voltages, are shown in Fig. 43. Six deep traps

(labeled as  $A_1$ , A, B, B', C and D) were observed in the temperature range 80 to 450 K and ii) three of these traps,  $A_1$ , A, and B', show significant increases in peak height as  $W_f$  increases from 0.2 to 20 ms. The "fingerprints" of these traps, i.e.  $E_T$  and  $\sigma_T$ , as determined from the Arrhenius plots of  $T^2/e_n$  versus  $1/T$ , are  $E_T=0.70$  eV and  $\sigma_T=1.7 \times 10^{-15}$  cm<sup>2</sup> for A;  $E_T=0.58$  eV and  $\sigma_T=2.4 \times 10^{-15}$  cm<sup>2</sup> for B;  $E_T=0.53$  eV and  $\sigma_T=1.5 \times 10^{-15}$  cm<sup>2</sup> for B';  $E_T=0.35$  eV and  $\sigma_T=1.6 \times 10^{-15}$  cm<sup>2</sup> for C; and  $E_T=0.25$  eV and  $\sigma_T=1.2 \times 10^{-15}$  cm<sup>2</sup> for D. Traps  $A_1$ , A, B, and D are commonly observed in epitaxial GaN grown by metalorganic chemical-vapor deposition (MOCVD), reactive molecular beam epitaxy (RMBE)<sup>116,117</sup> and HVPE.<sup>129</sup>

A significant increase in a DLTS signal as a function of  $W_f$ , as found for traps  $A_1$ , A, and B', usually suggests a small capture cross-section and/or a trap behaving as a "line-defect" which is typically associated with threading dislocations. Such behavior in connection with traps  $C_1$  and  $A_1$  in thin RMBE-GaN layers has been reported.<sup>116,117</sup> The prominence of trap C found in the Ga-face sample appears to be related to the surface damage caused by RIE, since this center can be detected only in the top 0.4- $\mu$ m, and is not present at all in the N-face sample which was etched by wet chemical etching to remove any damage present on the surface. Interestingly, the behavior of trap C found here is very similar to that of a sputter-deposition-induced trap  $E_{S3}$  in MOCVD-grown n-GaN, reported by Auret et al.<sup>118</sup> The new trap B' is found not only near the surface, but also in the deeper region. This trap has a small capture cross-section, and seems to be affected by the strength of the electric field in the depletion region.

For several of the N-face SBDs, measured at temperatures below 200 K, we observed trap D, but not trap C. However, in some of the N-face SBDs, we found trap  $E_1$ , which is shown in Fig. 44 as a function of  $W_f$ . The  $E_T$  and  $\sigma_T$  for trap  $E_1$  were determined to be 0.18 eV and  $4 \times 10^{-17}$  cm<sup>2</sup>, respectively. The much lower value of the capture cross-section for trap  $E_1$ , as compared to that of trap D, can explain the strong influence of  $W_f$  on the peak height of trap  $E_1$ . Trap  $E_1$  was also observed in thin GaN films grown at 750 °C by RMBE, as previously reported.<sup>117</sup> Through comparisons of the DLTS spectra in as-grown RMBE GaN and electron-irradiated MOCVD GaN, trap  $E_1$  is found to be very similar to the electron-irradiation-induced trap E, and is thus believed to be a complex involving the N vacancy. This assignment is supported by the fact that ammonia, the N source in RMBE growth, is rather stable at the low growth temperatures employed, and thus N vacancies might be expected. Also, the observation of trap  $E_1$  in the N-face SBDs of this study might be an indication of nitrogen deficiency in the early stages of HVPE growth.

Reiterating what was mentioned in the TEM section dealing with the HVPE films with varying thicknesses, the dislocation density increases from  $1 \times 10^8$  cm<sup>-2</sup> in the top region (at  $t=55$   $\mu$ m), up to  $3 \times 10^8$  cm<sup>-2</sup> in the middle region (at  $t=20$   $\mu$ m), then up to  $1.6 \times 10^9$  and  $1 \times 10^{10}$  cm<sup>-2</sup>

in the region close to the interface (at  $t=3$   $\mu$ m and 1  $\mu$ m, respectively). From a cross-sectional TEM image for the nominally 5- $\mu$ m-thick sample (not shown here), the dislocation densities at  $t=4.5$   $\mu$ m, 3  $\mu$ m and 1  $\mu$ m, are  $9 \times 10^8$  cm<sup>-2</sup>,  $1.7 \times 10^9$  cm<sup>-2</sup>, and  $4 \times 10^9$  cm<sup>-2</sup>, respectively. The results obtained in the 5- $\mu$ m-thick sample are very similar to those obtained in the interface region of the 55- $\mu$ m-thick sample. To summarize our observations, the deep level concentration, the leakage current in SBDs, and threading dislocation density decreases in thicker films. By analogy, one can argue the deep level density decreases away from the interface and are correlated to dislocations.

Threading dislocations in GaN are electrically active and cause defect states which act as traps and non-radiative recombination centers. This has been demonstrated by studies of scanning capacitance microscopy<sup>119</sup> and plan-view TEM along with cathodoluminescence imaging.<sup>120</sup> Recently, a theory of charged-dislocation-line scattering was developed within the framework of the Boltzmann transport equation<sup>121</sup> which describes the temperature-dependent Hall-effect data in GaN. Threading dislocations in GaN have been predicted to be of the  $V_{Ga}$  or  $V_N$  nature in their core structures, depending on doping (or type) and growth stoichiometry. The formation of the  $V_{Ga}$  structure is favored under N-rich conditions and is most stable in n-type material, whereas the formation of the  $V_N$  structure is favored under Ga-rich conditions and is most stable in p-type material.<sup>122</sup> Because of the uncertainty involved in the formation energy calculations, a mixture of core structures is also possible. Thus, edge dislocations may behave as electron traps in n-type GaN and may act as hole traps in p-type GaN, depending on growth conditions.

Regarding the possible point defect natures of the main centers found in n-GaN, we point out two important experimental observations: i) high concentrations of deep centers in n-GaN are closely associated with high dislocation densities regardless of the growth technique; ii) there exists an anti-correlation between centers  $A_1$  and B for the two thinnest samples investigated (see curves d and e in Fig. 45). The anti-correlation relationship was also observed in other n-GaN materials (e.g., for thin MOCVD-GaN<sup>123</sup> and for thin RMBE-GaN<sup>124</sup>, which means that a strong increase in trap B is generally accompanied by a significant reduction of trap  $A_1$ . The center B (also called  $E_2$  in the literature) has been extensively studied resulting in the suggestion that the center could be due to chemical impurities, such as C<sup>125</sup> or Mg.<sup>126</sup> In another investigation, the photoionization of  $E_2$  in n-GaN was characterized by using capacitance transient spectroscopy, which yielded an optical activation energy of  $E^0=0.85$  eV at 90 K and resulting in a Franck-Condon shift of 0.3 eV, indicating a possible defect nature.<sup>127</sup> A recent study showed that  $E_2$  could be effectively suppressed by isoelectronic In-doping and it was suspected of being a  $N_{Ga}$  defect.<sup>128</sup>

To gain a better insight into the nature of  $A_1$ , we need to refer to the EI-induced centers in n-GaN. In MOCVD-GaN layer after 1-MeV electron-irradiation (EI) trap E (at  $\sim 120$  K), which consisted of two components, each of which with a thermal activation energy of 0.06 eV, and trap  $A_2$  (at  $\sim 420$  K), with  $E_T=0.85$  eV appeared. There is good evidence that E is related to the nitrogen vacancy ( $V_N$ ), and because  $A_2$  shows a production rate close to that of E, it is possible that  $A_2$  might be a  $N_T$ -related defect, created by the reaction nitrogen leaving the substitutional site and creating an interstitial ( $N_N \rightarrow V_N + N_i$ ).<sup>129</sup> In addition the aforementioned observations, some pre-existing centers in MOCVD-GaN, including B, are not affected by 1-MeV EI at all, ruling out the possibility that defect B is related to the  $V_N$  defect. Since center  $A_1$  is very similar to the EI-induced center  $A_2$  and B shows an anti-correlation with  $A_1$ ,  $A_1$  is tentatively assigned to a  $N_T$ -related defect and B to  $N_{Ga}$ .  $N_{Ga}$  can be easily formed by the reaction  $V_{Ga} + N_i \rightarrow N_{Ga}$ . According to the predictions mentioned above,  $V_{Ga}$  could be present in n-GaN having a high dislocation density, which has been observed in undoped MOCVD-GaN by positron annihilation spectroscopy.<sup>130</sup> The center D, with  $E_T=0.17$ -0.23 eV, also shows a correlation with the thickness reduction or the dislocation increase, which means that D, as an electron trap, could possibly be a defect complex involving  $V_{Ga}$  (such as  $V_N$ - $V_{Ga}$ ). As a way of summary, Arrhenius plots of  $T^2/e_n$  for as-grown and electron beam induced deep centers in n-GaN are shown in Fig. 46. The results of the above investigation and summary of the discussion are tabulated in Table V below.

#### V.d. Minority Carrier lifetime

Electron beam and optical depth-profiling of thick (5.5-64  $\mu\text{m}$ ) n-type HVPE GaN samples were carried out using electron beam induced current (EBIC) and micro-photoluminescence (PL) to determine the minority carrier diffusion length,  $L$ , and minority carrier lifetime. The minority carrier diffusion length increased linearly from 0.25  $\mu\text{m}$ , at a distance of about 5  $\mu\text{m}$  from the GaN/sapphire interface, to 0.63  $\mu\text{m}$  at the GaN surface, for a 36- $\mu\text{m}$ -thick sample. The increase in  $L$  was accompanied by a corresponding increase in PL band-to-band radiative transition intensity as a function of distance from the GaN/sapphire interface. We attribute these observations in PL intensity and minority carrier diffusion length to a reduced carrier mobility and lifetime at the interface, due to scattering at threading dislocations. The results of EBIC and PL measurements are in good agreement with the values for dislocation density, obtained using TEM, which we discussed earlier in this report.

Minority carriers are captured by defect rather easily reducing their lifetime and diffusion length in the material. In addition to having important bearing on devices, the minority carrier lifetime can be used to assess the quality of the material. Since the TEM and DLTS results discussed above clearly indicated that the defects are reduced away from the interface, it is only logical to seek

the value of the minority carrier lifetime as a function of distance away from the interface. The thick HVPE films provide an excellent medium for this investigation. In this vein, electron beam and optical depth-profiling of thick (5.5-64  $\mu\text{m}$ ) quasi-bulk n-type GaN samples, grown by hydride vapor-phase epitaxy (HVPE), were carried out using electron beam induced current (EBIC), micro-photoluminescence (PL) and correlated to the transmission electron microscopy (TEM) results discussed above.<sup>51</sup> To cap the properties of the HVPE films used, room-temperature Hall measurements, after correction for the highly conductive  $\sim 200\text{nm}$  interfacial layer) showed electron concentrations (at the surface) ranging from  $8 \times 10^{16}$  to  $1.2 \times 10^{17} \text{ cm}^{-3}$ , and mobilities of 580 to 750  $\text{cm}^2/\text{Vsec}$ , respectively, the larger and lower mobilities being associated with the thicker films. The conductive interfacial layer was modeled to have an electron concentration of mid- $10^{19} \text{ cm}^{-3}$  and a mobility of about 50  $\text{cm}^2/\text{Vsec}$ .

EBIC measurements were carried out *in-situ* in a Scanning Electron Microscope (SEM) JEOL 6400F. A cartoon of the experimental set up is shown in Fig. 47. The accelerating voltage, used in these measurements, was varied from 10 to 20 kV. This corresponds to an electron range,  $R$ , of 0.36 to 1.20  $\mu\text{m}$ , respectively.<sup>131</sup><sup>132</sup> After cleavage, vertical gold (Au) stripes (Schottky barriers) of different sizes were formed on one of the edges of the samples by Au evaporation and subsequent lift off. The minority hole diffusion length,  $L$ , was derived from the line-scan EBIC measurements.<sup>133</sup><sup>134</sup> The measurements were carried out at distance,  $d$ , from the GaN/sapphire interface. In these measurements the electron beam (positioned perpendicular to the sample edge) was moved from the vertical wall of the Au/n-GaN Schottky barrier towards another Au-contact.  $L$  can be obtained from the EBIC current decay versus distance from the edge of the Schottky contact (for distances  $> 2L$ ). The details of the diffusion length extraction can be found elsewhere.<sup>133,134</sup> Since the samples used met the condition of thickness  $\gg 4L$ , no sample thickness correction in the measurements  $L$  was warranted as the sample could be construed as bulk.<sup>135</sup> Likewise, since the ratio  $R/L \leq 4$ , no EBIC resolution limitations would be expected.<sup>136</sup>

Micro-PL profiling across thick GaN samples was performed *in-situ* in the micro-photoluminescence setup. The micro-PL measurements were carried out using a 4 nsec-pulse 337 nm nitrogen laser with a power of  $\sim 100 \mu\text{J/pulse}$ . The laser beam focused to a 1.5  $\mu\text{m}$  diameter spot allowed probing of a region comparable to that studied by EBIC (electron beam line-scan length is  $\sim 4.4 \mu\text{m}$  at  $\times 25,000$  magnification). A translation stage with a 0.5  $\mu\text{m}$  step resolution was used for laser beam positioning at the predetermined distance from the GaN/sapphire interface.

The dependence of the so measured minority carrier diffusion length on distance from the GaN/sapphire interface for one of the samples under investigation (36  $\mu\text{m}$  thick) is shown in Fig. 48 as open circles. Also shown

in the figure are the minority carrier lifetime and minority carrier mobility (in the inset) which will be discussed below.  $L$  increases linearly from  $\sim 0.25 \mu\text{m}$  at the GaN/sapphire interface up to  $\sim 0.63 \mu\text{m}$  at the surface. This increase is in agreement with the average space between dislocations, calculated from the experimentally determined dislocation densities using TEM, and shown in Fig. 49.

Comparing the depth dependence of the dislocation density of Fig. 49 with that of  $L$  shown in Fig. 48, one notes that the decrease in minority carrier diffusion length towards the GaN/sapphire interface is correlated to an increase in the dislocation density. The minority carrier diffusion length at a certain distance from the interface agrees well with the spacing between two adjacent dislocations. For example,  $L = 0.63 \mu\text{m}$  at a distance of  $32 \mu\text{m}$  from the GaN/sapphire interface (Fig. 48). From Fig. 49, the average spacing between two adjacent dislocations at this distance is  $\sim 0.69 \mu\text{m}$ . Similarly,  $L = 0.25 \mu\text{m}$  at a distance of  $\sim 8 \mu\text{m}$  from the GaN/sapphire interface, while the spacing between two adjacent dislocations at this distance is  $\sim 0.35 \mu\text{m}$ . Hence, it is likely that the minority carrier diffusion length is determined by carrier recombination on the adjacent threading dislocations. This simply implies that samples used do not allow the measurement of the intrinsic diffusion length in GaN. It is then expected that larger figures would result in the GaN templates with dislocation density some two orders of magnitude lower than the films investigated in this particular study.

The hole diffusion length in n-GaN may decrease due to a degradation in diffusivity (or minority carrier mobility) and lifetime,  $\tau$ , or both through the expression  $L = \sqrt{D\tau}$ . The diffusivity,  $D$ , and mobility,  $\mu_p$ , are related via the Einstein equation. The calculation of minority carrier hole mobility,  $\mu_p$ , is a difficult problem in any semiconductor material, because of the degenerate valence bands. However, to get a first order estimate of  $\mu_p$  vs. dislocation density, one can simply assume a single valence band with an associated literature hole effective mass of  $2.0 m_0$ , and then follow previously reported treatments.<sup>121</sup> The results are presented in the inset of Fig. 48. Note that the  $\sim 150 \text{ cm}^2/\text{Vsec}$  value of mobility at low dislocation densities is much higher than that found in most *p-type* GaN samples. However, such samples are usually heavily doped (with Mg), and heavily compensated (perhaps by N vacancies), and thus may be expected to produce a much lower mobility than that calculated for a high quality n-type GaN under investigation. The intensity of PL emission can be related to carrier lifetime<sup>137</sup> which can be used to probe for any trend in  $\tau$  on  $d$ . This has been done as a function of distance away from the interface in a  $64 \mu\text{m}$  sample. This is the sample that we have been referring to as being  $68 \mu\text{m}$  layer. To summarize the results, the intensity of the room temperature band-to-band transition decreases as the probe moves closer to the GaN/sapphire interface. Since

the PL intensity is proportional to the carrier lifetime, we conclude that the latter parameter decreases at lower values of  $d$ .

With the dependence of diffusion length,  $L$ , and lifetime,  $\tau$ , the variation of the diffusion constant with position away from the interface can be discerned. Einstein's relation can then be used to determine the dependence of the minority carrier mobility, hole mobility in this case, on position away from the interface. Since the diffusion length correlates with dislocation density, the basic semiconductor parameters such as the diffusion constant, minority carrier lifetime and the minority carrier mobility can now be related to the dislocation density, which are shown in Fig. 48 and its inset. To find the dislocation density corresponding to a certain distance from the GaN/sapphire interface, at which the  $L$  measurements were carried out, one can use the dislocation-density-vs.- $d$  data, presented in Fig. 49. Since  $L$  depends linearly on  $d$  and on the square root of  $\tau$ , a quadratic fit for  $\tau$  vs.  $d$  results (see dashed line in Fig. 48). Note that the values of  $\tau$  so calculated are in agreement with the minority carrier lifetimes (1.4 - 2.3 nsec), probed in InGaN/GaN quantum well, *in-situ* in SEM, using time resolved cathodoluminescence.<sup>138</sup>

#### V.e. Positron Annihilation: Lincoln layers- Samsung layers. In Progress

Positron annihilation experiments have been conducted in HVPE films with varying thicknesses from 1 to  $68 \mu\text{m}$ . Other samples doped with Mg and bulk GaN samples grown at UNIPRESS were also investigated and the behavior of positron annihilation in Mg-doped samples established. Unlike in the Mg-doped samples, the positron lifetime in the HVPE samples under investigation increased as the lattice temperature was lowered. This was interpreted as meaning that the acceptors in these n-type samples are due to Ga-vacancies as opposed to relatively shallow acceptor impurities. The similarities in the behavior of these samples and those investigated in a previous study where the III/V ratio was changed also lend support to the Ga-vacancy argument. The previous investigation established that as the III/V is lowered by increasing the ammonia flow during the growth, the Ga-vacancy concentration increased. Using Mg-doped samples as standard, the vacancy concentration was determined to be about  $10^{17} \text{ cm}^{-3}$  near the surface for the layer with a thickness greater than  $30 \mu\text{m}$  (could be as high as  $68 \mu\text{m}$ ). Assuming that the growth parameters in the set of layers with varying thicknesses that were investigated are the same, the Ga-vacancy concentration increases to mid  $10^{19} \text{ cm}^{-3}$  near the interface. Since the interfacial region is n-type and highly conductive, this region must also contain even larger concentrations of O and/or N-vacancies which lead to n-type material. SIMS results already indicate mid  $10^{19} \text{ cm}^{-3}$  levels of O being present in this region. This has been attributed to O outdiffusion from sapphire as previously reported. Moreover, the preliminary data in sample LH1232.  $2.6 \mu\text{m}$

thick sample, suggest that this sample contains vacancy clusters instead of Ga vacancies.

Positrons get trapped at neutral and negative vacancies due to the missing positive charge of the ion cores.<sup>139</sup> The reduced valence and core electron densities at vacancies increase the positron lifetime and narrow the positron-electron momentum distribution. While the previous positron experiments in GaN showed negative Ga vacancies in  $10^{18} \text{ cm}^{-3}$  range in unintentionally doped n-type layers and bulk crystals,<sup>101</sup> vacancies are observed in semi-insulating or p-type GaN.<sup>140, 101</sup> The Ga vacancy concentration correlates with the intensity of the yellow luminescence at 2.2 eV, suggesting that the acceptor states of  $V_{\text{Ga}}$  are involved in this optical transition.<sup>101</sup> The vacancy defects in the HVPE grown GaN layers were investigated by implanting positrons from a monoenergetic beam to the depths of up to 1  $\mu\text{m}$  from the surface. The Doppler broadening of the 511 keV annihilation radiation was recorded using a Ge detector and a stabilized multichannel analyzer system. The shape of the 511 keV line was described using the conventional low and high electron-momentum parameters  $S$  and  $W$ .<sup>139</sup> When positrons annihilate at vacancies, the  $S$  parameter increases and the  $W$  parameter decreases, because a larger fraction of annihilations takes place with the valence electrons with lower momentum. Consequently, the lower the  $S$  parameter, the less the concentration of Ga vacancies,  $V_{\text{Ga}}$ .

The lifetime of the positron annihilation depends on the presence of vacancies or the vacancy-related complexes in solids that are primarily negatively charged.<sup>141</sup> With this technique, which has recently been refined for semiconductors, it is possible to estimate concentration of the vacancies, bivalencies or the vacancy related complexes in the material and to predict their charge state. Vacancies can be unambiguously identified along with their open volume (monovacancy/bivacancy/larger cluster) and atomic surrounding (i. e. the sublattice of the vacancy). In many cases, whether a vacancy is surrounded by impurity atoms can also be discerned. Positrons are sensitive to neutral and negative vacancies with differentiation possible. Positive vacancies are not detected due to the Coulomb repulsion, unless they are first converted to a neutral or negative charge state (e. g. by excitation with photons). The sensitivity is in the concentration range  $10^{15} - 10^{20} \text{ cm}^{-3}$ . Against a calibrated sample, The relative vacancy concentrations in the samples can be determined to an accuracy of better than 10 %. The absolute concentration scale is known within a factor of two. The positron spectroscopy can be applied to both bulk crystals and epitaxial layers. The minimum thickness of the layer being > 100 nm, although thicknesses of about 1 micron (or preferable much more) are usually preferred. Positrons can be used to determine the depth profile of vacancies close to the surface of the sample at 0 - 2 microns. The depth resolution is typically 20 % of the depth. In addition to vacancies, positron spectroscopy is useful for studying other defects containing open volume, like voids, dislocation lines with

open volume, DX centers, etc. There are no limitations concerning the conductivity (n-type, SI, p-type) of the sample except the charged state of the defect being examined. The technique has been applied to vacancies in GaN already.<sup>101, 130</sup>

In previous investigations, the lowest  $S$  parameter was obtained in the Mg-doped reference layer, where a figure of  $S = 0.434$  at  $E = 5-15 \text{ keV}$  was obtained.<sup>130</sup> The Doppler parameters in Mg-doped layer previously investigated are very close to those estimated for defect-free GaN by combining positron lifetime and Doppler broadening techniques.<sup>101</sup> When temperature is lowered to 20 K, the  $S$  parameter in the Mg-doped reference layer decreased gradually to  $S = 0.433$ . This behavior is expected for delocalized positrons in a defect-free lattice, and it has been attributed to thermal expansion of the lattice.<sup>139</sup> One can conclude that the Mg-doped sample is free of vacancy defects that trap positrons and can be used as reference.

The  $S$  parameter in all the n-type layers under investigation previously and during this investigation is larger than that in the Mg-doped reference sample mentioned above. Such increase in  $S$  parameter is indicative of the fact that the positron-electron momentum distribution gets narrowed as compared to that vacancy-free reference sample. This narrowing is ascribed to positron annihilation by trapping at vacancy sites where the electron density is lower and the probability of annihilation with high-momentum core electrons is reduced compared to that of delocalized positrons in the lattice.<sup>139</sup> The increased  $S$  parameter is thus a clear sign of vacancy defects present in the n-type GaN layers. Another, albeit indirect, evidence for Ga vacancies for being the cause of the defects annihilating positron is the experiments conducted in samples grown with different group III/V ratio. As this parameter was increased, which would plausibly cause Ga vacancies, the  $S$  parameter increased indicative of increased vacancy defects.<sup>130</sup>

Positron annihilation experiments were performed by Prof. Kimmo Saarinen in HVPE samples grown at Lincoln Laboratories. The samples ranged in thickness from 1 to 68  $\mu\text{m}$  in an effort to map the Ga vacancy concentration as a function of the sample thickness. Specifically, the experiments were performed in the following samples: LH1089(3,1) 1  $\mu\text{m}$ , LH1106(3,1) 5  $\mu\text{m}$ , LH1059(3,1) 10 - 14  $\mu\text{m}$ , LH706(3,1) 36 - 39  $\mu\text{m}$ , LH266(3,-1) 49 - 68  $\mu\text{m}$ , and LH1232(1,-3) 2.6  $\mu\text{m}$ . Recall that the deep level concentration decreased with increased thickness, the electron mobility increased with increased thickness and the acceptor concentration decreased with increased thickness. Since, the all of the holes ionized and negatively charged in n-type samples, positron annihilation experiments would add support to the suggestion that the acceptors are caused by Ga vacancies,  $V_{\text{Ga}}$ . Also, complexes with substitutional impurities such as  $\text{O}_{\text{N}}$  and  $\text{Si}_{\text{Ga}}$  present in the films can be investigated.

Thick (> 30  $\mu\text{m}$ ) samples LH706 and LH266 are suitable for the positron lifetime spectroscopy because the

energetic ( $\sim 200$  keV) positrons emitted directly from the  $\beta^+$ -decay of  $^{22}\text{Na}$  source do not penetrate through the thick GaN layers. About  $2 \times 10^6$  positron-electron annihilation events were collected in each lifetime spectrum during a time of 3 hours. The temperature dependence of positron lifetimes was studied by measuring about 40 lifetime spectra in each sample at 10–550 K. All samples were characterized by measuring the Doppler broadening of positron-electron annihilation radiation. Positrons were implanted from a monoenergetic (0–25 keV) positron beam at depths of 0–1.2  $\mu\text{m}$  from the surface of GaN epilayer. Experiments varying both the incident positron energy and sample temperature were completed in a total time of about 2 months.

Positron annihilation spectra were taken in a thick ( $> 30$   $\mu\text{m}$ ) n-type HVPE GaN sample at 550 K and 80 K as shown in Fig. 50. Data taken at 550 K with the aid of the exponential decay of the form  $p_n(t) = \sum I_i \exp(-t/\tau_i)$  led to a single lifetime  $\tau_B = 160$  which is what one would expect from the Mg-doped samples which are descriptive of films with very little if any vacancies. At 80 K, the exponential decay could be described by a two-lifetime process. The lifetime, for positron annihilation by vacancies,  $e^+$  lifetime, was deduced to be  $\tau_V = 235$  ps. The experimental lifetime  $\tau_V = 235$  ps can be attributed to the Ga vacancy (relaxed outwards) but not to the nitrogen vacancy<sup>142</sup> as show in Fig. 51. Using the Mg-doped sample as the reference, the density of Ga vacancies,  $V_{\text{Ga}}$  was thus determined to be about  $10^{17} \text{ cm}^{-3}$  near the surface. The vacancies can be positively identified as Ga vacancies and they are responsible for the acceptors in the film as the concentration of likely acceptors such as Mg ( $< 10^{15} \text{ cm}^{-3}$ ) and C ( $< 10^{16} \text{ cm}^{-3}$ ) determined by SIMS are much less than the vacancy figure. Although, these experiment alone cannot distinguish between the isolated and complexed Ga vacancies in one sample, the body of evidence presented in this report and elsewhere<sup>143,144,145,146</sup> lend support to the premise that the Ga vacancies are associated with defect complexes (such as  $\text{VGa} - \text{ON}$  or  $\text{VGa} - \text{SiGa}$ ).

Again the thicknesses of the film used are 1, 5, 10-14, 36-39, 49-68  $\mu\text{m}$ , 49-68  $\mu\text{m}$  simply representing the thickness variation across the two inch wafer. The Doppler broadening experiments indicate that the thinner layers ( $< 30$   $\mu\text{m}$ ) also contain Ga vacancies at even larger densities, as would be expected. The increased S parameter as the thickness of the film is reduced is indicative of larger concentrations of Ga vacancies as shown in Fig. 52. A Mg-doped sample containing very little if any Ga vacancies is used as the reference (here the reference S parameter, which depends slightly on the resolution of the detection system, is  $S = 0.459$ ). Since the films are reproducible and thinner films represent the earlier stages of growth in thicker films, it is concluded that the Ga vacancy concentration increases toward the interface as is the case with dislocations. In addition, as shown in Fig. 52, the implantation energy can be used to determine the extent of positron in the films giving a

measure of the S parameter as a function of depth in each of the films independently. Fig. 53 shows the W (core annihilation parameter) versus S (valence annihilation parameter) parameter plot for all the samples, from 1 to 68  $\mu\text{m}$  inclusive of the reference Mg-doped sample. The slope of the curve supports the argument that Ga vacancy is the same in all the films at the same distance from the interface regardless of the eventual total thickness of the film. The Ga vacancy concentration was determined in each of the samples and plotted vs layer thickness which is considered as the distance from the interface and is shown in Fig. 54. The density drops from some  $10^{20}$  in 1  $\mu\text{m}$  thick film to below  $10^{17} \text{ cm}^{-3}$  in the nominally 68  $\mu\text{m}$  thick films. Since the interfacial region is determined to be n-type and highly conductive, this region must also contain even larger concentrations of O and or N-vacancies with lead to n-type material. SIMS results already indicate mid  $10^{19} \text{ cm}^{-3}$  O being present in the layer. This has been attributed to O outdiffusion from sapphire as previously reported.<sup>147</sup> Moreover, the preliminary data in sample LH1232. 2.6  $\mu\text{m}$  thick sample, suggest that this sample contains vacancy clusters instead of Ga vacancies.

At lower temperatures, the average positron lifetime increases, indicating that positrons get trapped more efficiently due to attractive Coulomb interaction, lending further support to the proposition that Ga vacancies are negatively charged (i. e. acceptors). If positrons were trapped at negative impurities, such as  $\text{Mg}_{\text{Ga}}$  ions as was the case in the measurement conducted in highly n-type bulk GaN such as UNIPRESS bulk GaN crystals, the average lifetime would have decreased at low temperatures, not increased. Observation of the opposite effect in the HVPE samples to that in the bulk crystals is a good indication that Ga vacancies are the only negatively charged defects. One can then conclude that the Ga vacancies are the dominant acceptors in thick HVPE layers and or in the regions of the layer that are more than 5 microns away from the GaN/ $\text{Al}_2\text{O}_3$  interface. In short, formation of  $\text{VGa}$  depends on the thickness of the layer and is strongly enhanced close to the GaN/ $\text{Al}_2\text{O}_3$  interface. In one sample, LH1232, instead of isolated vacancies, preliminary data suggest that this sample contains vacancy clusters. The results of these particular investigations as well as those preceding them, we can conclude that the vacancy concentration in n-type GaN:  $[V_{\text{Ga}}] \approx 10^{17} - 10^{18} \text{ cm}^{-3}$ .

#### V.f. FTIR, EPR and ODMR

FTIR, ODMR and EPR measurements have been made in both Lincoln and Samsung HVPE layers. In FTIR measurements, two absorption bands corresponding to binding energies of 30.9 and 33.9 meV were found. The former is of higher concentration than the latter and is attributed to Si donors. Splitting of the binding energies with magnetic field is consistent with an effective mass of 0.22  $m_0$ . The ODMR signal in a 5-10  $\mu\text{m}$  thick GaN layer from the 2.2 eV peak, the notorious yellow peak, with magnetic field perpendicular and parallel to the c-axis showed signatures of shallow donor (effective mass like)

and deep donor transitions with 1.95 and 1.99 g-values, respectively. The 3.27 eV peak, which is the blue peak observed in many GaN films grown by a variety of growth methods, was attributed to transitions involving shallow acceptors and has a g-value of about 2.1. The 2.4 eV "green" PL band from the Samsung free-standing layer is a shallow donor (effective mass like) transition and has a g-value of 1.95. The larger linewidth, relative to the Lincoln layers, associated with the Samsung template is indicative of a lower concentration of this center, which leads to a reduced hyperfine interaction. EPR studies confirmed the notable difference between the Lincoln and Samsung layers, notably the larger linewidths in the Samsung material due to lower concentration. Specifically, the Samsung free-standing sample has about  $6 \times 10^{15} \text{ cm}^{-3}$  uncompensated donors per  $\text{cm}^3$  while the Lincoln sample has a concentration about a factor of four higher.

Fourier Transform InfraRed (FTIR) measurements in the frequency range of 120 to 320 wavenumbers ( $\text{cm}^{-1}$ ) in a transmission mode were undertaken. At frequencies corresponding to vibrational modes of impurities incorporated in the lattice resonant absorption occurs and valuable information about the local nature of impurities can be garnered. Spectral position is unique to a specific impurity and absorption intensity is proportional to concentration. Absorption features in the IR transmission have been obtained in an unintentionally doped GaN layer on sapphire and the results of such an experiment are shown in Fig. 55.

As can be seen, at two distinct energies, 187 and  $211.1 \text{ cm}^{-1}$  for zero magnetic field, where distinct absorption bands were observed. Fig. 55 also shows the dependence of those absorption bands on magnetic field up to 12 T. The frequency of the absorption band is indicative of the donor binding energy where the intensity of absorption is related to the concentration of donors. Needless to say that the data point to two donors with binding energies of about 30.9 meV and 33.9 meV. The former is believed to be due to unintentionally introduced Si while the genesis of the latter, which has a much lower concentration, is not clear. The splitting due to the magnetic field, shown with lines emanating from each donor absorption band at zero magnetic field, is consistent with an electron effective mass of  $0.22 m_0$ .

Many defects have electron levels, which split due to different internal fields: exchange interaction, the Jahn-Teller effect, spin-orbit interaction, etc. Such defects may be paramagnetic or rendered paramagnetic under illumination and, thus, can be detected by magnetic resonance techniques. The electron paramagnetic resonance (EPR) method can be used for identification and a thorough study of a predominant defect in the sample. In thin epitaxial layers with defect concentrations at the part per million levels, a more efficient method is often the optical detection of magnetic resonance (ODMR) which is really EPR and PL in one. It is based on changes of the PL intensity under varying applied dc magnetic

field and resonant microwave absorption. The magnetic resonance methods give the spin Hamiltonian parameters of the defect (g-factor, hyperfine interaction tensor, etc.) and, thus, can reveal the symmetry of the defect, the character of the defect wave function, and (in principle) the chemical identity of the defect.

Native defects (vacancies, antisites, and complexes), that are present in semiconductors in moderate concentrations, can be produced in large amounts by electron or particle irradiation of the sample. Comparison of the magnetic resonance or luminescence before and after irradiation can augment efforts to identify native defects. Defects may be created or healed by annealing. Annealing in hydrogen or oxygen environment can reveal the related defects in the samples.

The ODMR method has already been applied to the study of GaN. The ubiquitous yellow luminescence in undoped GaN, and different bands in Mg-doped GaN were studied by Glaser et al.<sup>148</sup> Identification of transitions suggested in these investigations is inconsistent with the models proposed in conjunction with PL studies.<sup>149,150</sup> The reason may be a two-step process involving spin-dependent capture followed by radiative recombination.<sup>150</sup> Recently, two deep defects in electron-irradiated undoped GaN have been observed and studied by the ODMR method.<sup>151</sup> One of them, responsible for the broad band at about 0.95 eV, is related to interstitial-Ga defect. Another band with a sharp zero-phonon line at 0.88 eV is not yet identified.

More insight into the nature of defects such as their symmetry can be gleaned from ODMR and EPR techniques. These techniques could determine whether defects are interstitials, vacancies, impurities, etc. EPR/ODMR could play an important role here, combined with theory. Samples in which nitrogen vacancies are likely to be present are electron-irradiated n-type GaN. We must sort out whether we are dealing with isolated vacancies or with complexes. EPR typically probes the ground state of the system while ODMR reveals information on the excited states. ODMR relies on the spin-dependence of recombination processes and combines PL with EPR. The PL provides the high sensitivity needed to study defects at the part-per-million level or less while the EPR provides the high resolution required to reveal the local symmetry and hyperfine structure of the defect. EPR and ODMR are complementary techniques that will be brought to bear to determine the atomic and electronic structure of residual defects and dopants in GaN. Experimentally, obtaining a "fingerprint" of the nitrogen vacancy will be essential.

ODMR is useful in determining the nature of the centers causing extrinsic transitions. In the context of this work, ODMR has been applied to the investigation of unintentionally doped GaN grown by HVPE on sapphire substrate at Lincoln Laboratories (5-10  $\mu\text{m}$ ) and a Samsung layer, the latter being free-standing. Note that the ODMR was done on the same samples as investigated by EPR. Representative ODMR spectra are shown in

Figs. 56 and 57 with the following observation to be made. The resonance with a  $g$ -value of  $\sim 1.950$ , assigned to shallow (effective-mass-like) donors from previous work, was found for both the 2.2 eV "yellow" PL band from LH1106 and the 2.4 eV "green" PL band from the Samsung free-standing layer (see Fig. 58). As also observed in the EPR studies which will be discussed below, the notable difference is the larger linewidth of this feature in the Samsung material.

The broadening is consistent with the reduced concentration of (shallow) donors as suggested by Hall effect and EPR measurements (the broadening arises from an increase of the electron-nuclear hyperfine interaction in this regime of nearly isolated donors, i.e.,  $N_D \sim 1-3 \times 10^{16} \text{ cm}^{-3}$ ; see, for example, Glaser et al.<sup>152</sup> The second feature with  $g=1.989$  observed on the 2.2 eV band from LH1106 is typically found on this emission from (as-grown)  $n$ -type GaN and is ascribed to a deep defect (suggested by some groups to involve Ga vacancies). A different resonance with donor-like character and of deeper nature (based on the  $g$ -value of  $\sim 1.975$  and larger linewidth compared to that found for the effective mass (EM) donor resonance) was found for the 2.4 eV PL band. The weak feature labeled by an arrow at  $\sim 840 \text{ mT}$  with  $B$  rotated  $30^\circ$  from the  $c$ -axis is more pronounced with  $B$  parallel to the  $c$ -axis (not shown). The corresponding  $g$ -value of  $\sim 2.02$  suggests an assignment of this feature to (deep) acceptors. Distinct ODMR spectra were observed for the 1.8 eV PL bands from LH1059 and the Samsung samples (see Fig. 56). In particular, different acceptor-like isotropic resonances with  $g$ -values of 2.000 and 2.019, respectively, were found for this emission. The same shallow donor resonance ( $g_{\parallel} = 1.950$  and  $g_{\perp} = 1.947$ ) as observed for the 2.2 eV PL band was also observed for the 1.8 eV emission band from LH1059. A resonance with a slightly different  $g$ -tensor ( $g_{\parallel} = 1.958$  and  $g_{\perp} = 1.954$ ) was found for the 1.8 eV PL from the Samsung sample. This line is likely associated with "quasi"-shallow or perturbed donors. As suggested by preliminary fits to the spectra, two additional features (labeled by arrows) are also possibly revealed in this emission. More work is planned to clarify the assignments discussed above.

In addition to the ODMR, EPR measurements were also undertaken in one HVPE layer from Lincoln Laboratory (LH1059) and a free-standing GaN template from Samsung (177). All samples had a resonance due to residual donors as shown in Fig. 59. The Samsung free-standing sample has about  $6 \times 10^{15} \text{ cm}^{-3}$  uncompensated donors/ $\text{cm}^3$  while the Lincoln sample has a concentration about a factor of four higher. Note that the Samsung sample has a volume of  $5 \text{ mm}^3$  vs.  $0.1 \text{ mm}^3$  for the Lincoln sample. The linewidth for the Samsung sample is 27 Gauss (G) vs. 12 G for the Lincoln sample and less than 10 G for typical MOCVD films. The narrower widths observed in Lincoln and MOCVD samples are consistent with more isolated donors. In these samples with higher concentration, the hyperfine interaction with the lattice nuclei is "averaged" out and the lineshape is

very Lorentzian. Due to a lower concentration of donors, the Samsung sample exhibits a lineshape that has a significant Gaussian character due to unresolved hyperfine interactions. With somewhat purer samples, we can expect to perhaps resolve hyperfine interaction with nearest neighbor lattice nuclei and establish whether the residual donor is on the Ga, N or interstitial site. Note also that these spectra were taken at 20 K: this is necessary because the signals (especially in the Samsung sample) are easily saturated at 4 K. This is again indicative of isolated donors.

#### V.f. Scanning Micro-Cathodoluminescence Spectroscopy

Micro cathodoluminescence with scanning capability was used to probe optical transitions along the edge of the wafer extending from the surface into the substrate. Evolution of the GaN bandedge and sapphire related peaks were monitored. In addition to the commonly observed 2.2 eV peak which diminished toward the interface, an emission line 2.9 eV emerged at the interface. The underlying mechanisms are under investigation.

As described in the previous section, there exists an interface layer which is very highly conductive and is most likely caused by increased concentration of defects, as well as impurities the interface. Positron annihilation experiments point to increased Ga-vacancy concentration at the interface which act as acceptors and will be discussed in detail later. However, there is also a large concentration of O incorporation at the interface which acts as donors. TEM experiments indicate a larger dislocation concentration at the interface than in the bulk of the sample, and EBIC experiments indicate lower diffusion lengths at the interface. Impurities such as O, as well as native defects and other states associated with large concentration of extended defects, could diffuse from the interface during the initial stages of the growth. In order to assess the nature of the degenerate near-interface doping, Brillson et al. at Ohio State used micro CLS, (Cathodo-Luminescence Scan) technique to measure the spatial distribution of electrically-active defects throughout the epilayer and at the GaN-sapphire junction. The micro-CLS cross sectional technique is well suited for this kind of an investigation and was applied to HVPE films grown at Lincoln Labs. The spectra showed deep level and near band edge (NBE) features characteristic of specific interface states whose energies and intensities vs. depth and vs. sample correlated with the interface conductivity.

Though the work is in progress, a picture is beginning to emerge. Shown in Fig. 60 are the spectra taken across the cleaved face of the sample at various positions with respect to the interface. Positive thickness values correspond to the GaN layer, while negative ones relate to the sapphire substrate. The interface is at zero. The spectra near the surface of this some  $30 \mu\text{m}$  thick Lincoln sample show the usual band edge emission, a 2.2 eV yellow emission, and a peak at 1.67 eV. As the probe moves closer to the GaN/sapphire, the 2.2 and 1.67 eV emission

lines decrease in intensity which could have its genesis in increased non-radiative recombination centers.

Very near the interface, broad peaks at 2.9 and 3.8 eV appear. A sharp peak at 1.78 eV also appears due to Cr impurities in the sapphire. The 3.8 eV peak decays over several microns into the sapphire and appears due to interdiffusion, possibly an Al-N-O complex. However, the 2.9 eV blue peak is interface-related. A log vs. linear plot displays its emergence more clearly. Similar measurements were also made in a sample obtained from ATMI with a higher carrier concentration. The associated data are displayed in Fig. 61 where the spatial (in cross-section) variation of the 3.4 (band edge emission of GaN), 3.8 eV (most likely sapphire related) and 2.9 eV transitions. It is clear that as the interface is approached, the 2.9 eV peak intensity increases substantially. The behavior of the GaN band edge emission is peculiar in that its intensity is low except near the interface. Further experiments indicated that the intensity of the blue emission increases with increased carrier concentration in the film. Zn is the only impurity reported to date that gives 2.9 eV emission in n-type GaN.<sup>153</sup> Interfacial Zn is plausible since Lincoln Labs and others employ a ZnO buffer on Al<sub>2</sub>O<sub>3</sub> that is thermally desorbed prior to GaN growth. Such treatment can result in a Zn-spinel structure and residual Zn impurities near the interface.<sup>154</sup> However, such emission is observed even for ATMI and Linköping HVPE GaN on sapphire for which no Zn treatment is claimed. Additional experiments are clearly needed for a better understanding of the underlying mechanisms.

Very recent low temperature (10K) studies of the GaN near band edge emission peaks reveals the appearance of a peak feature that can account for the n-type doping of the interface region. For distances less than a micron from the ATMI GaN/Al<sub>2</sub>O<sub>3</sub> interface, an peak feature appears 34 meV below the donor-bound exciton that corresponds to an additional donor, correlating closely with the 32-37 meV trap depth for O donors in GaN reported by Götz.<sup>155</sup> Furthermore, SIMS measurements of this specimen show strong O diffusion over 2  $\mu\text{m}$  with [O] as high as  $7 \times 10^{19} \text{ cm}^{-3}$  decreasing to mid- $10^{18} \text{ cm}^{-3}$  over the 1  $\mu\text{m}$  range in which the CLS emission is observed. No other GaN impurity is localized in this depth range. Similar CLS and SIMS behavior is observed for other specimens. Hence, both the spectral energy of the shallow donor level and its intensity vs. depth distribution indicate that O impurities diffused from the Al<sub>2</sub>O<sub>3</sub> are responsible for the high sheet carrier concentration. Further investigation is needed in order to determine the diffusion path(s) and lengths for O and other impurities into the GaN, e.g., via grain boundaries, dislocations, its dependence on growth temperature and time, and methods to suppress such diffusion.

## VI. Theory

Calculations indicate that incorporation of Si has a negligible effect on the lattice constant, but O and Mg can lead to an observable expansion of the lattice. Since

values of the GaN lattice constant have often been based on bulk crystals that are now known to contain large concentrations of oxygen, the "true" GaN lattice constant is actually smaller than what has been measured for such crystals. Boron is an unintentional impurity that can be introduced during MBE growth. There has been speculation about whether B might act as an acceptor in GaN; this would require it to be incorporated on the nitrogen site. Our computations indicate that incorporating B on the N site is energetically unfavorable. Even if it did incorporate there, it would act as a *deep*, rather than a shallow acceptor.

As is the case for defects, impurities too have far reaching consequences in the analysis of the material as well as devices fabricated from it. In addition to the usual effect dealing with carriers associated with impurities, impurities have been shown to affect residual strain in epitaxial layers also, particularly at high concentrations. Does this mean that the impurities themselves affect the lattice constant? And/or do they somehow affect strain relaxation, plastic deformation, etc? And how does all of this depend on layer thickness? A rigorous answer to the first question can be obtained from first-principles calculations. This would also shed light on the question: what is the actual lattice constant of defect-free, undoped GaN? Accepted lattice constant values in the literature have been derived from the UNIPRESS bulk material -- which is now known to contain high concentrations of oxygen! The presence of oxygen affects the lattice constant. This needs to be sorted out in order to establish the true lattice constant. Moreover, impurities in high concentrations have the beneficial effect of reducing dislocation propagation if such propagation is through point defects.

The purpose of this discussion is to review our understanding of native point defects and impurities in III-nitride semiconductors, and the role they play in materials characteristics and device performance. The enhanced understanding will undoubtedly form the basis for better control of impurity and defect incorporation in the growth process. Through close interaction with experiment, emphasis is placed on those defects, which most crucially affect device performance.

### *Effects of impurities on the lattice constant*

As alluded to earlier, impurities could affect the lattice constant of the semiconductor into which they incorporate. Calculations indicate that incorporation of Si has a negligible effect on the lattice constant, but O and Mg can lead to an observable expansion of the lattice. Since values of the GaN lattice constant have often been based on bulk crystals that are now known to contain large concentrations of oxygen, the "true" GaN lattice constant is actually smaller than what has been measured for such crystals.<sup>160</sup>

Let us take a closer look at the effect of impurities on the lattice constant. Nitride semiconductors frequently contain large concentrations of impurities, which are introduced either intentionally (in the case of dopants such

as Mg or Si) or unintentionally (in the case of contaminants such as oxygen). Thin epitaxial nitride films are also usually strained. The role of impurities as a cause of this strain has been debated; a first-principles investigation of these effects has been performed.<sup>157,159</sup>

Incorporation of dopant impurities has two distinct effects on the lattice constant. The first effect is purely a *size* effect, related to the difference in atomic radius between the impurity and the host atom which it replaces. The second effect is an *electronic* effect, related to deformation potentials. For instance, in the case of *n*-type doping donors are contributing electrons to the conduction band. The energy of the system can therefore be lowered if the conduction band energy can be decreased (on an absolute energy scale). Such a shift in the position of the conduction band can occur if the volume of the material is changed; hydrostatic strain indeed leads to a change in the conduction-band energy, with a proportionality factor given by the deformation potential. Such strain also bears a cost, of course, because of the elastic energy associated with the deformation. This elastic energy, however, varies as the *square* of the strain, whereas the energy gain due to the deformation varies *linearly* with the strain; the system can therefore lower its energy by undergoing a deformation. We have studied both the size and the electronic effect on the basis of first-principles calculations, using density-functional theory in the local-density approximation, *ab initio* pseudopotentials, and a supercell geometry.

The size effect can be addressed by studying the relaxation of host atoms around the impurity. Even though we are dealing with wurtzite semiconductors, we treat the material as isotropic. Our results indeed indicate that the anisotropy of the atomic relaxations is very small compared to the magnitude of the overall relaxations. It is customary to define a parameter  $\beta_{\text{size}}$ , which relates the fractional change in the lattice constant to the impurity concentration:

$$\Delta a/a = \beta_{\text{size}} N, \quad (1)$$

where  $N$  is the impurity concentration. To determine the change in lattice constant, we follow a procedure described earlier.<sup>156</sup> The recently calculated<sup>159, 157</sup> values for  $\beta_{\text{size}}$  are listed in Table VI.

The electronic effect can be derived by performing a minimization of the sum of the elastic energy cost (quadratic in the strain) and the energy gained due to lowering of the conduction band (in the case of *n*-type doping), occupied with a certain number of electrons (linear in the strain). Similar to the parameter  $\beta_{\text{size}}$  defined in Eq. (1), one can define a parameter  $\beta_e$ , where the subscript indicates the deformation-potential effect for electrons:

$$\Delta a/a = \beta_e n \quad (2)$$

where  $n$  is the electron concentration. Note that the carrier concentration  $n$  is not necessarily equal to the donor

concentration, because of compensation or incomplete ionization. Similar expressions hold for holes, where of course the shift in the valence band and the hole concentration need to be taken into account. The shift of the band-edge extrema is described by the "absolute" deformation potentials,  $a_c$  and  $a_v$ , as defined earlier<sup>156</sup> and calculated.<sup>158</sup>

For Si, Table VI shows that the size effect and deformation-potential effects have similar magnitudes but are of opposite sign, resulting in a very small net strain. Assuming complete ionization, we can write  $\Delta a/a = \beta_{\text{tot}} [\text{Si}]$ , with  $\beta_{\text{tot}} = \beta_{\text{size}} + \beta_e = -0.1 \times 10^{-24} \text{ cm}^3$ . For  $[\text{Si}] = 5 \times 10^{19} \text{ cm}^{-3}$  the expected in-plane strain is  $-5 \times 10^{-6}$ , a value which would be difficult to detect experimentally. Therefore we conclude that the changes in lattice constant that have been observed as a function of Si concentration<sup>159</sup> can *not* be attributed to lattice distortions caused by the substitution.

For oxygen, the contributions from size and electronic effects are additive, and lead to an expansion of the lattice. Let us consider the effect of incorporating a large concentration  $[\text{O}]$  of oxygen in GaN. Since oxygen is a common unintentional impurity in GaN, this is an important case. Assuming that all of the oxygen is residing on substitutional nitrogen sites, and that it is all electrically active, we find:  $a/a = \beta_{\text{tot}} [\text{O}]$ , with  $\beta_{\text{tot}} = \beta_{\text{size}} + \beta_e = +2.0 \times 10^{-24} \text{ cm}^3$ . For an oxygen concentration of  $10^{20} \text{ cm}^{-3}$ , which is not uncommon, this leads to a lattice expansion  $\Delta a/a = 0.0002$ , which is measurable in X-ray diffraction. We suggest that the observed difference in lattice constants of bulk crystals between "undoped" GaN and "Mg-doped" GaN, observed by Porowski<sup>160</sup> is due to this effect. The "undoped" material is more appropriately called "not intentionally doped"; it has been shown to contain large concentrations of oxygen<sup>161</sup> and exhibits *n*-type conductivity consistent with this high donor concentration. The "Mg-doped" material is grown by introducing Mg in the growth chamber; it is at present not clear whether the Mg (and/or other impurities) are incorporated in the bulk crystal. The conductivity of these "Mg-doped" crystals is much lower, however, than that of the unintentionally-doped (i.e., oxygen-doped) material. The lattice constant of the oxygen-doped material is larger than that of the "Mg-doped" material by a fraction ranging from 0.00016 to 0.00044, consistent with a change induced by the incorporation of oxygen in concentrations ranging from  $8.0 \times 10^{19} \text{ cm}^{-3}$  to  $2.2 \times 10^{20} \text{ cm}^{-3}$ . For Mg, finally, Table VI shows a fairly large lattice expansion, mainly due to the size effect. Incorporation of Mg in the large concentrations required to achieve adequate *p*-type conductivity may thus lead to an observable change in the lattice constant.

#### Unintentional impurities in GaN

Boron is an unintentional impurity that can be introduced during MBE growth. There has been speculation about whether B might act as an acceptor in GaN;<sup>162</sup> this would require it to be incorporated on the nitrogen site. The computations we will report here

indicate that incorporating B on the N site is energetically unfavorable. Even if it did incorporate there, it would act as a *deep*, rather than a shallow acceptor.

It is often assumed that isoelectronic impurities are electronically inactive. For instance, incorporation of As in GaN has traditionally been assumed to lead to substitution on the N site.<sup>163</sup> In small concentrations, As was assumed to have no effect, while in large concentrations it was assumed to lead to formation of GaAsN alloys. Van de Walle and Neugebauer<sup>164</sup> recently showed that As may actually also incorporate on the Ga site. The driving force is mainly the large size mismatch that exists between As and N: placing As on a N site creates large strains, whereas As "fits" quite nicely on a Ga site. There is, of course, an "electronic" mismatch for As on a Ga site: since As is two columns to the right of Ga in the periodic table, it acts as a double donor.

It is interesting to contemplate whether similar effects may occur for other isoelectronic impurities. Boron is a particularly important case. It may occur as an unintentional impurity during MBE growth,<sup>165</sup> and there has been some speculation that B might act as an acceptor in GaN. The driving force for this behavior would again be a preference for the impurity to occupy the site on which the size mismatch is minimized: B would prefer the N site, from this point of view. On this site, it should act as a double acceptor.

Here we report the results of first-principles calculations of the atomic and electronic structure for B on both types of sites. The results for formation energies are summarized in Fig. 62, for N-rich conditions and assuming equilibrium with BN; these choices do not affect our conclusions. The higher the formation energy, the more difficult it is to incorporate the impurity on a given site. We thus see that B overwhelmingly prefers the Ga site – although we note that even on this site its formation energy is rather high. Formation of BGaN alloys will thus be difficult, and may require conditions far from equilibrium. The configuration with B on a N site is much higher in energy, and is thus exceedingly unlikely to form. The main reason is that in this configuration, B needs to form bonds with the surrounding Ga atoms, which is energetically much less favorable than forming B-N bonds. If B would incorporate on the N site, it would behave as a double acceptor, as shown by the formation energies for 0, -, and 2- charge states in Fig. 62. The transitions between these charge states occur deep in the gap (more than 1.2 eV above the valence band). B<sub>Ga</sub> is thus a *deep* acceptor, and would not be useful for *p*-type doping of GaN.

#### Hydrogen in nitride semiconductors

Hydrogen is another unintentional impurity that can have a major effect on the properties of nitride semiconductors. Since hydrogen is present in many of the commonly used growth environments for nitrides, its incorporation (if energetically favorable) can hardly be avoided. We previously performed a comprehensive investigation of hydrogen in GaN<sup>166,167,168</sup>, and found

that hydrogen acts as a donor ( $H^+$ ) in *p*-type GaN, and as an acceptor ( $H^-$ ) in *n*-type GaN (see Fig. 63). Hydrogen is thus an *amphoteric* impurity, always acting as a compensating center and counteracting the dominant electrical conductivity of the material. The solubility of hydrogen was found to be significantly higher in *p*-type GaN than in *n*-type material.

We have now set out on an investigation of hydrogen in AlN and InN. Indeed, device structures usually incorporate layers of InGaN and/or AlGaN, and also pure AlN and InN are being investigated in their own right; a thorough understanding of hydrogen in these materials is therefore essential.

Our results for AlN (see Fig. 64) show that the behavior of H in AlN is very similar to GaN:  $H^+$  dominates in *p*-type,  $H^-$  in *n*-type. Due to the larger band gap of AlN, the solubility of H could be significantly larger than in GaN under both *p*-type and *n*-type conditions.

Our results for H in InN (Fig. 65) revealed a true surprise, however: H in InN behaves exclusively as a donor, i.e., it is *not* amphoteric as in GaN and AlN, but actually contributes to the *n*-type conductivity of the material. This donor behavior is due to the fact that  $H^0$  and  $H^-$  are always higher in energy than  $H^+$ , making  $H^+$  the *only* stable charge state for all positions of the Fermi level.

This result may help explain why, to date, all InN samples have been found to be highly *n*-type. Fig. 66 illustrates our findings for donor impurities in InN in general; the results for oxygen and silicon were taken from Ref.<sup>169</sup>, and our new results for hydrogen were added. We see that all potential donor impurities in InN have relatively low formation energies, making them really easy candidates for unintentional incorporation. Of all the donors, hydrogen actually has the lowest formation energy. Further investigations, e.g. about the diffusivity of H in InN, are planned.

#### VII. Thermal Conductivity determined by Scanning Thermal Microscopy

Scanning thermal microscopy (SThM) has been applied to measure the local thermal conductivity of epitaxial GaN. Since the thermal conductivity is affected to a large extent by phonon scattering, a closer to the true value of this parameter can be obtained by a local measurement in areas of lower defect concentration such as those found in the wing regions of lateral epitaxially grown GaN. The method relies on a thermo-resistive tip forming one quadrant of a Wheatstone bridge. The bridge is balanced with the tip heated ( $\sim 40$ - $50^\circ\text{C}$ ) followed by bringing the tip in contact with the sample under test which tends to cool down this tip due to thermal dissipation. However, the feedback circuit attempts to keep the thermo-resistance and thus the tip temperature the same. The square of the feedback voltage necessary for this compensation is proportional to the thermal conductivity. Accurate values can be obtained with

calibration using known materials such as GaSb, GaAs, InP, Si and Al metal. Using SThM, thermal conductivity,  $\kappa$ , values in the 2.0 – 2.1 W/cm-K in the wing regions of lateral epitaxially grown GaN, 1.70 – 1.75 W/cm-K in HVPE grown GaN, and 3.0 – 3.3 W/cm-K for free-standing AlN have been measured.

GaN and other group III-nitride semiconductors are considered for high power/high temperature electronic and opto-electronic devices where a key issue is the thermal dissipation. Consequently, thermal conductivity ( $\kappa$ ) is an extremely important material property. In an indirect manner the thermal conductivity is also a measure of materials quality as it degrades in defective material. Scanning thermal microscopy (SThM)<sup>170</sup> provides nondestructive, absolute measurements of the thermal conductivity with a high spatial/depth resolution of about 2 – 3  $\mu\text{m}$ . Thermal imaging achieved using a resistive thermal element incorporated at the end of a cantilever/AFM type feedback as shown in Fig. 67. The resistive tip forms one element of a Wheatstone bridge as shown in Fig. 68. Upon contact with the sample, the tip tends to cool down due to heat conduction into the sample, which is related to its thermal conductivity,  $\kappa$ . The bridge circuit applies a compensating voltage ( $U_{\text{out}}$ ) to maintain its target operating temperature. The details of the cantilever are as follows: The arms of cantilever made of Wollaston process wire: silver wire  $\sim 75$   $\mu\text{m}$  in diameter with a platinum/10% rhodium core. The tip section is  $\sim 3$   $\mu\text{m}$  in diameter. The resistive element at its end comprises a 200  $\mu\text{m}$  length of platinum/10% rhodium that has been exposed by removal of the silver and bent into a "V" shape (radius of curvature  $\sim 1$   $\mu\text{m}$ ), which acts as the probe. Spatial/depth resolution estimated to be  $\sim 2$ -3  $\mu\text{m}$  for GaN and AlN.

The feedback signal for constant resistance is a measure of the thermal conductivity of the material with which the tip is in contact, specifically  $(U_{\text{out}})^2$  is proportional to  $\kappa$  since power dissipation is the mechanism here. Measurements of the absolute values of  $\kappa$  are based on a recently developed calibration procedure. This simply comprises calibrating the feedback signal,  $U_{\text{out}}^2$ , for a constant thermal element resistance against that for samples with known conductivities such as GaSb, GaAs, InP, Si, and Al metal as shown in Fig. 69.

The SThM method has been applied to the measurement of the room temperature thermal conductivity on both fully and partially coalesced lateral epitaxial overgrown (LEO) GaN/sapphire (0001) samples.<sup>170</sup> A correlation between low threading dislocation density and high thermal conductivity values was established. The reduction in the thermal conductivity with increased dislocation density is expected as threading dislocations degrade the sound velocity and increase the phonon scattering in the material. In fact, due to the high defect concentrations in early films, the thermal conductivity value measured was 1.3 W/cm-K.<sup>171</sup> The highest GaN  $\kappa$  values to date, in the 2.0 – 2.1 W/cm-K range, were found on samples at the regions that were

laterally grown which contain the lowest density of threading dislocations. Even then it falls short of the recent predictions by Witek.<sup>172</sup>

The thermal conductivity has also been correlated doping levels in hydride vapor phase epitaxy (HVPE) *n*-GaN/sapphire (0001) by SThM on two sets of samples.<sup>173,174</sup> In both sets of data the thermal conductivity decreased linearly with  $\log n$ ,  $n$  being the electron concentration, the variation being about a factor of two decrease in  $\kappa$  for every decade increase in  $n$ . Significantly, it was concluded that the decrease in the lattice contribution to  $\kappa$ , due to increased phonon scattering from impurities and free electrons, predominates over the increase in the electronic contribution. Also, a correlation between film thickness and improved thermal conductivity was found which is consistent with the observed general reduction of both extended (dislocations) and point defects with film thickness.<sup>51,174</sup> The  $\kappa$  values at 300K before and after plasma-induced effects on a series of *n*-GaN/sapphire (0001) samples fabricated by HVPE was also measured.<sup>175</sup> The sample thicknesses were  $50 \pm 5$   $\mu\text{m}$  and the carrier concentrations  $\sim 8 \times 10^{16} \text{ cm}^{-3}$ , as determined by Hall effect measurements. The thermal conductivity before treatment was found to be in the 1.70 – 1.75 W/cm-K range, similar to that previously reported for HVPE material with this carrier concentration and thickness.<sup>173,174</sup> The  $\kappa$  value was reduced however when the samples were processed under constant Ar gas flow and pressure for a fixed period of time (5 min). The only variable processing parameter was the DC bias voltage (125 – 500 V). After the initial 125 V procedure  $\kappa$  exhibited a decrease linear in the DC voltage in the investigated range. At 125 V the thermal conductivity was only slightly less ( $\kappa \sim 1.65$  W/cm-K) than the untreated case. The values of  $\kappa$  had dropped to  $\sim 0.3$  W/cm-K for the 500 V case.

Another semiconductor, which forms the other binary end next to GaN in the formation of AlGaIn, is AlN, which is often mentioned as a substrate material for GaN. AlN is a very good thermal conductor, a point that was recognized very early on with predicted values near 3.2 W/cm-K in a simulated material containing the experimentally observed amounts of O.<sup>176</sup> A more recent prediction for the value in AlN is 5.4 W/cm-K.<sup>172</sup> Values in the 3.0 – 3.3 W/cm-K range were measured on bulk (300 – 800  $\mu\text{m}$  thick free-standing material) AlN samples.<sup>177</sup> The samples were grown by HVPE on Si (111) substrates, which were subsequently and selectively removed by chemical etching. The dislocation density in the free-standing AlN templates was about  $10^8 \text{ cm}^{-2}$ .<sup>178</sup> These are the highest reported to date in AlN and bodes well for the heat dissipation capability of this material.

## VIII. Conclusions

Extended defects by TEM, the density of defects by decorating them with chemical etches, point defects as manifested in the form of deep levels, by DLTS, PL, positron annihilation, and EPR, and scattering due to

ionized impurities by temperature and magnetic field dependent Hall measurements have been analyzed. The HVPE films were exhaustively characterized with sophisticated and sensitive electrical, optical and analytical tools, and augmented by theory dealing with defect and impurity behavior.

TEM analyses indicated that in Hydride VPE samples the dislocation density is near  $10^{10} \text{ cm}^{-2}$  in 1.5  $\mu\text{m}$  thick films and dropped to about  $10^8 \text{ cm}^{-2}$  near the surface of a 55  $\mu\text{m}$  thick sample. The dislocation density at the interface was about  $10^{13} \text{ cm}^{-3}$ . Assuming reproducibility, these figures represent the depth distribution of extended defects. Photoenhanced chemical etching in KOH and hot phosphoric acid etching indicated the defect concentration near the surface to be about  $8 \times 10^8 \text{ cm}^{-3}$ , in good agreement with TEM.

Hall measurements (mobility improves from 190 and 740  $\text{cm}^2 \text{V}^{-1} \text{s}^{-1}$  in the same thickness range while the electron concentration drop from about  $10^{18} \text{ cm}^{-3}$  for the 5  $\mu\text{m}$  film to about  $10^{17} \text{ cm}^{-3}$  for those thickest sample which was as thick as 68  $\mu\text{m}$  in places), SIMS depth profiles, and minority carrier lifetime measurements, DLTS analysis all agree that the films improve with thickness. Six deep levels were and in conjunction with electron beam induced defects, their likely origins determined. Differential Hall measurements indicate that the mobility near the surface could be as high as 1200  $\text{cm}^2 \text{V}^{-1} \text{s}^{-1}$ . Both O and Si concentrations drop rapidly away from the surface into the sample from mid  $10^{19} \text{ cm}^{-3}$  for O and mid  $10^{18} \text{ cm}^{-3}$  for Si down to about  $10^{17} \text{ cm}^{-3}$  for Si and high  $10^{16} \text{ cm}^{-3}$  for O.

The diffusion length increased linearly from 0.25  $\mu\text{m}$ , at a distance of about 5  $\mu\text{m}$  from the GaN/sapphire interface, to 0.63  $\mu\text{m}$  at the GaN surface of the thickest film. Positron annihilation experiments indicate the Ga-vacancy concentration to be mid  $10^{19} \text{ cm}^{-3}$  near the interface and about  $10^{17} \text{ cm}^{-3}$  near the surface for the layer with a thickness greater than 30  $\mu\text{m}$  (could be as high as 68  $\mu\text{m}$ ). ODMR and EPR measurements have been made in both Lincoln and Samsung HVPE layers. The ODMR signal in a 5-10  $\mu\text{m}$  thick GaN layer from the 2.2 eV peak, the notorious yellow peak, with magnetic field perpendicular and parallel to the c-axis show signatures of shallow donor (effective mass like) and deep donor transitions with 1.95 and 1.99 g-values, respectively. The thermal conductivity of these sorts of HVPE films was determined to be about 1.75 W/cm-K. This figure degrades with defects and electrons as they scatter phonons.

Several of the Samsung freestanding GaN templates were also analyzed in similar fashion. The substrate side was confirmed to be N-face. The density of dislocations near the N-face was determined to be, in order,  $3 \pm 1 \times 10^7$  and  $4 \pm 1 \times 10^7$  by cross-sectional TEM and plan-view TEM, respectively. Identical observations on the Ga-face revealed the defect concentration to be less than  $1 \times 10^7 \text{ cm}^{-2}$  by plan-view TEM and  $5 \times 10^5 \text{ cm}^{-2}$  by cross-sectional TEM. Defect revealing etches led to

concentrations on Ga and N-faces of about  $5 \times 10^5 \text{ cm}^{-2}$  for the former and about  $1 \times 10^7 \text{ cm}^{-2}$  for the latter, which are in very good agreement with TEM observations.

The Samsung template investigated had peaks with FWHM values of 20.6 and 24 arcmin for [002] and [104] diffractions, respectively, on the Ga-face when a 2 mm slit size was used. When the slit size was reduced to 0.02 mm, the Ga and N-face [002] peaks reduced to 69 and 160 arcseconds. This may indicate that the sample may have been bowed since the dislocation density is low and can not account for the observed broadening. A bowing radius of 1.2 m was calculated for the observed broadening with wider slits. The Ga-face SIMS profile in the Samsung template indicates levels below mid  $10^{16} \text{ cm}^{-3}$  for all three of the impurities whereas the N-side has an impurity concentration that is 1-3 orders of magnitude higher than that for the Ga-face. Particularly the concentration of O and C is high, albeit some drop occurs as one goes deeper into the film. This should be re-examined in a sample where the N-surface etched.

Detailed transport measurements were undertaken at AFRL and VCU in Samsung HVPE material in an effort to gain insight to impurities and defect including their depth profiles, and scattering events. The Samsung free-standing GaN template made it possible for us to remove some 30  $\mu\text{m}$  of the interfacial layer to make sure that the measurements were not affected by the highly conductive what would have been the interfacial layer before laser separation leading to electron mobilities of 1425  $\text{cm}^2/\text{Vs}$  at  $T=273 \text{ K}$  and 7385  $\text{cm}^2/\text{V}\cdot\text{s}$  at 48.2 K. Excellent fit to the measured mobility in the temperature range of 30 – 273 K was obtained by using an iterative BTE method, so was the case for the temperature dependent electron concentration. Utilizing the acceptor concentration determined from the fit to the Hall data ( $2.4 \times 10^{15} \text{ cm}^{-3}$ ), and the charge balance equation, a donor concentration of  $1.6 \times 10^{16} \text{ cm}^{-3}$ , and donor activation energy of 26 meV, the latter being the highest reported in the literature for GaN.

Deep centers in n-GaN have been characterized by DLTS in HVPE-grown Samsung templates. A collation of all the deep centers and their known characteristics are shown in Table V in the text. Centers  $A_1$  and  $E_1$  found in as-grown and thin HVPE-GaN are very similar to the centers  $A_2$  and E induced by electron-irradiation, indicating their point-defect nature. The Samsung template exhibited a new trap B, with parameters  $E_T=0.53 \text{ eV}$  and  $\sigma_T=1.5 \times 10^{-15} \text{ cm}^2$  on the Ga-face, in addition to the four traps commonly observed in various epitaxial GaN layers. For the N-face sample, a N-vacancy related trap  $E_1$ , with  $E_T=0.18 \text{ eV}$  and  $\sigma_T=4 \times 10^{-17} \text{ cm}^2$ , was observed. On the other hand, the Ga-face sample contained trap C, with  $E_T=0.35 \text{ eV}$  and  $\sigma_T=1.6 \times 10^{-15} \text{ cm}^2$ . This trap may be related to surface damage caused by the RIE process employed. A Side benefit of the DLTS investigations is that the barrier heights of Ni/Au Schottky contacts were determined to be 1.27 eV and 0.75 eV for the Ga face and N face, respectively.

Freestanding thick Samsung material along its high quality made it possible to use polarizations where the E field in the c-plane, commonly done in all PL, and along the c-axis, very uncommon to distinctly observe to types of A exciton. The former polarization favors the  $\Gamma_5$  and the latter favors the  $\Gamma_6$  free excitons. In the latter geometry the light is coupled from the side of the sample, which is rendered possible due to freestanding thick sample. Focusing on the defect region of the PL spectrum, the N-face of the sample exhibited the usual yellow line. However, the Ga-face exhibited a broad band encompassing both yellow and green bands. Upon increased below gap radiation, the yellow band saturated while the green continued to grow. It is suggested that the green line is due to Ga vacancy, where as the yellow band may be due to the same vacancy complexed with dislocations which are more abundant on the N-face than on the Ga-face.

For deeper transitions associated with defects, experiments with variation of excitation intensity and excitation energy showed two bands with maxima at about 2.15 eV (yellow luminescence) and 2.43 eV (green luminescence). Unlike in RMBE, RF-MBE and MOCVD and other HVPE grown GaN samples, the yellow luminescence in the freestanding template is weak and can be easily saturated. In contrast, the green luminescence is dominant and is attributed to the isolated defect involving gallium vacancy, whereas the yellow luminescence is related to the same defect bound to dislocation or surface bound structural defect.

FTIR measurements point to two donor levels with binding energies of 30.9 and 33.9 meV in an Lincoln sample. The former is of higher concentration than the latter and is attributed to Si donors. Splitting of the binding energies with magnetic field leads to  $m^* = 0.22 m_0$ . ODMR and EPR measurements led us to conclude that the 2.4 eV "green" PL band from the Samsung free-standing layer is a shallow donor (effective mass like) transition and has a g-value of 1.95. The larger linewidth, relative to the Lincoln layers associated with the Samsung template is indicative of reduced hyperfine interaction due to a lower concentration of this center. The Samsung free-standing sample has about  $6 \times 10^{15} \text{ cm}^{-3}$  uncompensated donors/cm<sup>3</sup> while the Lincoln sample has a concentration about a factor of four higher.

Optical transitions along the edge of the wafer extending from the surface into the substrate were investigated by micro cathodoluminescence with scanning capability. Evolution of the GaN bandedge and sapphire related peaks were monitored. In addition to the commonly observed 2.2 eV peak, which diminished toward the interface, an emission line 2.9 eV emerged at the interface. The former may be correlated with Zn pretreatments of the growth template. The latter is temporarily attributed to O diffusion.

Calculations indicate that incorporation of Si has a negligible effect on the lattice constant, but O and Mg can

lead to an observable expansion of the lattice. Since values of the GaN lattice constant have often been based on bulk crystals that are now known to contain large concentrations of oxygen, the "true" GaN lattice constant is actually smaller than what has been measured for such crystals. Boron is an unintentional impurity that can be introduced during MBE growth. There has been speculation about whether B might act as an acceptor in GaN; this would require it to be incorporated on the nitrogen site. Our computations indicate that incorporating B on the N site is energetically unfavorable. Even if it did incorporate there, it would act as a *deep*, rather than a shallow acceptor. Formation energies of H in AlN and GaN have also been calculated. The behavior of H in AlN is very similar to GaN: H<sup>+</sup> dominates in *p*-type, H in *n*-type. Surprisingly, H in InN behaves exclusively as a donor, i.e., it is *not* amphoteric as in GaN and AlN, but actually contributes to the *n*-type conductivity of the material.

Scanning thermal microscopy (SThM) has been applied to measure the local thermal conductivity of epitaxial GaN. Using SThM, thermal conductivity,  $\kappa$ , values in the 2.0 – 2.1 W/cm-K in the wing regions of lateral epitaxially grown GaN, 1.70 – 1.75 W/cm-K in HVPE grown GaN, and 3.0 – 3.3 W/cm-K for free-standing AlN have been measured.

#### Acknowledgements

The research reported here has been funded by ONR (Dr. C. E. C. Wood) and AFOSR (Dr. G. L. Witt) through a group grant to VCU, WSU and NR, with VCU as the primary institution, and individual grants to other participants. Prof. K. Saarinen of the Helsinki University of Technology contributed to the project because of his interest in the scientific problems. This report was written by Hadis Morkoç based on the material he collected from the participants detailed at the outset of this report, and the results obtained in his own group and through collaborations with his colleagues elsewhere.

## References

- 1 H. Morkoç, "Nitride Semiconductors and Devices," Springer Verlag, Heidelberg 1999.
- 2 S. N. Mohammad and H. Morkoç, "Progress and Prospects of Group III-V Nitride Semiconductors," *Progress in Quantum Electronics* 20(5 and 6), 361-525, 1996.
- 3 S. N. Mohammad, A. Salvador, and H. Morkoç, "Emerging GaN Based Devices," *Proc. IEEE* 83, 1306-1355, 1995.
- 4 H. Morkoç, S. Strite, G. B. Gao, M.E. Lin, B. Sverdlov, and M. Burns, "A Review of Large Bandgap SiC, III-V Nitrides, and ZnSe Based II-VI Semiconductor Structures and Devices," *J. Appl. Phys. Reviews* 76(3), 1363-1398, 1994.
- 5 S.T. Strite and H. Morkoç, "GaN, AlN, and InN: A Review," *J. Vacuum Science and Technology B* 10, 1237-1266, 1992.
- 6 O. Ambacher, "Growth and applications of Group III-Nitrides", *J. Phys. D: Appl. Phys.* Vol. 31, pp. 2653-2710, (1998).
- 7 S. J. Pearton, J. C. Zolper, R. J. Shul, and F. Ren, "GaN: Processing, defects, and devices", *J. Appl. Phys.* Vol. 86, pp. 1-78, (1999)
- 8 M.T. Duffy, C.C. Wang, G'D. O'Clock, S.H. McFarlane III and P.J. Zanzucchi, "Epitaxial growth and piezoelectric properties of AlN, GaN, and GaAs on sapphire or spinel" *J. Elect. Mat.* 2, 359, (1973).
- 9 M. Razeghi and A. Rogalski, "Semiconductor Ultraviolet Detectors," *J. Appl. Phys.* 79, 7433-7473, 1996.
- 10 G. Y. Xu, A. Salvador, W. Kim, Z. Fan, C. Lu, H. Tang, H. Morkoç, G. Smith, M. Estes, B. Goldenberg, W. Yang, and S. Krishnankutty, "Ultraviolet Photodetectors based on GaN p-i-n and AlGaIn(p)-GaN(i)-GaN(n) Structures," *Appl. Phys. Lett.* 71(15), 2154-156, 1997.
- 11 I. J. Fritz and T. J. Drummond, "AlN-GaN Quarter-wave Reflector Stack Grown by Gas-source MBE on (100) GaAs," *Electron. Lett.* 31, 68-69, 1995.
- 12 S. Nakamura, T. Mukai, and M. Senoh, "Candela-class High-brightness InGaIn/AlGaIn Double-heterostructure Blue Light-emitting Diodes," *Appl. Phys. Lett.* 64, 1687-1689, 1994.
- 13 For a review see: H. Morkoç and S. N. Mohammad, "High Luminosity Gallium Nitride Blue and Blue-Green Light Emitting Diodes," *Science Magazine* 267, 51-55, 1995.
- 14 For a review, see: H. Morkoç and S. N. Mohammad, "Light Emitting Diodes," in *Wiley Encyclopedia of Electrical Engineering and Electronics Engineering*, J. Webster, ed. (John Wiley and Sons, New York 1999).
- 15 S. Nakamura, M. Senoh, N. Nagahama, N. Iwara, T. Yamada, T. Matsushita, H. Kiyoku, Y. Sugimoto, T. Kozaki, H. Umemoto, M. Sano, and K. Chocho, "InGaIn/GaN/AlGaIn-Based Laser Diodes with Modulation-Doped Strained-Layer Superlattices," *Jpn. J. Appl. Phys.* 38, L1578, 1997.
- 16 H. Morkoç, "Wurtzite GaN Based Heterostructures by Molecular Beam Epitaxy," *IEEE J. Selected Topics in Quantum Electronics*, R. Miles and I. Akasaki, eds., Vol. 4, Number 3, pp. 537-549, 1998.
- 17 J. Schetzina, North Carolina State University, Private communication.
- 18 H. Temkin, Texas Tech University, Private communication.
- 19 J. C. Campbell, University of Texas at Austin, Private communication.
- 20 J. Schetzina et al. In *Proceedings of the International Conference on Silicon Carbide and Related Materials*, October 10-15, 1999, Research Triangle Park, NC USA
- 21 B. K. Ridley, "Exact electron momentum-relaxation times in GaN associated with scattering by polar-optical phonons", *Journal of Applied Physics*, vol.84, no.7, 1, pp.4020-4021 Oct. (1998).
- 22 U. V. Bhapkar, M. S. Shur, "Monte Carlo calculation of velocity-field characteristics of wurtzite GaN", *J. Appl. Phys* 82, 1649 (1997)
- 23 J. Kolnik, I.H. Oguzman, K.F. Brennan, R. Wang, P.P. Ruden, and Y. Wang, *J. Appl. Phys.* 78, pp. 1033-1038 (1995).
- 24 H. Morkoç, "Beyond SiC! III-V Nitride Based Heterostructures and Devices," in *SiC Materials and Devices*, Y. S. Park, ed., Academic Press, Willardson and Beer Series, eds. Willardson and Weber, Vol. 52, Chapter 8, pp. 307-394, 1998.
- 25 S. T. Sheppard, K. Doverspike, W. L. Pribble, S. T. Allen, J. W. Palmour, L. T. Kehias and T. J. Jenkins, "High Power Microwave GaN/AlGaIn HEMTs on Semi-insulating Silicon Carbide Substrates," *IEEE Electron. Dev. Lett.*, 20(4), 161, (1999).
- 26 Y.-F. Wu, B. P. Keller, P. Fini, S. Keller, T. J. Jenkins, L. T. Kehias, S. P. DenBaars, U. K. Mishra, "High Al-Content AlGaIn/GaN MODFET's for Ultrahigh Performance," *IEEE Electron. Dev. Lett.* 19(2), 50-53, 1998.
- 27 A. T. Ping, Q. Chen, J. W. Yang, M. A. Khan, and I. Adesida, "DC and Microwave Performance of High-Current AlGaIn/GaN Heterostructure Field Effect Transistors Grown on p-Type SiC Substrates," *IEEE Electron. Device Lett.* 19(2), 54-56, 1998.
- 28 G. J. Sullivan, M. Y. Chen, J. A. Higgins, J. W. Yang, Q. Chen, R. L. Pierson, and B. T. McDermott, "High-power 10-GHz Operation of AlGaIn HFET's on Insulating SiC," *IEEE Electron. Dev. Lett.* 19, 198-199, 1998.

- 29 S. Binari, J.M. Redwing, G. Kelner, and W. Kruppa, "AlGaIn/GaN HEMTs Grown on SiC Substrates," *Electron. Lett.* 33(3), 242-243, 1997.
- 30 N. Nguyen and C. Nguyen, and of HRL Laboratories, private communication.
- 31 T. Henderson, M.I. Aksun, C.K. Peng, H. Morkoç, P.C. Chao, P.M. Smith, K.H.G. Duh and L.F. Lester, "Microwave Performance of a Quarter Micron Gate Low Noise Pseudomorphic InGaAs/AlGaAs Modulation Doped Field Effect Transistor," *IEEE Electron. Dev. Lett.*, Vol. EDL-7, pp. 649-651, 1986.
- 32 R. J. Molnar, W. Goetz, L. T. Romano, and N. M. Johnson, "Growth of gallium nitride by hydride vapor-phase epitaxy". *Journal of Crystal Growth*, vol.178, no.1-2, , pp.147-56, June (1997)
- 33 S. Yamaguchi, M. Kariya, S. Nitta, T. Takeuchi, C. Wetzel , H. Amano, I. Akasaki, "Structural properties of InN on GaN grown by metalorganic vapor-phase epitaxy". *Journal of Applied Physics*, vol.85, no.11, 1, pp.7682-7688. June (1999).
- 34 D. C. Look, D. C. Reynolds, J. W. Hemsky, J. R. Sizelove, R. L. Jones, and R. J. Molnar, *Phys. Rev. Lett.* 79, 2273 (1997).
- 35 S. Nakamura, T. Mukai, and M. Senoh, *J. Appl. Phys.* 71, 5543 (1992).
- 36 M. E. Lin, B. Sverdlov, G. L. Zhou, and H. Morkoç, *Appl. Phys. Lett.* 62, 3479 (1993).
- 37 H. M. Ng, D. Doppalapudi, T. D. Moustakas, N. G. Weimann, and L. F. Eastman, *Appl. Phys. Lett.* 73, 821 (1998).
- 38 D. C. Look and J. R. Sizelove, *Phys. Rev. Lett.* 82, 1237 (1999);
- 39 N. G. Weimann, L. F. Eastman, D. Doppalapudi, H. M. Ng, and T. D. Moustakas, *J. Appl. Phys.* 83, 3656 (1998).
- 40 Z. Q. Fang, D. C. Look, W. Kim, Z. Fan, A. Botchkarev, and H. Morkoc, *Appl. Phys. Lett.* 72, 2277 (1998);
- 41 K. Wook, A. E. Botchkarev, H. Morkoc, Z. Q. Fang, D. C. Look, and D. J. Smith, *J. Appl. Phys.* 84, 6680 (1998)
- 42 B. Heying, I. Smorchkova, C. Poblentz, C. Elsass, P. Fini, and S. Den Baars, U. Mishra, and J. S. Speck, "Optimization of the surface morphologies and electron mobilities in GaN grown by plasma-assisted molecular beam epitaxy", *Applied Physics Letters*, Vol. 77, No. 18, pp. 2885-2887, 30 October 2000
- 43 M. J. Manfra, L. N. Pfeiffer, K. W. West, H. L. Stormer, K. W. Baldwin, J. W. P. Hsu, D. V. Lang, and R. J. Molnar, "High-mobility AlGaIn/GaN heterostructures grown by molecular-beam epitaxy on GaN templates prepared by hydride vapor phase epitaxy" *Applied Physics Letters -- Volume 77, Issue 18, pp. 2888-2890, October 30, 2000*
- 44 J. Cui, and A. Sun, M. Reshchikov, F. Yun, A. Baski, and H. Morkoç, "Preparation of Sapphire for High Quality III-Nitride Growth", *MRS Internet Journal - The URL for the front page is <http://nsr.mij.mrs.org/5/7/>*.
- 45 Powell, J. A., D. J. Larkin and A. J. Trunek (1998). Use of Gaseous Etching for the Characterization of Structural Defects in Silicon Carbide Single Crystals. *Silicon Carbide, III-Nitrides, and Related Materials*. G. Pensl, H. Morkoc, B. Monemar and E. Janzen. Sweden, Trans Tech Publications. 264-268: 421-424.
- 46 E. J. Tarsa, B. Heying, X. H. Wu, P. Fini, S. P. DenBaars, and J. S. Speck, *J. Appl. Phys.* 82, 5472 (1997)
- 47 B. Heying, R. Averbeck, L. F. Chen, E. Haus, H. Riechert, and J. S. Speck, *J. Appl. Phys.* 88, 1855 (2000).
- 48 N. Grandjean, CHREA-CNRS, Valbonne, France Private communication,
- 49 R.J. Molnar, W. Götz, L.T. Romano, and N.M. Johnson, *J. Cryst. Growth* 178, 147 (1997).
- 50 T. Detchprohm, K. Hiramatsu, H. Amano, I. Akasaki, *Appl. Phys. Lett.* 61, 2688 (1992).
- 51 Z-Q. Fang, D.C. Look, J. Jasinski, M. Benamara, Z. Liliental-Weber, K. Saarinen, R.J. Molnar, "Evolution of deep centers in GaN grown by hydride vapor phase epitaxy", *Appl. Phys. Lett.* (2000), submitted.
- 52 J. Jasinski, W. Swider, Z. Liliental-Weber, P. Visconti, K. M. Jones, M. A. Reshchikov, F. Yun, H. Morkoç, S. S. Park and K. Y. Lee, "Characterization of free-standing HVPE GaN" *Appl. Phys. Lett.*, pending.
- 53 M. K. Kelly, R. P. Vaudo, V. M. Phanse, L. Gorgens. O. Ambacher. M. Stutzmann, *Japanese Journal of Applied Physics* vol.38, no.3A, pp. L217-219, 1.March 1999.
- 54 Z-Q. Fang, D.C. Look, P. Visconti, D-F. Wang, C-Z. Lu, F. Yun, H. Morkoç, S.S. Park, and K.Y. Lee, *Appl. Phys. Lett.* Pending.
- 55 L. Chernyak, A. Osinsky, G. Nootz, A. Schulte, J. Jasinski, M. Benamara, Z. Liliental-Weber, D.C. Look, R.J. Molnar, *Appl. Phys. Lett.* 77, 875 (2000).
- 56 Z-Q. Fang, D.C. Look, J. Jasinski, M. Benamara, Z. Liliental-Weber, K. Saarinen, R.J. Molnar, *Appl. Phys. Lett.* (2000), in press.
- 57 T. Kozawa, T. Kachi, T. Ohwaki, Y. Taga, N. Koide, M. Koike, *J. Electrochem Soc.*, 143, No.1, L17 (1996).
- 58 S. K. Hong, T. Yao, B. J. Kim, S.Y. Yoon, T. I. Kim, *Appl. Phys. Lett.*, 77, 82 (2000).
- 59 S. K. Hong, B. J. Kim, H. S. Park, Y. Park, S. Y. Yoon, T. I. Kim, *J. of Crystal Growth*, 191, 275-278 (1998).
- 60 K. Shiojima, *J. Vac. Sci. Technol. B* 18 (1), 37 (2000)
- 61 T. Hino, S. Tomiya, T. Miyajima, K. Yanashima, S. Hashimoto, and M. Ikeda, *Appl. Phys. Lett.* 76, 3421 (2000).

- 62 D. A. Stocker, E. F. Schubert, J. M. Redwing, Appl. Phys. Lett. **73**, 2654 (1998).
- 63 C. Youtsey, L. T. Romano, and I. Adesida, Appl. Phys. Lett., **73**, 797 (1998).
- 64 C. Youtsey, L. T. Romano, R. J. Molnar, and I. Adesida, Appl. Phys. Lett., **74**, 3537 (1999).
- 65 P. Visconti, K. M. Jones, M. A. Reshchikov, R. Cingolani, H. Morkoç, and R. Molnar, "Investigation of defects in GaN by photo-electrochemical and hot wet etching" Appl. Phys. Lett., **77**, 3532 (2000).
- 66 L. T. Romano, B. S. Krusor, R. J. Molnar, Appl. Phys. Lett. **71**, 2283 (1997).
- 67 W. Götz, L. T. Romano, B. S. Krusor, N. M. Johnson, R. J. Molnar, Appl. Phys. Lett. **69**, 242 (1996).
- 68 D. Kapolnek, X. H. Wu, B. Heying, S. Keller, B. P. Keller, U. K. Mishra, S. P. DenBaars, and J. S. Speck, Appl. Phys. Lett. **67**, 1541 (1995).
- 69 E. J. Tarsa, B. Heying, X. H. Wu, P. Fini, S. P. DenBaars, and J. S. Speck, J. Appl. Phys. **82**, 5472 (1997).
- 70 M. K. Kelly, R. P. Vaudo, V. M. Phanse, L. Gorgens, O. Ambacher, M. Stutzmann, Japanese Journal of Applied Physics vol.38, no.3A, pp. L217-219, 1.March 1999.
- 71 P. Visconti, K. M. Jones, M. A. Reshchikov, F. Yun, R. Cingolani, H. Morkoç, S. S. Park and K. Y. Lee, "Characteristics of Free Standing Hydride Vapor Phase Epitaxy Grown GaN with very low defect concentration", Appl. Phys. Lett., in press.
- 72 F. Yun, M. A. Reshchikov, K. M. Jones, P. Visconti, H. Morkoç, S. S. Park and K. Y. Lee, "Electrical, Structural, and Optical Characterization of Free-standing GaN Template Grown by Hydride Vapor Phase Epitaxy", Solid State Electronics, Vol. **44**, pp. 2225 (2000).
- 73 B. Heying, X. H. Wu, S. Keller, Y. Li, B. Keller, S. P. DenBaars, and J. S. Speck, Appl. Phys. Lett. **68**, 643(1996)
- 74 T. Metzger, P. Hopler, E. Born, O. Ambacher, M. Stutzmann, R. Stommer, M. Schuster, H. Gobel, S. Christiansen, M. Albrecht and H. P. Strunk: Philos. Mag. **A77**, 1013(1998)
- 75 W. S. Wong, T. Sands, and N. W. Cheung, Appl. Phys. Lett. **72**, 599(1998)
- 76 M. Leszczynski, T. Suski, H. Teisseyre, P. Perlin, I. Grzegory, J. Jun, S. Porowski and T. D. Moustakas, J. Appl. Phys. **76**, 4909(1994)
- 77 D.C. Look and R.J. Molnar, Appl. Phys. Lett. **70**, 3377 (1997).
- 78 C.E. Stutz, M. Mack, M.D. Bremser, O.H. Nam, R.F. Davis, and D.C. Look, J. Electronic Mater. **27**, L26 (1998)
- 79 D.C. Look, J. Appl. Phys. **57**, 377 (1985)
- 80 D. Huang, F. Yun, P. Visconti, M. A. Reshchikov, K. M. Jones, D. Wang, H. Morkoç, D. L. Rode, L. A. Farina, Ç. Kurdak, K. T. Tsen, S. S. Park and K. Y. Lee, "Hall mobility and carrier concentration in GaN free-standing templates grown by hydride vapor phase epitaxy with high quality", pending.
- 81 D. L. Rode, "Low field electron transport", Semiconductors and Semimetals **10**, pp1-89, (Academic, New York 1975).
- 82 H. Brooks, Phys. Rev. **83**, 879(1951)
- 83 D. C. Look: Electrical Characterization of GaAs Materials, Devices (Wiley, New York 1989).
- 84 H. Ehrenreich, J. Phys. Chem. Solids, **8**, 130(1959)
- 85 D. A. Anderson and N. Aspley, Semicond. Sci. Technol., **1**, 187(1986)
- 86 L. Hsu, and W Walukiewicz, Phys. Rev. B **56**, 1520 (1997)
- 87 C. Eginsoy, Phys. Rev. **79**, 1013(1950)
- 88 M.E. Lin, Z. Ma, F.Y. Huang, Z. F. Fan, L.H. Allen, and H. Morkoç, "Low Resistance Ohmic Contacts on Wide Bandgap GaN," Appl. Phys. Lett. Vol. **64**, pp. 1003- , (1994).
- 89 D. C. Reynolds, D. C. Look, B. Jogai, A.W. Saxler, S.S. Park, Y., J. Hahn, "Identification of the  $\Gamma_5$  and  $\Gamma_6$  free excitons in GaN", Applied Physics Letters, vol.77, no.18, 30 Oct. 2000, pp.2879-81.
- 90 J. J. Hopfield and D. G. Thomas, Phys. Rev. **122**, 35 (1961).
- 91 D. C. Reynolds, D. C. Look, B. Jogai, C. W. Litton, T. C. Collins, M. T. Harris, M. J. Callahan, and J. S. Bailey, J. Appl. Phys. **86**, 1 (1999).
- 92 M. A. Reshchikov, P. Visconti, and H. Morkoç, "Blue photoluminescence activated by surface states in GaN", Appl. Phys. Lett., in press.
- 93 Michael A. Reshchikov, Paolo Visconti, Hadis Morkoç, Richard J. Molnar and Cole W. Litton, "Blue Photoluminescence Activated by Surface States in GaN" International Workshop on Nitride Semiconductors, Sept. 25-27, 2000, Nagoya, Japan.
- 94 D. C. Reynolds, D. C. Look, B. Jogai, A. W. Saxler, S. S. Park and J. Y. Hahn, "Identification of the  $\Gamma_5$  and  $\Gamma_6$  free excitons in GaN" Applied Physics Letters, Vol. **77**, No. **18**, pp. 2879-2881, 30 October 2000
- 95 J. J. Hopfield and D. G. Thomas, Phys. Rev. **122**, 1 (1961).
- 96 K. Kornitzer, T. Ebner, K. Thonke, R. Sauer, C. Kirchner, V. Schwegler, M. Kamp, M. Leszczynsky, I. Grzegory and S. Porowski, Phys. Rev. B **60**, 1471 (1999).
- 97 M. A. Reshchikov and H. Morkoç, S. S. Park and K. Y. Lee, "Yellow and Green Luminescence in free-standing GaN template" Appl. Phys. Lett., pending.
- 98 M. A. Reshchikov, F. Yun, H. Morkoç, S. S. Park and K. Y. Lee, "Defect-related transient photoluminescence in freestanding GaN" Appl. Phys. Lett., pending.

- 99 E. R. Glaser, T. A. Kennedy, K. Doverspike, L. B. Rowland, D. K. Gaskill, J. A. Freitas, Jr, M. Asif Khan, D. T. Olson, J. N. Kuznia, and D. K. Wickenden, *Phys. Rev. B* **51**, 13326 (1995).
- 100 T. Ogino and M. Aoki, *Jap. J. Appl. Phys.* **19**, 2395 (1980).
- 101 K. Saarinen, T. Laine, S. Kuisma, J. Nissilä, P. Hautojärvi, L. Dobrzynski, J. M. Baranowski, K. Pakula, R. Stepniewski, M. Wojdak, A. Wyszomolek, T. Suski, M. Leszczynski, I. Grzegory, and S. Porowski, *Phys. Rev. Lett.* **79**, 3030 (1997).
- 102 J. Neugebauer and C. G. Van de Walle, *Appl. Phys. Lett.* **69**, 503 (1996).
- 103 T. Mattila and R. M. Nieminen, *Phys. Rev. B* **55**, 9571 (1997).
- 104 I. Shalish, L. Kronik, G. Segal, Y. Rosenwaks, Y. Shapira, U. Tisch, and J. Salzman, *Phys. Rev. B* **59**, 9748 (1999).
- 105 E. Calleja, F. J. Sanchez, D. Basak, M. A. Sanchez-Garsia, E. Munoz, I. Izpura, F. Calle, J. M. G. Tijero, J. L. Sanchez-Rojas, B. Beaumont, P. Lorenzini and P. Gibart, *Phys. Rev. B* **55**, 4689 (1997).
- 106 M. A. Reshchikov, F. Shahedipour, R. Y. Korotkov, M. P. Ulmer, and B. W. Wessels, *Physica B* **273-274**, 103 (1999).
- 107 J. Elsner, R. Jones, M. I. Heggie, P. K. Sitch, M. Haugk, Th. Frauenheim, S. Öberg, and P. R. Briddon, *Phys. Rev. B*, **58**, 12571 (1998).
- 108 P. Visconti, K. M. Jones, M. A. Reshchikov, F. Yun, R. Cingolani, H. Morkoç, S. S. Park and K. Y. Lee, *Appl. Phys. Lett.* **77**, 3743 (2000).
- 109 M. A. Reshchikov, G.-C. Yi, and B. W. Wessels, *Phys. Rev.* **59**, 13176 (1999).
- 110 The upper limit of the deep donor concentration has been estimated from accounting for the electron scattering by neutral impurities.<sup>72</sup>
- 111 D. G. Thomas, J. J. Hopfield, and W. M. Augustyniak, *Phys. Rev.* **140**, A202 (1965).
- 112 M. A. Reshchikov, H. Morkoç, S. S. Park and K. Y. Lee, unpublished.
- 113 L.C. Kimerling, in "Defects in Semiconductors", Ed. S. Narayan and T. Y. Tan, Material Research Society Proceedings, Vol. 2 North Holland, New York 1981. Get something by Dave Lang
- 114 R.J. Molnar, W. Götz, L.T. Romano, and N.M. Johnson, *J. Crystal Growth* **178**, 147 (1997)].
- 115 Z.-Q. Fang, D.C. Look, P. Visconti, D.-F. Wang, C.-Z. Lu, F. Yun, H. Morkoç, S.S. Park and K.Y. Lee, "Deep centers in a free-standing GaN Template", *Appl. Phys. Letts.* Pending,
- 116 Z.-Q. Fang and D. C. Look, W. Kim and Z. Fan, A. E. Botchkarev and H. Morkoç, "Deep centers in n-GaN grown by reactive molecular beam epitaxy", *Appl. Phys. Lett.*, Vol. 72, No. 18, pp. 2277-2279, 1998.
- 117 W. Kim, A. E. Botchkarev, H. Morkoç, Z.-Q. Fang, D. C. Look, and D. J. Smith, "Effect of Ammonia Flow Rate on Impurity Incorporation and Material Properties of Si-Doped GaN Epitaxial Films Grown by Reactive Molecular Beam Epitaxy", *J. Appl. Phys.* vol.84, no.12, pp.6680-6685, 15 Dec. 1998
- 118 F.D. Aulet, S.A. Goodman, F.K. Koschnick, J-M. Spaeth, B. Beaumont, and P. Gibart, *Appl. Phys. Lett.* **74**, 2173 (1999).
- 119 P.J. Hansen, Y.E. Strausser, A.N. Erickson, E.J. Tarsa, P. Kozodoy, E.G. Brazel, J.P. Ibbetson, U. Mishra, V. Narayanamurti, S.P. DenBaars, and J.S. Speck, *Appl. Phys. Lett.* **72**, 2247 (1998).
- 120 T. Sugahara, H. Sato, M. Hao, Y. Naoi, S. Kurai, S. Tottori, K. Yamashita, K. Nishino, L.T. Romano, and S. Sakai, *Jpn. J. Appl. Phys.* **37**, pt 2, L398 (1998).
- 121 D.C. Look and J.R. Sizelove, *Phys. Rev. Lett.* **82**, 1237 (1999).
- 122 A.F. Wright and U. Grossner, *Appl. Phys. Lett.* **73**, 2751 (1998).
- 123 W. Götz, N.M. Johnson, D.P. Bour, C. Chen, H. Liu, C. Kuo, and W. Imler, *Mater. Res. Soc. Symp. Proc.* **395**, 443 (1996).
- 124 Z.-Q. Fang, D.C. Look, W. Kim, and H. Morkoç, *Mater. Res. Soc. Symp. Proc.* **595**, W11.84 (2000).
- 125 W.I. Lee, T.C. Huang, J.D. Guo, and M.S. Feng, *Appl. Phys. Lett.* **67**, 1721 (1995).
- 126 P. Hacke, H. Nakayama, T. Detchprohm, K. Hiramatsu, and N. Sawaki, *Appl. Phys. Lett.* **68**, 1362 (1996).
- 127 P. Hacke, P. Ramvall, S. Tanaka, Y. Aoyagi, A. Kuramata, K. Horino, and H. Munekata, *Appl. Phys. Lett.* **74**, 543 (1999).
- 128 H.M. Chung, W.C. Chuang, Y.C. Pan, C.C. Tsai, M.C. Lee, W.H. Chen, W.K. Chen, C.I. Chiang, C.H. Lin, and H. Chang, *Appl. Phys. Lett.* **76**, 897 (2000).
- 129 Z.-Q. Fang, L. Polenta, J.W. Hemsky, and D.C. Look, to be published in the Proceedings of the 11th Conference on Semiconducting and Insulating Materials (SIMC-XI), Canberra, Australia, 2000.
- 130 K. Saarinen, P. Seppälä, J. Oila, P. Hautojärvi, C. Corbel, O. Briot, and R.L. Aulombard, *Appl. Phys. Lett.* **73**, 3253-3255 (1998).
- 131 H.J. Leamy, *J. Appl. Phys.* **53**, R51 (1982).
- 132 Z.Z. Bandi, P.M. Bridger, E.C. Piquette, T.C. McGill, *Solid-State Electron.* **44**, 221 (2000)
- 133 L. Chernyak, A. Osinsky, H. Temkin, J.W. Yang, Q. Chen, M.A. Khan, *Appl. Phys. Lett.* **69**, 2531 (1996)
- 134 L. Chernyak, A. Osinsky, V. Fuflyigin, E.F. Schubert, *Appl. Phys. Lett.* **77**, 875 (2000).

- 135 C.A. Dimitriadis, *J. Phys. D* **14**, 2269 (1981).
- 136 K.L. Luke, O. von Roos, L.-J. Cheng, *J. Appl. Phys.* **57**, 1978 (1985)
- 137 M.E. Aumer, S.F. LeBoeuf, M. Smith, L.Y. Lin, H.X. Jiang, S.M. Bedair, Electronic Materials Conference, June 21-23, 2000, University of Denver, Denver, CO.
- 138 X. Zhang, D.H. Rich, J.T. Kobayashi, N.P. Kobayashi, P.D. Dapkus *Appl. Phys. Lett.* **73**, 1430 (1998)
- 139 K. Saarinen, P. Hautojärvi, and C. Corbel, in *Identification of Defects in Semiconductors*, edited by M. Stavola (Academic, New York, 1998).
- 140 L. V. Jorgensen, A. C. Kruseman, H. Schut, A. v. Veen, M. Fanciulli, and T. D. Moustakas, *Mater. Res. Soc. Symp. Proc.* **449**, 853 (1997).
- 141 E. Calleja et al., *Phys. Rev. B* **58**, 1550 (1998).
- 142 J. Neugebauer and C. Van de Walle: *Appl. Phys. Lett.* **69**, 503 (1996).
- 143 K. Saarinen, in *III-V Nitride Semiconductors: Electrical, Structural and Defects properties*, edited by M. O. Manasreh (Gordon and Breach, Amsterdam), in press.
- 144 K. Saarinen, J. Nissilä, P. Hautojärvi, J. Likonen, T. Suski, I. Grzegory, B. Lucznik, and S. Porowski, *Appl. Phys. Lett.* **75**, 2441 (1999).
- 145 K. Saarinen, T. Suski, I. Grzegory, and D. C. Look, submitted for publication.
- 146 J. Oila, V. Ranki, J. Kivioja, K. Saarinen, P. Hautojärvi, J. Likonen, J. M. Baranowski, K. Pakula, T. Suski, M. Leszczynski, and I. Grzegory, *Phys. Rev. B*, in press
- 147 Galina Popovici, Wook Kim, Andrei Botchkarev, Haipeng Tang, James Solomon, and Hadis Morkoç, "Impurity Contamination of GaN Epitaxial Films From Sapphire, SiC, and ZnO Substrates", *Appl. Phys. Lett.* Vol. 71, pp. 3385-3387, (1997).
- 148 E. R. Glaser, T. A. Kennedy, K. Doverspike, L. B. Rowland, D. K. Gaskill, J. A. Freitas Jr, M. Asif Khan, D. T. Olsen, J. N. Kuznia and D. K. Wickenden, *Phys. Rev. B* **51**, 13326 (1995).
- 149 T. Suski, P. Perlin, H. Teisseyre, M. Leszczynski, I. Grzegory, J. Jun, M. Bockowski, S. Porowski and T. D. Moustakas, *Appl. Phys. Lett.* **67**, 2188 (1995).
- 150 M. A. Reshchikov, G.-C. Yi and B. W. Wessels, *Phys. Rev. B* **59**, 13176 (1999).
- 151 C. Bozdog et al., *Phys. Rev. B* **59**, 12479 (1999).
- 152 E. Glaser et al., *Physica B* **273-274**, 58 (1999), to be published
- 153 J.I. Pankove and J.A. Hutchby, *J. Appl. Phys.* **47**, 5387 (1976).
- 154 S. Gu et al., *Appl. Phys. Lett.* **76**, 3453 (2000).
- 155 W. Götz, et al., *Mater. Res. Soc. Symp. Proc.* **449**, 525 (1997).
- 156 G. S. Cargill III, J. Angilello, and K. L. Kavanagh, *Phys. Rev. Lett.* **61**, 1748 (1988).
- 157 C. G. Van de Walle, to be published.
- 158 C. G. Van de Walle and J. Neugebauer, *Appl. Phys. Lett.* **70**, 2577 (1997).
- 159 L. T. Romano, C. G. Van de Walle, J. W. Ager III, W. Götz, and R. S. Kern, *J. Appl. Phys.* **87**, 7745 (2000).
- 160 S. Porowski, *J. Cryst. Growth* **189/190**, 153 (1998).
- 161 P. Perlin, T. Suski, A. Polian, J. C. Chervin, W. Knap, J. Camassel, I. Grzegory, S. Porowski and J. W. Erickson, *Mater. Res. Soc. Symp. Proc.* **449**, 519 (1997).
- 162 M. Yoder, private communication.
- 163 T. Mattila and A. Zunger, *Phys. Rev. B* **58**, 1367 (1998).
- 164 Chris G. Van de Walle and J. Neugebauer, *Appl. Phys. Lett.* **76**, 1009 (2000).
- 165 T. H. Myers, West Virginia University, private communication.
- 166 J. Neugebauer and C. G. Van de Walle, *Appl. Phys. Lett.* **68**, 1829 (1996).
- 167 J. Neugebauer and C. G. Van de Walle, *Phys. Rev. Lett.* **75**, 4452 (1995).
- 168 J. Neugebauer and C. G. Van de Walle, in *Hydrogen in Semiconductors II*, edited by N. H. Nickel, *Semiconductors and Semimetals Vol. 61*, Treatise Eds. R. K. Willardson and E. R. Weber (Academic Press, Boston, 1999), p. 479.
- 169 C. Stampfl, C. G. Van de Walle, D. Vogel, P. Krüger, and J. Pollmann, *Phys. Rev. B* **61**, R7846 (2000).
- 170 D.I. Florescu, V.M. Asnin, F.H. Pollak, A.M. Jones, J.C. Ramer, M.J. Schurman, and I. Ferguson, *Appl. Phys. Lett.* **77**, 1464 (2000).
- 171 E.K. Sichel and J.I. Pankove, *J. Phys. Chem. Solids* **38**, 330, (1977).
- 172 A. Witek, "Some aspects of thermal conductivity of isotopically pure diamond-a comparison with nitrides", *Diamond & Related Materials*, vol.7, no.7, pp.962-964, July 1998.
- 173 D.I. Florescu, V.M. Asnin, F.H. Pollak, and R.J. Molnar, *Mater. Res. Soc. Symp. Proc.* **595**, 3.89.1 (2000).
- 174 D.I. Florescu, V.M. Asnin, F.H. Pollak, R.J. Molnar, and C.E.C. Wood, *J. Appl. Phys.* **88**, 3295 (2000).
- 175 D.I. Florescu, F.H. Pollak, William B. Lanford, Farid Khan, I. Adesida, and R.J. Molnar, to be published in *Mater. Res. Soc. Symp. Proc.* 2001.
- 176 G.A. Slack, *J. Phys. Chem. Solids* **34**, 321, (1973).
- 177 D.I. Florescu, F.H. Pollak, A.M. Jones, J.C. Ramer, M.J. Schurman, I. Ferguson, A.E. Nikolaev, Yu V. Melnik, Katie Tsvetkov, and Vladimir Dmitriev, private communications.

---

178 A. Nikolaev, I. Nikitina, A. Zubrilov, M. Mynbaeva,  
Y. Melnik, and V. Dmitriev, Mater. Res. Soc. Symp. Proc.  
595, 6.5.1 (2000).

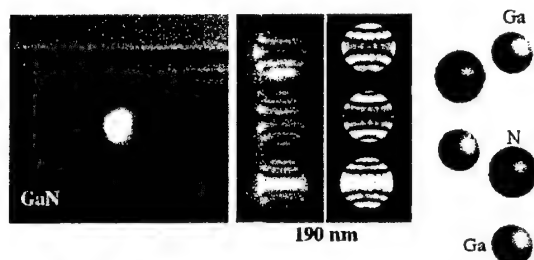


Fig. 1. Polarity determination for LH2661 (-7,3)G layer

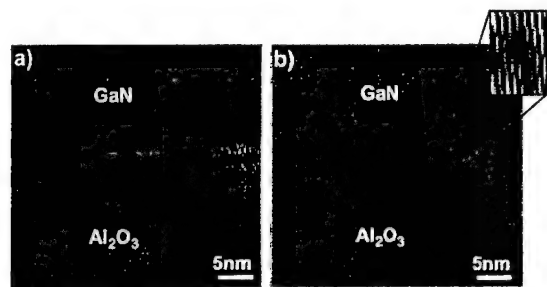


Fig. 2. High resolution electron microscopy (HREM) image of the interface in LH2661 (-7,3)G sample (a). An appropriate filtering in the Fourier space enhances visibility of misfit dislocations present at this interface (b). Inset shows clearly one of such dislocations.

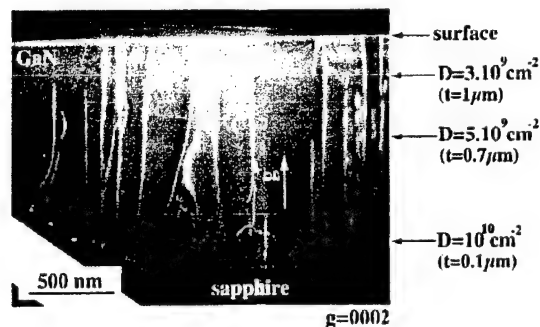


Fig. 3. Determination of density of threading dislocations in LH1089 (1,-3)G layer.

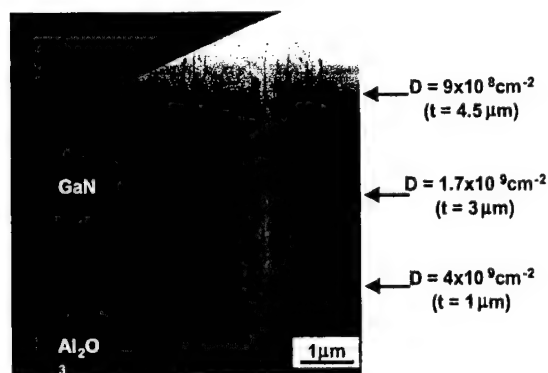


Fig. 4. Determination of density of threading dislocations in LH1106 (7,-5)G layer.

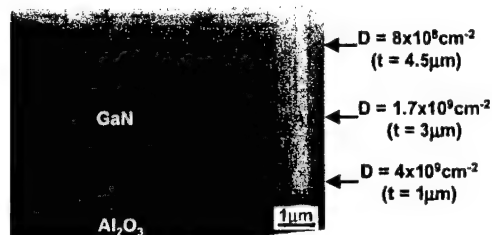


Fig. 5. Determination of density of threading dislocations in LH1106 (1,-5)G layer.

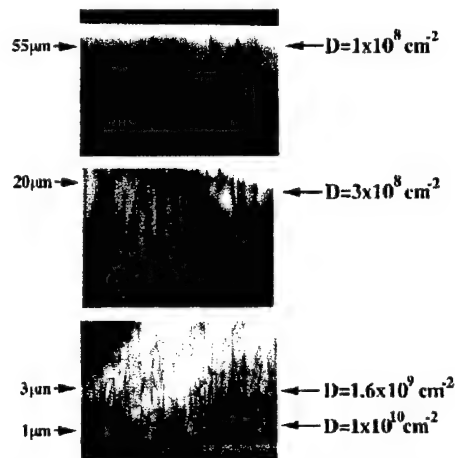


Fig. 6. Determination of density of threading dislocations in LH1106 (7,-5)G layer.

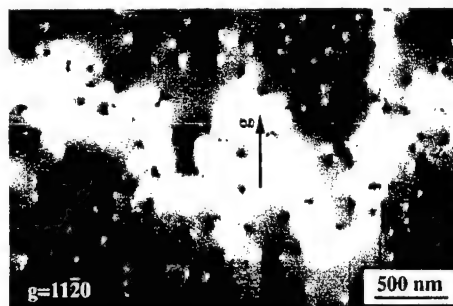


Fig. 7. Threading dislocations at the surface of LH1089 (1,-3)G layer ( $D = 2 \times 10^9 \text{ cm}^{-2}$ ).

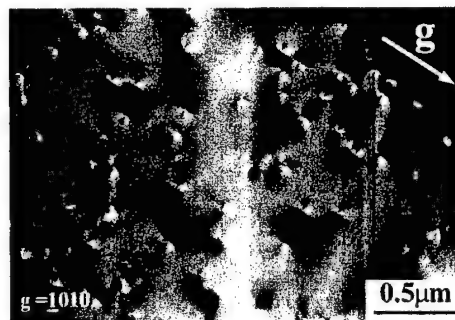


Fig. 8. Threading dislocations at the surface of LH1106 (1,-5)G layer ( $D = 1 \times 10^9 \text{ cm}^{-2}$ ).

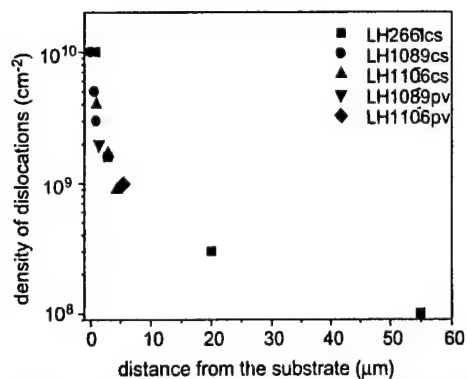


Fig. 9 Density of threading dislocations vs. distance from the interface.

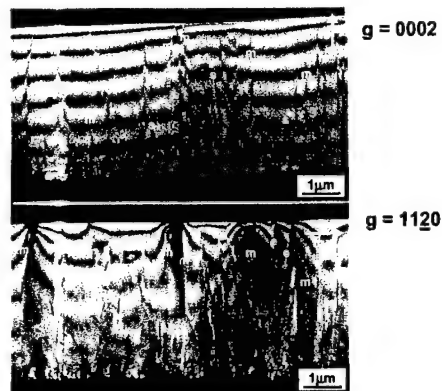


Fig. 12. Threading dislocations type determination for LH1106 (1,-5)G layer.

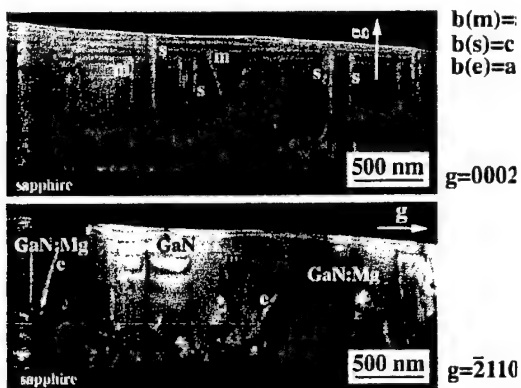


Fig. 10. Threading dislocations type determination for LH1089 (1,-3)G layer

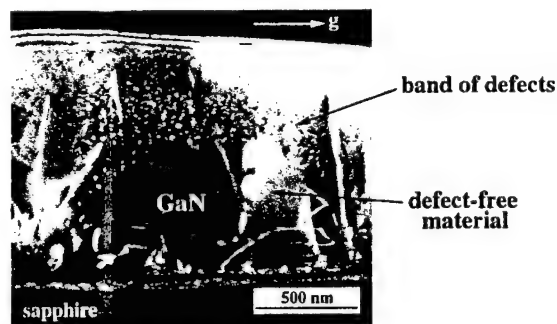


Fig. 13. A band of pyramidal defects observed in LH1089 (1,-3)G layer

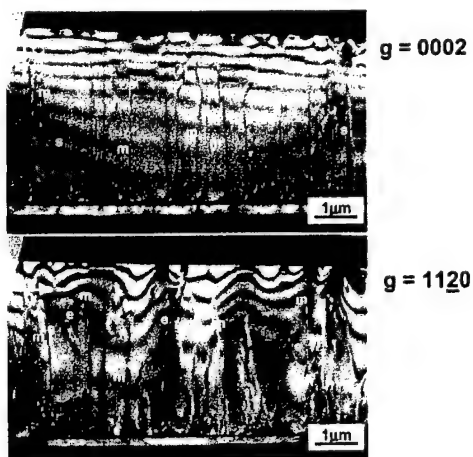


Fig. 11. Threading dislocations type determination for LH1106 (7,-5)G layer

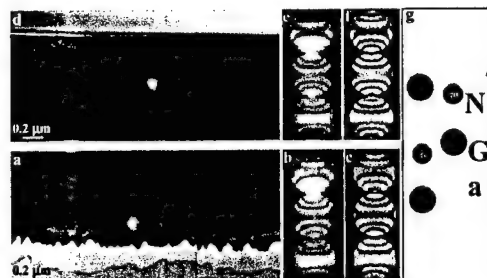
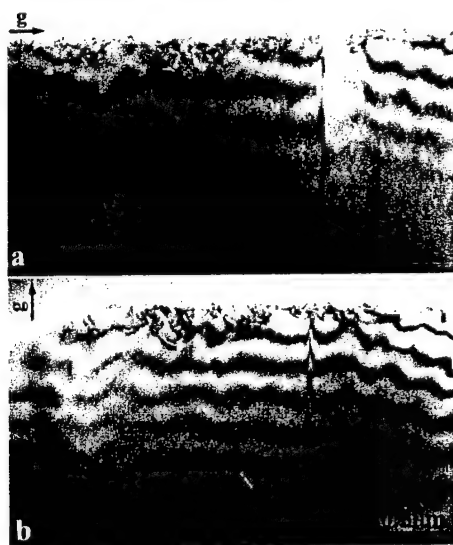


Fig. 14. TEM micrographs taken near surfaces (a) previously attached to the substrate and (d) top surface of the template. Experimental [1100] CBED patterns (b and e) taken from marked areas shown in images a and d, respectively. Simulated (for 185 nm and 200 nm, respectively) CBED patterns (c and f). Distribution of N and Ga atoms along the c-axis (g). Growth direction is shown by arrow.



**Fig. 15.** Bright-field TEM micrograph of a plan-view sample prepared for the N-face (a) and Ga-face (b), respectively. Visible edge-on dislocations are marked with arrows



**Fig. 16.** Bright field TEM micrographs of a cross-section sample near the N-face side for the g-vectors perpendicular (a) and parallel (b) to the c-axis. Note that both dislocations are visible in both images.

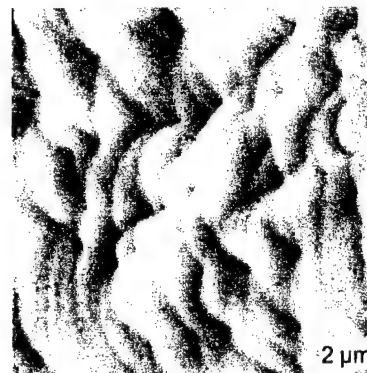


**Fig. 17.** AFM image ( $2 \times 2 \mu\text{m}^2$ ) of as-grown GaN. Some point defects (pits) have positioned at surface step terminations are visible. The average step height is of 0.8 nm and the root mean square (Rms) roughness of 0.4 nm. The vertical scale ranges from 0 to 10nm

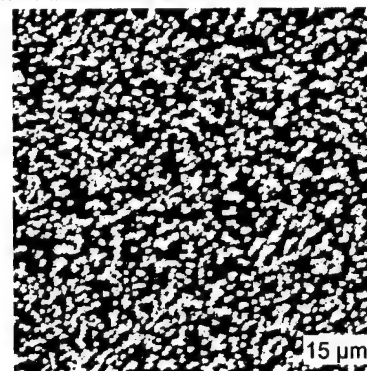


**Fig. 18.** AFM image ( $15 \times 15 \mu\text{m}^2$ ) of the GaN sample etched by PEC process. "Whisker-like" features revealed by etching are present on the surface. We estimate the height of the features to be about 700 nm and the lateral size of the order of 100 nm. The density is approximately  $2 \times 10^9 \text{ cm}^{-2}$ . The vertical scale ranges from 0 to 1200 nm.

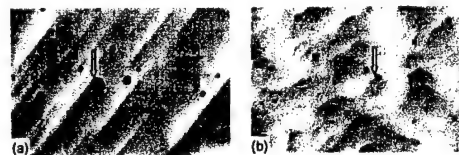


**Fig. 19.** AFM images ( $2 \times 2 \mu\text{m}^2$ ) of the GaN samples etched by wet etching (a) surface morphology of GaN sample after etching by molten KOH for 2 min. at 210 °C. Etch pits are revealed on the surface with a density of  $1 \times 10^9 \text{ cm}^{-2}$ . (b) surface morphology of GaN sample after etching by molten  $\text{H}_3\text{PO}_4$  for 6 min. at 160 °C. The EPD is the same found for the KOH etched sample. The vertical scale ranges from 0 to 10 nm.

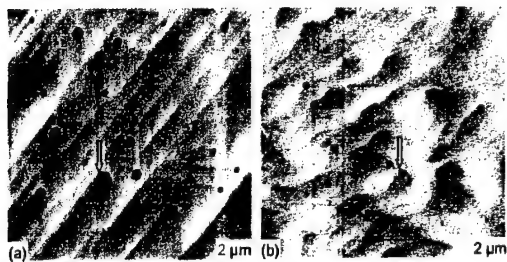


**Fig. 20.** AFM image ( $15 \times 15 \mu\text{m}^2$ ) of the GaN sample etched for 10 min at 200 °C using  $\text{H}_3\text{PO}_4$ . Two different types of etch pits with different sizes are revealed on the etched surface. Altogether, we estimated the EPD to be  $1 \times 10^8 \text{ cm}^{-2}$ . The vertical scale ranges from 0 to 450 nm.

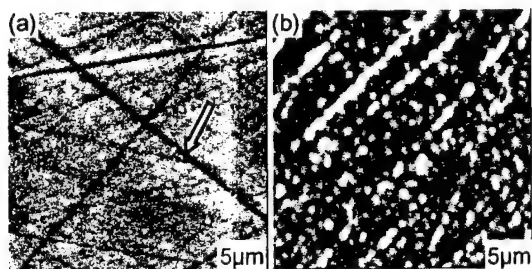


**Fig. 21.** AFM images of the mechanical-chemically polished and dry etched Ga face (a), and the mechanical-chemically polished N face (b) of the GaN substrate. The lines visible in (a) result from the mechanical polishing of the Ga face. Less distinct lines can also be seen on the N face (b).

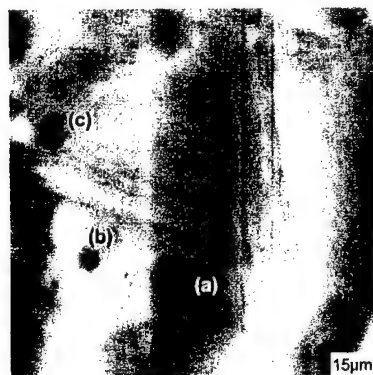


**Fig. 22.** AFM image of the N face of the substrate after etching in  $\text{H}_3\text{PO}_4$  for 15 seconds at 160°C. The surface has been significantly etched at defect sites; so much that valleys, ridges and terraces have been formed on the surface. The deep etch pits on the surface marked (a), (b), and (c) are 2.1  $\mu\text{m}$ , 1.2  $\mu\text{m}$ , and 1.5  $\mu\text{m}$  wide by 6 nm, 4.7 nm, and 8 nm deep respectively.

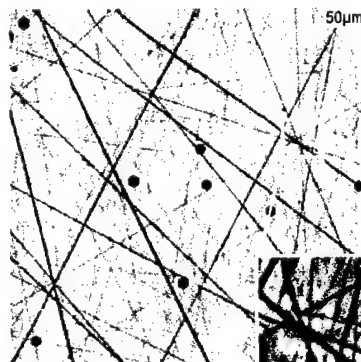


**Fig. 23.** AFM image of the Ga face etched for 50 min at 160°C in  $\text{H}_3\text{PO}_4$ . The lines from the etching are still visible on the surface, indicating that the non-defective GaN has not been significantly etched. The point defect sites on the surface have been etched by the acid. There are three discrete sizes of defects found on the surface. The large defects are roughly 1.5  $\mu\text{m}$  wide, the medium sized defects (upper left corner of image) are generally 800 nm wide, and the small defects are approximately 200 nm wide. A small defect can be seen in the inset, which is a zoom into the boxed region.

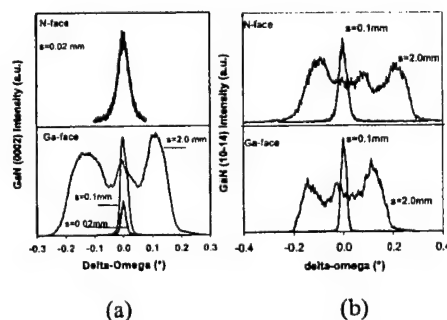


**Fig. 24.** High-resolution x-ray rocking curve (omega scan) from the unetched Ga-face and the N-face of the freestanding bulk GaN sample. (a) The symmetric (0002) peak is plotted for both the Ga- and the N-faces with the source slit width ranging from 0.02 mm to 2.0 mm; (b) The asymmetric (10-14) peak is plotted for both the Ga- and N-faces with slit width of 0.1 mm and 2.0 mm.

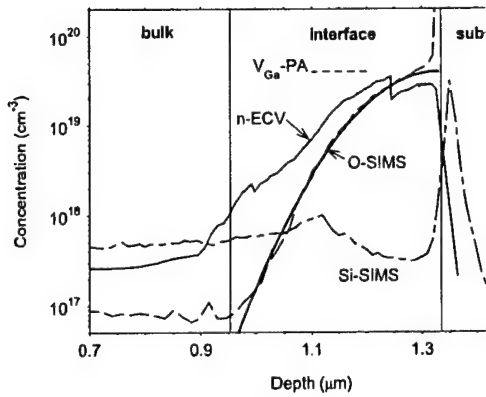


Fig. 25. SIMS profiles in a HVPE GaN layer on sapphire substrate showing the depth distributions of O and Si concentrations. The average  $n$  and true  $n$  (from Hall measurements) in HVPE GaN on  $\text{Al}_2\text{O}_3$  are also shown. For a discussion of the average and true electron concentrations, refer to the "Transport Properties section".

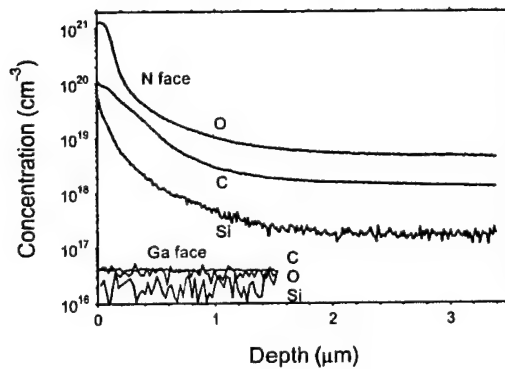


Fig. 26. SIMS profiles in a HVPE GaN template showing the depth distributions of O, C, and Si concentrations from both N- and Ga- faces with Ga-face figures being below mid  $10^{16} \text{ cm}^{-3}$ .

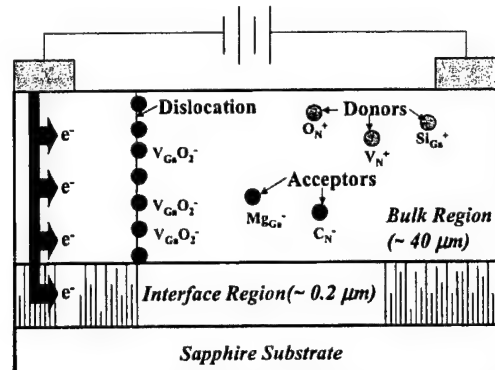


Fig. 27. Current Transport in HVPE GaN showing the possible scatterers and the highly conductive interfacial region.

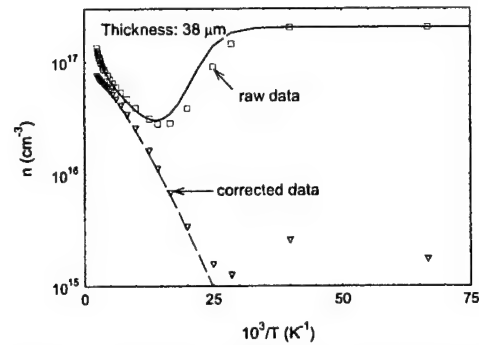


Fig. 28. Carrier concentration of HVPE GaN layer on  $\text{Al}_2\text{O}_3$  before, upper curve, and after correction, lower, for degenerate interface layer.

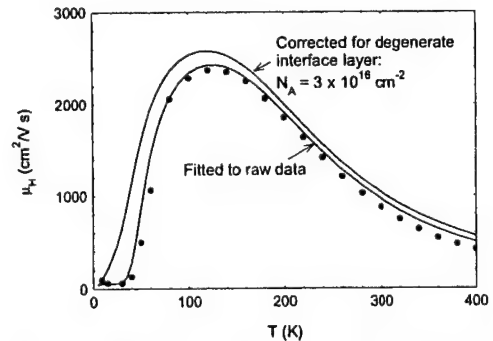


Fig. 29. Temperature dependence of Hall mobility in a  $\sim 68 \mu\text{m}$  thick HVPE GaN layer. The raw data are in solid circles. Also shown are the fitted Hall mobility calculated with the iterative method of Rode and the same calculations after correcting for the highly conductive interfacial layer. The best fit is obtained for an acceptor concentration of  $3 \times 10^{16} \text{ cm}^{-3}$ .

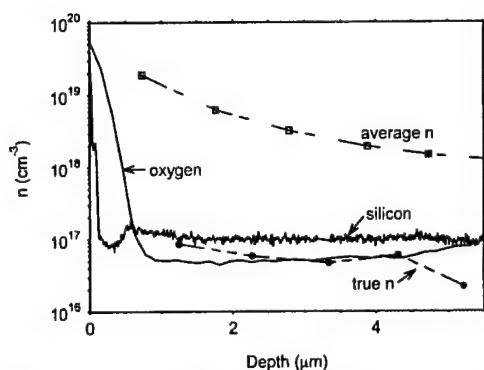


Fig. 30. Profiles of [O], [Si], average  $n$  and true  $n$  (from Hall measurements) in HVPE GaN on  $\text{Al}_2\text{O}_3$

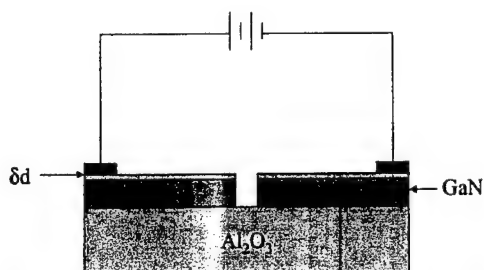


Fig. 31. Cross-section of structure used for differential Hall measurements.

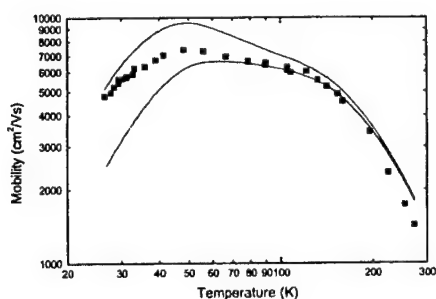


Fig. 32. Experimental mobility vs. temperature data (open circles) of the freestanding bulk GaN sample. Solid lines indicate the calculated values, using an iterative method of Boltzmann Transport Equation, for acceptor concentrations of  $3.4 \times 10^{16} \text{ cm}^{-3}$ ,  $2.4 \times 10^{16} \text{ cm}^{-3}$ , and  $1.4 \times 10^{16} \text{ cm}^{-3}$ . The best fit is obtained for an acceptor concentration of  $2.4 \times 10^{16} \text{ cm}^{-3}$ . No adjustable fitting parameter was used. The GaN parameters used in the simulations are listed in Table IV.

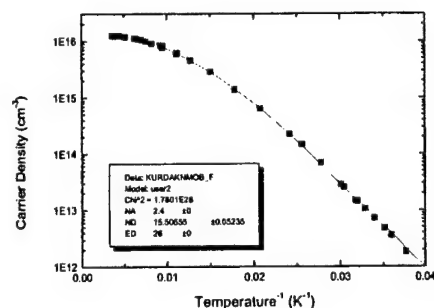


Fig. 33. Temperature dependence of the electron concentration in a Samsung free-standing GaN template. One donor model fits the data well with a donor activation energy of  $\sim 52 \text{ meV}$ .

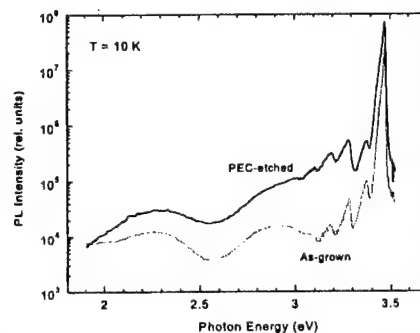


Fig. 34. PL spectrum of HVPE grown sample # 958 before and after PEC etching. The PL was measured in the same conditions and the intensity is plotted in relative units. Excitation density was  $0.01 \text{ W/cm}^2$ .

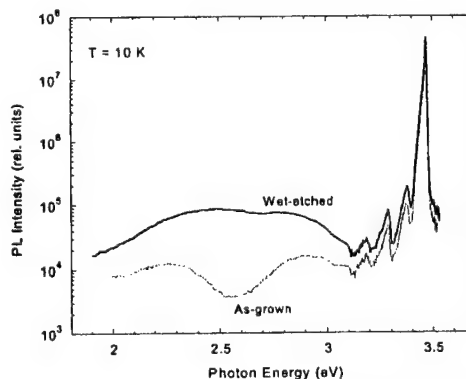


Fig. 35. PL spectrum of HVPE-grown GaN sample # 958 before and after etching in  $\text{H}_3\text{PO}_4$  at  $160^\circ\text{C}$  for 2 minutes. Excitation density is  $0.01 \text{ W/cm}^2$ .

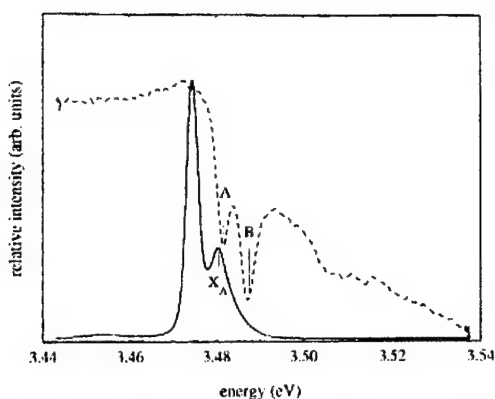


Fig. 36. Emission, solid line, and reflection, dashed line, for  $K||c$ . A polarizer was not used in this configuration.

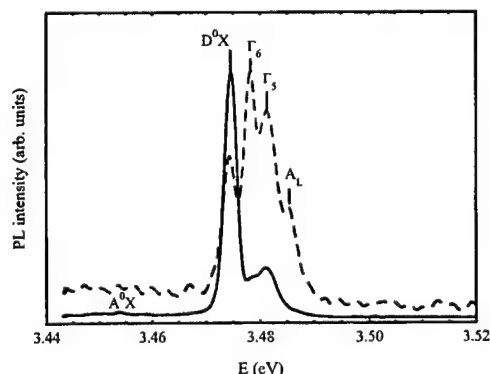


Fig. 37. Emission for  $k^cin$  in a Samsung GaN template. The polarizer is oriented  $E^c$ , solid line,  $E||c$ , dashed line. The polarizer was a Glan Thompson prism.

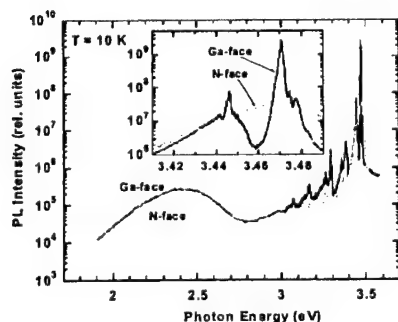


Fig. 38. PL spectrum of freestanding GaN template at 10 K excited with He-Cd laser (3.81 eV) for both Ga and N-faces. The inset shows the expanded view of the bandedge region.

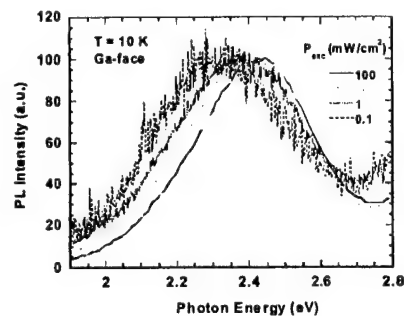


Fig. 39. Defect-related PL spectrum from Ga-face of the sample at different excitation intensities. The excitation energy is 3.81 eV. The PL intensity is normalized to the value at maximum.

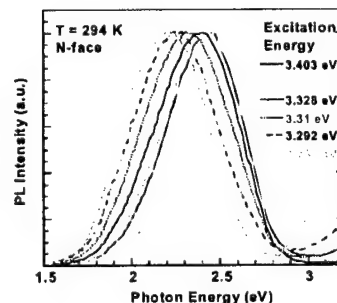


Fig. 40. PL spectrum in the defect-range taken at different photon excitation energies below-band-edge. The excitation density is about 1 W/cm<sup>2</sup>.

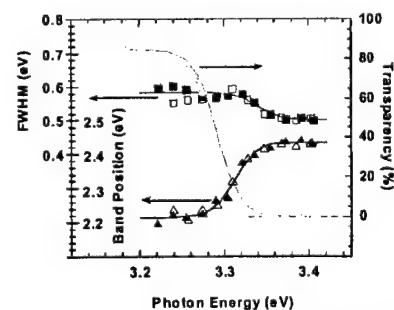


Fig. 41. Position of band maximum, band FWHM and transparency of the 200 mm-thick sample as a function of incident light energy at room temperature. The excitation density is about 1 W/cm<sup>2</sup>. Full squares and triangles are related to illumination of the Ga-face, empty squares and triangles are related to illumination of the N-face of the sample. Solid lines are guides for eye.

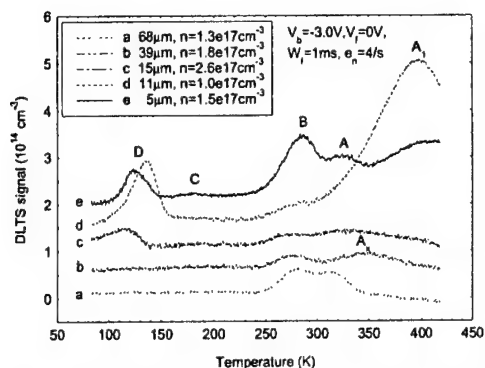


Fig. 42. Typical DLTS spectra for 5 HVPE-GaN samples with different thicknesses. The carrier concentration of each sample is shown in the legend.

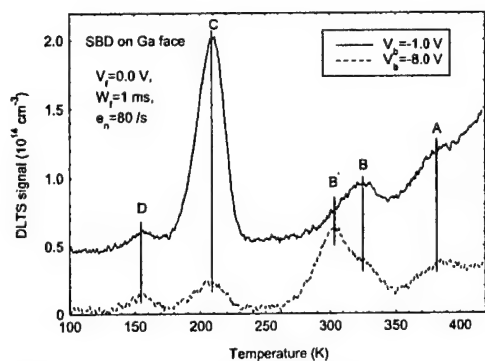


Fig. 43. DLTS spectra for the Ga-face of the free-standing GaN template measured as a function of temperature for a series of filling pulse widths ( $W_f$ ) at 0 and -8 V reverse bias voltages.

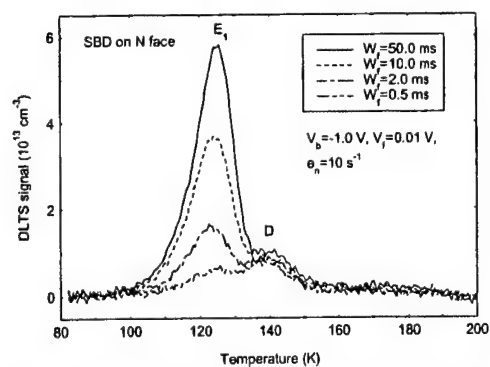


Fig. 44. DLTS spectra for the N-face of the free-standing GaN template measured as a function of temperature for a series of filling pulse widths ( $W_f$ ) at 0.01 and -1 V reverse bias voltages.

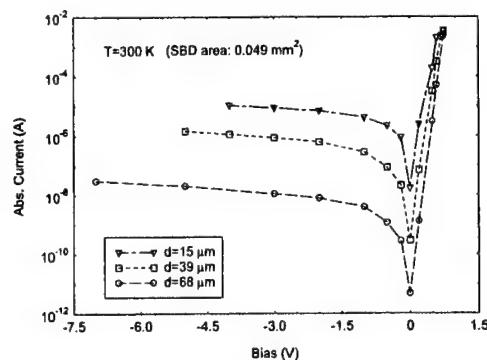


Fig. 45. I-V characteristics of SBDs on HVPE-GaN with different thicknesses; 1, 5, 39 and 68  $\mu\text{m}$ .

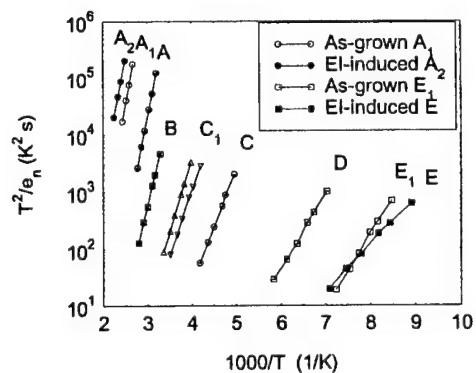


Fig. 46. Arrhenius plots of  $T^2/e_n$  for as-grown and electron beam induced deep centers in n-GaN

Fig. 47. Schematic diagram of the experimental setup used for measuring electron beam induced current (EBIC).

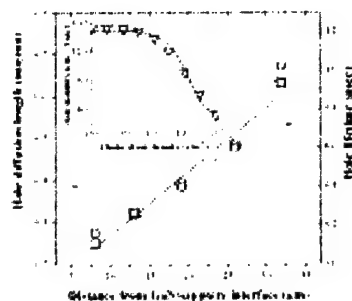


Fig. 48. Experimental minority hole diffusion length dependence (open squares) on the distance,  $d$ , from the n-GaN/sapphire interface, measured for a 36  $\mu\text{m}$  thick sample. The solid line shows a fit. The open circles show the calculated values of minority hole lifetime,  $\tau$ , using equation (1). The dashed line represents a second-order polynomial fit (cf. equation (1)). Inset: theoretical minority hole mobility dependence on dislocation density.

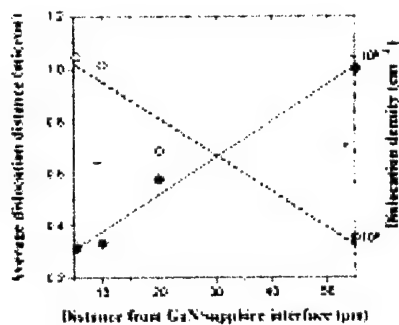


Fig. 49. Experimental dependence of threading dislocation density vs. distance from the GaN/sapphire interface (open circles). The measurement error range is illustrated by the horizontal bars. The dashed line represents the fit. Also shown is average dislocation spacing (solid circles), calculated from the experimentally determined dislocation density. The linear fit is shown by the solid line.

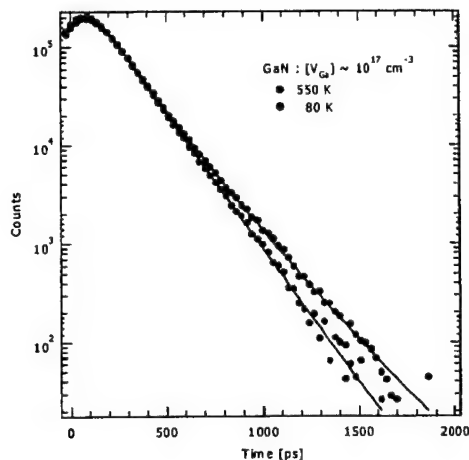
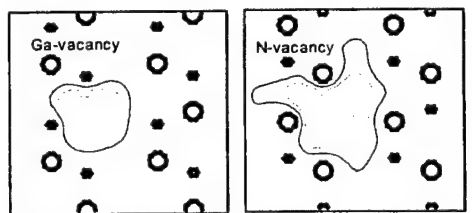


Fig. 50. Positron lifetime spectra in thick,  $>30\mu\text{m}$ , HVPE GaN showing an annihilation lifetime of 235 ps indicative of vacancies labelled as Ga vacancies.



Ga vacancy:  $\tau_v = 209$  ps      N vacancy:  $\tau_v = 160$  ps

Neugebauer and Van de Walle: Appl. Phys. Lett. 69, 503 (1996).

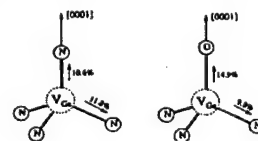


Fig. 51. Schematic of positron densities at Ga and N vacancies, not complexed, in GaN and the lattice diagram showing the local symmetry of a simple VGa and one with a neighboring substitutional O atom on a N-site. The experimental lifetime  $\tau_v =$

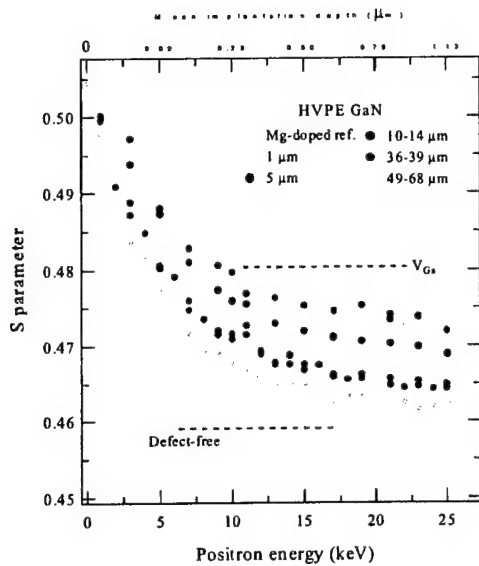


Fig. 52. Ga vacancies and 1, 5, 10-14, 36-39, 49-68  $\mu\text{m}$  thick HVPE GaN layers indicating increased S parameter, thus increased Ga vacancy concentration toward the GaN/ $\text{Al}_2\text{O}_3$  interface in each of the films. A Mg-doped p-type sample with very low if any Ga vacancy is shown as the reference

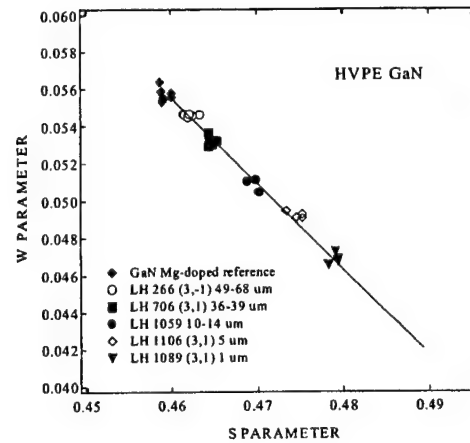
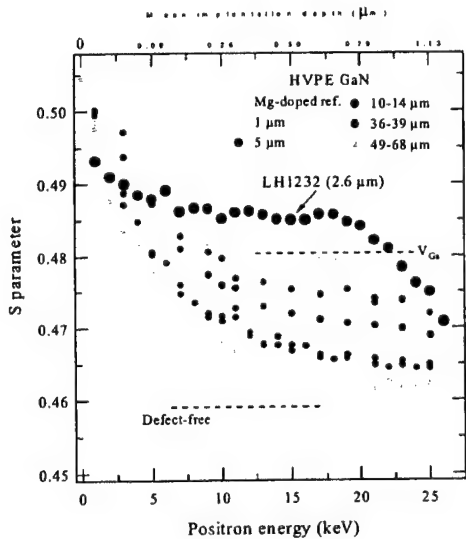


Fig. 53 shows the W (core annihilation parameter) versus S (valence annihilation parameter) parameter plot for all the samples. The slope of the curve points to the same Ga vacancy concentration at a given distance from the interface regardless of the layer. Slide 11



The same as Fig. 52, but inclusive of LH1232, 2.6  $\mu\text{m}$

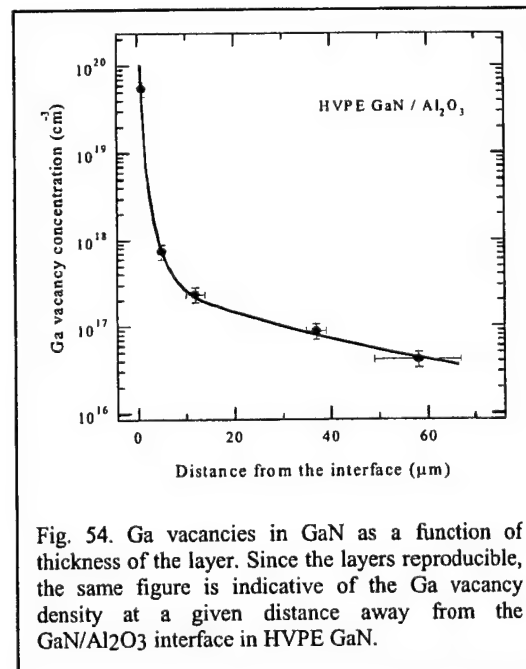


Fig. 54. Ga vacancies in GaN as a function of thickness of the layer. Since the layers reproducible, the same figure is indicative of the Ga vacancy density at a given distance away from the GaN/ $\text{Al}_2\text{O}_3$  interface in HVPE GaN.

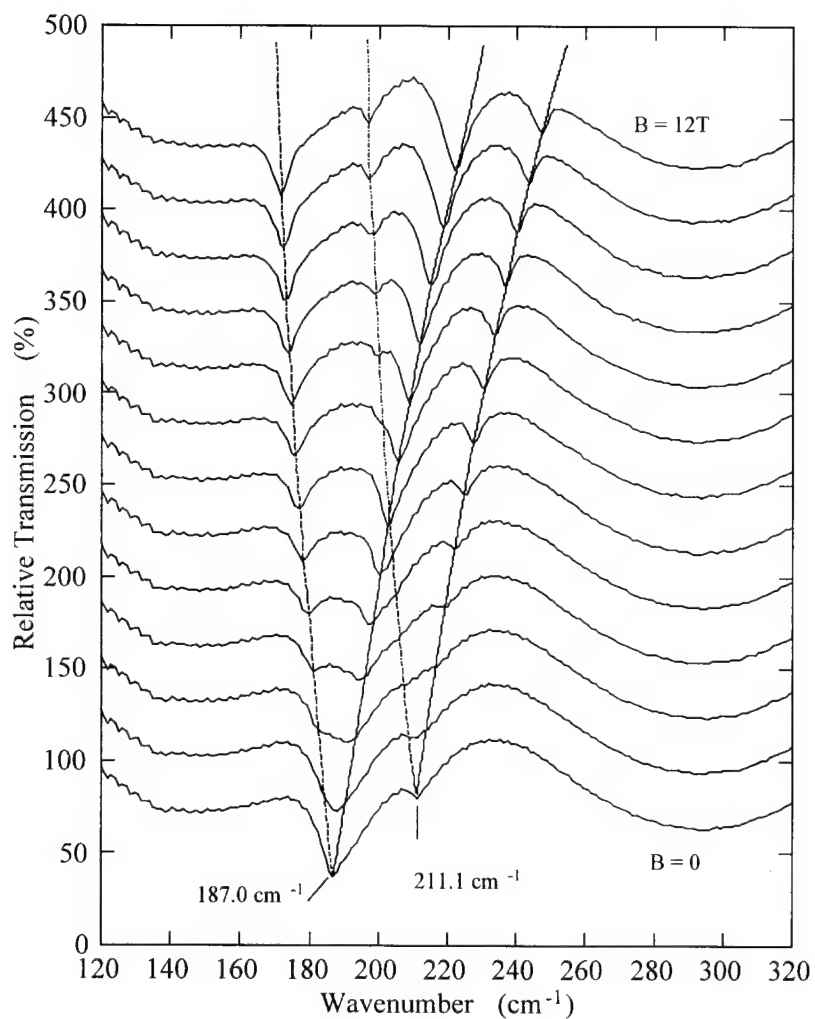
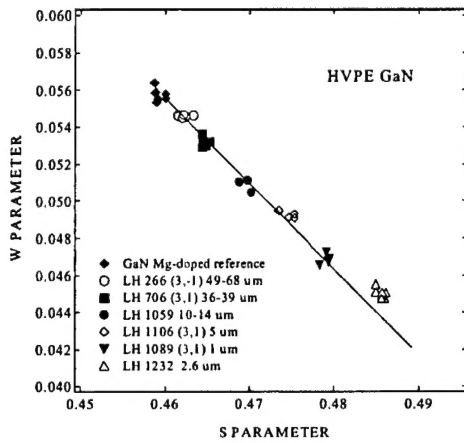
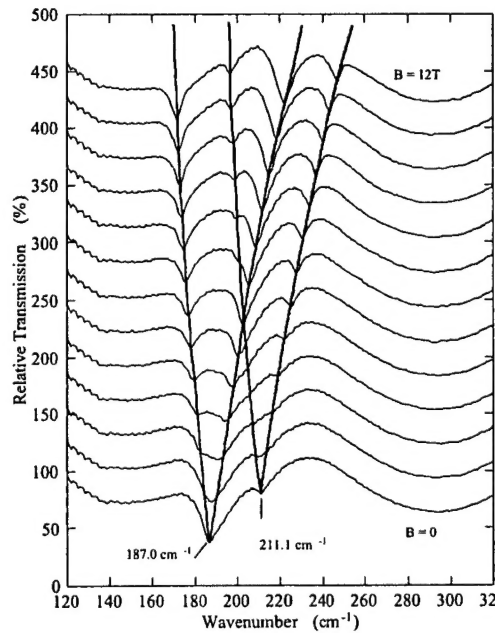


Fig. 55. FTIR absorption measurements in the 120 to 320  $\text{cm}^{-1}$  frequency range and up to a magnetic field of 12 T. The frequency of the absorption bands lead to two donors with binding energies of 30.9 meV and 33.9 and the splitting with magnetic field lead to an effective mass of  $0.22 m_0$ . Data obtained at NRL.



The same as Fig. 53, but inclusive of LH1232, 2.6.  $\mu\text{m}$



FTIR absorption measurements in the 120 to 320  $\text{cm}^{-1}$  frequency range and up to a magnetic field of 12 T. The frequency of the absorption bands lead to two donors with binding energies of 30.9 meV and 33.9 and the splitting with magnetic field lead to an

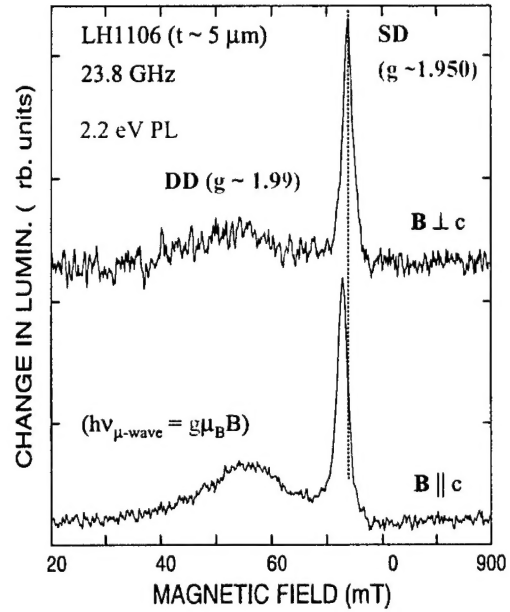


Fig. 56. ODMR signal in a 5-10 mm thick GaN layer from the 2.2 eV peak for the magnetic field perpendicular and parallel to the c-axis. The SD and DD transitions with their associated g-values are given.

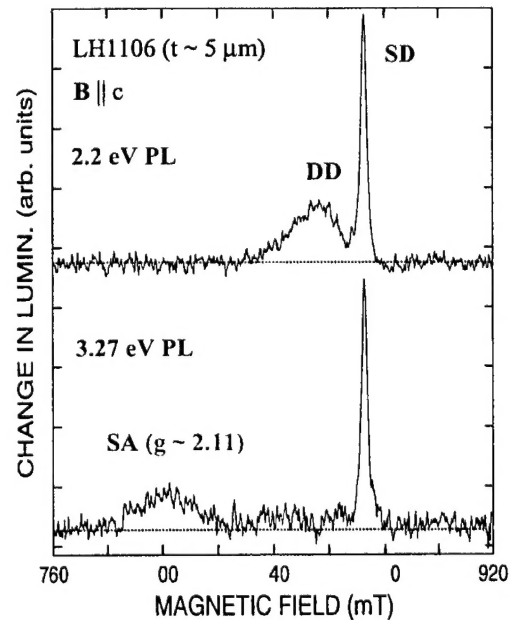


Fig. 57. ODMR signal in a 5-10 mm thick GaN layer from the 2.2 (SD) and 3.27 (SD) eV peaks. In both cases, distinct, but broad, DD and Shallow Acceptor (SA) peaks are observable.

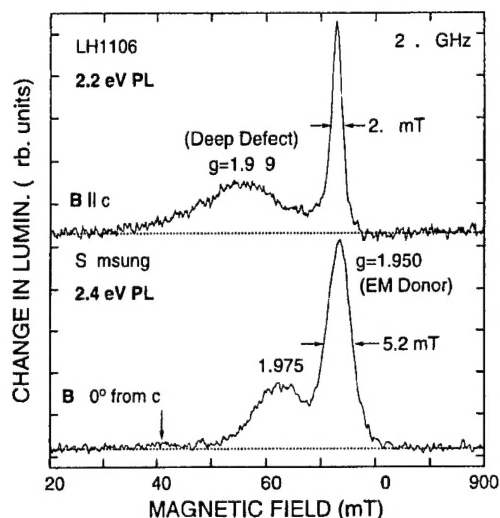


Fig. 58. ODMR signal on 2.2 eV and 2.4 PL for GaN grown at both Lincoln Labs (2.2 eV) and Samsung (2.4 eV), the latter one being a free-standing template. In the case of the Lincoln sample, the B field is parallel to the c-axis. In the case of the Samsung free-standing template, the B field is rotated 30° off the c-axis. This polarization is shown because the weak feature labeled by an arrow at ~ 840 mT does not appear when B is parallel to the c-axis.

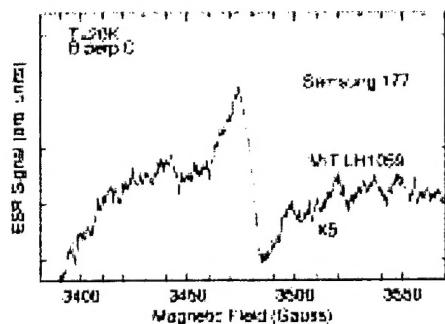


Fig. 59. Electron Paramagnetic Resonance investigation of HVPE samples.

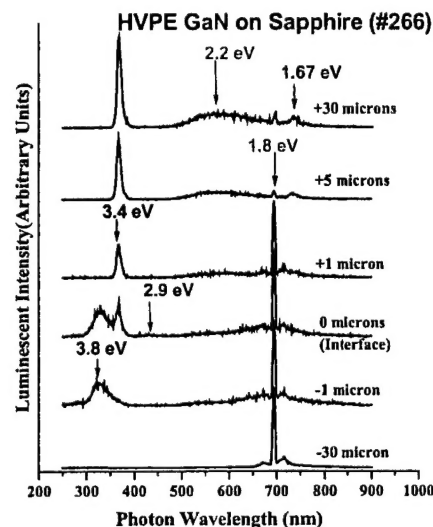


Fig. 60. Micro-CL Cross Sectional Spectra of a Lincoln HVPE GaN layer on sapphire substrate indicating the evolution of optical transition across the interface and in both GaN and sapphire bulk.

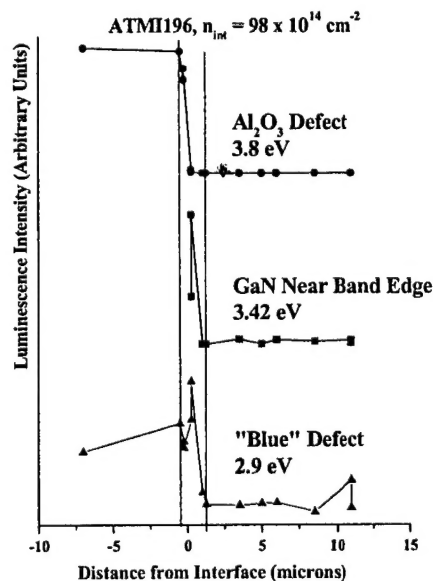


Fig. 61. High Energy, 2.9, 3.42 and 3.8 eV transitions vs distance from the surface in an ATMI GaN/Al<sub>2</sub>O<sub>3</sub> layer. Note the increased intensity of the 2.9 eV peak at the interface.

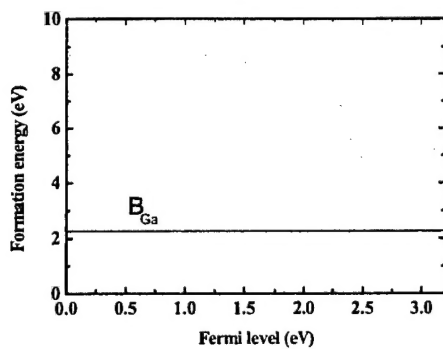


Figure 62: Calculated formation energies for B on substitutional sites in GaN.

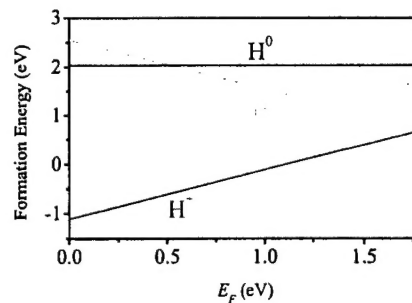


Figure 65: Calculated formation energies of hydrogen in InN. Note that  $H^+$  is the most stable charge state over the entire range of Fermi levels.

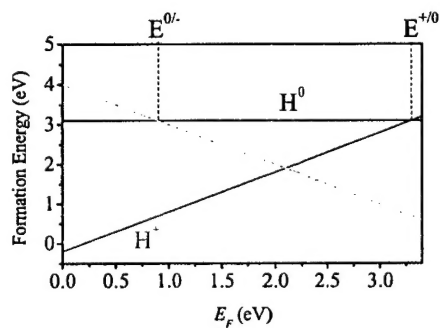


Figure 63: Calculated formation energies of hydrogen in GaN (From Ref.12 in Chris' version).

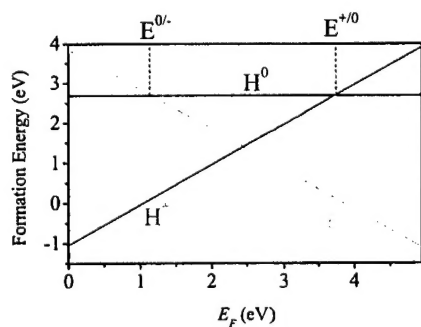


Figure 64: Calculated formation energies of hydrogen in AlN.

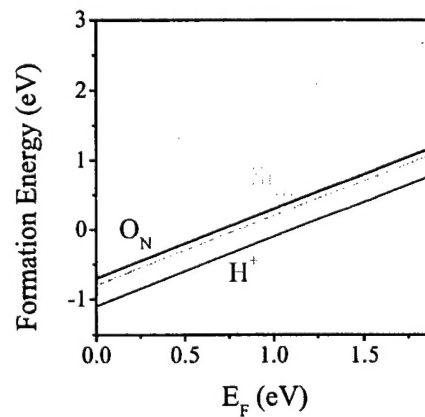


Figure 66: Calculated formation energies for various donor impurities in InN.

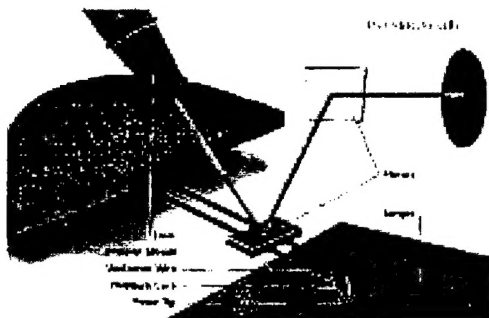


Fig. 67. An artist's view of Scanning thermal microscope

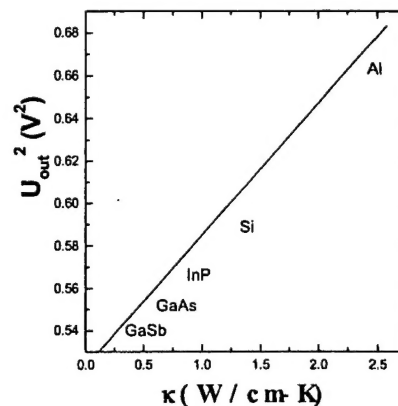


Fig. 69. The feedback signal,  $U_{out}^2$ , which is a measure of the thermal conductivity of the material under test, for a constant thermal element resistance for samples with known conductivities such as GaSb, GaAs, InP, Si, and Al metal.

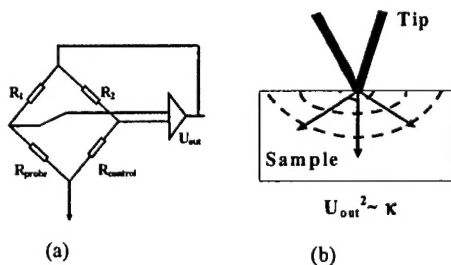


Fig. 68. (a) Winston bridge arrangement in which the tip temperature is kept constant before and after contact with the material whose thermal conductivity is being measured. The feedback signal  $U_{out}$  is related to thermal conductivity,  $\kappa$ . A calibration against known samples such Si, GaAs and GaP, lead to absolute values of  $\kappa$ . (b), Schematic of heat dissipation into the sample from the tip.